CENTER FOR INFRASTRUCTURE ENGINEERING STUDIES

ASSESSMENT OF TECHONOLOGIES OF MASONRY RETROFITTING WITH FRP

by

Davide Tinazzi

Antonio Nanni

University of Missouri-Rolla

CIES
2000

ABSTRACT

The use of Fiber Reinforced Polymer (FRP) materials has proved to be one of the most exciting and effective technologies for external strengthening of masonry structures. The present study, part of the collaboration project between the University of Missouri – Rolla and University of Padua, investigates in-plane and out-of-plane load conditions applied to different constructive typologies of FRP strengthened masonry panels.

From an interesting investigation on an in field application new ideas emerged to improve the structural effectiveness and appearance of FRP based reinforcement approaches. The successive laboratory experimental program includes a preliminary material characterization, bonding investigations and coupon wall testing. Diagonal compression and flexural tests are performed on clay and concrete masonry wallettes in order to identify the influence of different combinations of FRP reinforcement systems. Parameters such as strengthening set-up, anchoring details, installation and strip width are evaluated.

Original failure mechanisms are modified, increasing noticeably ultimate capacities and introducing semi-ductile behaviors. Some specimens subjected to shear load cycles present high levels of energy-dissipation and remarkable post-damage load bearing capacity.

A new technology consisting in embedding composite rods into mortar joints following a specific procedure, called FRP "Structural Repointing", introduces aesthetic and rapid application advantages. Proposed as a reinforcement system to solve shear, flexural, and creep problems, suitable for load bearing walls as well as façades, this technology can be combined with FRP laminates when hybrid systems are required on particular surfaces.

Detailed finite element models are implemented: from the material characterization non linearity and frictional behaviors are introduced to describe failure mechanisms, stress and strain redistributions and predict ultimate capacities.

As result of the present work, design guidelines are proposed for applications of FRP-Structural Repointing in flexural and shear strengthening of masonry.

ACKNOWLEDGEMENTS

This project was funded by the University of Missouri - Rolla Transportation Center and NSF Industry/University Cooperative Research Center on Repair of Building and Bridges with Composites. Support for the exchange experience was also provided by A. Gini Foundation in Padova, Italy. A different profile of support, global could be the word, is the one received from D.N. Mazza University College in Padova, Italy.

All these supports are gratefully acknowledged.

I wish to express my sincere gratitude to my advisors: Prof. Claudio Modena and Dr. Antonio Nanni, for the support and guidance that made a research project a truly enriching experience. I am grateful also to Prof. Alberto Bernardini for his accuracy and expertise.

I would like to acknowledge the outstanding technical skills of Marco Arduini: I really appreciated his contribution and collaboration. Special thanks go also to CIES faculty member Dr. John Myers and the staff: Ravonda McGauley, Gayle Spitzmiller and Steve Haug for their continuous assistance whenever I needed it. Many thanks to Jeff Bradshaw and Steve Gabel, who both were very helpful for the performance of the experimental tests. My gratitude also to RTI for the collaboration. I am truly grateful to my fellow graduate and undergraduate students in the Center for Infrastructure Engineering Studies (CIES). I will never forget their outstanding help and support throughout the course of the work, along with the many social moments we shared.

I am also grateful to my Italian friends, who did not ever forget to give me their support and make me feel their friendship even from overseas.

Finally, I wish words could express my gratitude to my family, for their never-ending trust and support.

TABLE OF CONTENTS

ABSTRACT 1

ACKNOWLEDGENTS 2

SECTION 1: PRESENTATION

1.1 PREFACE 3

1.2 DESCRIPTION OF THE PROJECT 4

1.2.1 Background
1.2.2 The project

1.3 DESCRIPTION OF THE FRP-STRUCTURAL REPOINING TECHNOLOGY 6

SECTION 2: LITERATURE REVIEW

2.1 FRP OVERVIEW 8

2.2 FRP BARS 10

2.3 PREVIOUS WORKS ON FRP RODS 14

2.3.1 Introduction
2.3.2 Experimental projects
2.3.3 Field projects

2.4 DIAGONAL TEST STRESS DISTRIBUTION 22

2.5 ROD-SUBSTRATE BOND FAILURE MECHANISMS 26

2.5.1 Background on Bond of Steel Rebars to Concrete
2.5.2 Background on Bond of FRP Rebars to Concrete

SECTION 3: EXPERIMENTAL PROGRAM

3.1 MATERIALS USED IN THE EXPERIMENTAL PROGRAM 33

3.1.1. Introduction
3.1.2. Material Characterization Tests

3.2 FRP FLEXURAL STRENGTHENING 34

3.2.1 Concrete block walls
3.2.2 Clay masonry beams

3.3 FRP SHEAR STRENGTHENING 37

3.4 AXIAL LOADING TEST 43

SECTION 4: TEST RESULTS

4.1 ABSTRACT 44

4.2 MATERIAL PROPERTIES LIST 44

4.3 FLEXURAL PERFORMANCE 47

4.2.1 Concrete block walls
4.2.2 Clay masonry beams

4.4 SHEAR PERFORMANCE 53

4.5 POST DAMAGE PERFORMANCE 65

SECTION 5: ANALYTICAL STUDY

5.1 DESIGN APPROACH FOR FRP-STRUCTURAL REPOINTING STRENGTHENING OF MASONRY COUPON BEAMS 69

5.1.1 Unreinforced beams
5.1.2 Reinforced beams

5.2 GENERAL ANALITICAL MODEL FOR SHEAR STRENGTHENING OF MASONRY WALLS 77

5.2.1 Validation of the experimental program
5.2.2 Analytical model proposal for masonry shear strengthening with FRP laminates and rods.

5.3 DESIGN APPROACH FOR FRP-STRUCTURAL REPOINTING SHEAR STRENGTHENING OF MASONRY WALLS 81

5.3.1 Introductory Considerations
5.3.2 Background
5.3.3 Existing codes provisions

5.3.4 Research approaches
5.3.5 Contribution of FRP-Structural Repointing to Shear Capacity
5.3.6 Shear strength design
5.3.7 Final Considerations

SECTION 6: CONCLUSIONS AND FUTURE RESEARCH 94

APPENDICES

APPENDIX A: An in-field experimental project:
The MALCOLM BLISS HOSPITAL- St. Louis 97

A1 Background
A2 Material Characterization
A3 Analytical Model

APPENDIX B: MATERIAL CHARACTERIZATION 122

B1 Mortar
B2 Concrete block masonry
B3 Clay brick masonry
B4 Epoxy paste
B5 GFRP rods
B6 GFRP laminates

APPENDIX C: FINITE ELEMENT MODEL 130

BIBLIOGRAPHY 138

1 PRESENTATION

1.1 PREFACE

Unreinforced masonry walls often present inadequacies of ultimate capacities and/or serviceability performances, resulting from deficiencies due to lateral load variation, occupancy change, deterioration, construction or design errors. Load bearing walls are sensitive to lateral cyclic actions, which may cause sudden loss of capacity and brittle failure due to instability; infill panels are also susceptible to pulling apart from floors or snap through during earthquakes or blasting shocks. For these reasons, strengthening of masonry walls is of importance during building retrofitting operations.

In order to restore the original structural function of already damaged masonry members, rehabilitation techniques usually require delicate retrofit that could even be detrimental if a disturbing process is involved. Low-impact approaches based on non-intrusive and non-destructive methods of rehabilitation are in demand when induced or potential damages are fundamental issues.

Structural and architectural maintenance are preventive countermeasures taken to avoid any cause of degradation on historically or architecturally remarkable buildings. Masonry walls are the main focus of this concern. Current techniques hardly reconcile strengthening with appearance, and often tend to periodically replace deteriorated materials instead of preventing moisture infiltration and corrosion. Preservation, instead, might involve reversible installations that have to be removable once certain conditions change; for this reason many traditional strengthening methods cannot be considered for this purpose.

Repointing is the common name for a technique involving the application of short steel rods across cracks caused by creep of the masonry assemblage under long-term high-level dead loads (Binda et al., 1999). Those rods are anchored by cementitious injections. This technology aims to solve circumscribed problems and does not have a global structural function.

FRP materials exhibit several properties, such as high tensile strength and corrosion insensitivity, which make them suitable for use as structural reinforcement. While design procedures have been established specifically for the use of FRP as concrete reinforcement, the outline of masonry strengthening with composites is still in a phase of analytical and experimental basic research.

Previous works based on field experimentations (Tumialan et al., 2000) indicated that in case of out of plain cyclic loads, FRP laminates are not suitable to provide boundary anchoring to prevent pulling apart and neither can be externally applied as façade reinforcement.

It is in this contest that, with the use of advanced materials, a new technology is introduced in order to offer a valid alternative to traditional masonry strengthening systems.

1.2 DESCRIPTION OF THE PROJECT

1.2.1 Background

A field evaluation of URM walls strengthened with FRP composites was performed at the Old City Hospital complex in St. Louis, Missouri, which has been decommissioned and scheduled for demolition (Tumialan et al., 2000. [49]). Before the demolition takes place, one of the buildings within the complex, the Malcolm Bliss Hospital, was selected as a research test bed (see Figure 1.1).

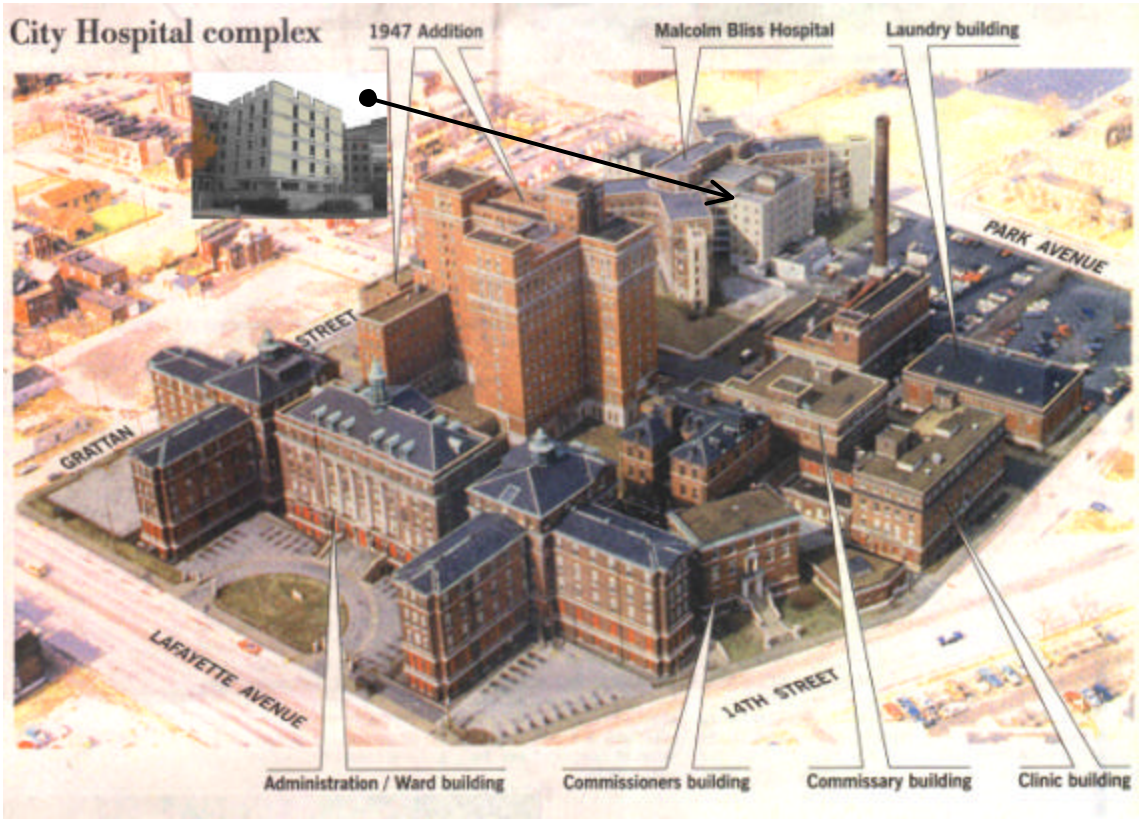

Fig.1.1: City Hospital Complex overview and picture of the Malcolm Bliss Hospital addition.

The building of interest, a five-story reinforced concrete frame addition built in 1964, offered a unique opportunity for performing field experimentation on masonry walls strengthened with Glass, Aramid, and Carbon Fiber Reinforced Polymers (GFRP, AFRP and CFRP, respectively), as well as Glass Rods. The walls belonging to the field experimental program were strengthened on the inner side and subjected to out-of-plane

loading cycles and up to failure. Parameters such as the type of composite system, strip width, and FRP installation methods were evaluated. A mechanism of failure caused by a shear-compression effect lead to the fracture of either the upper or lower boundary masonry units. Due to this failure mode, the walls were not able to develop a higher capacity compared to the control specimen. As this mechanism is not commonly observed in tests performed in a laboratory environment, where simply supported boundary conditions are considered, it is not usually considered in the quantification of upgraded wall capacities, which can dangerously lead to overestimate the wall response during a seismic event.

1.2.2 The project

It was in this context that the present project of "Assessment Of Technologies Of Masonry Retrofitting With FRP" was thought. Evidently, it was necessary to conduct a material characterization experimental program on the hospital walls in order to later relate their properties into a model describing the mechanism of failure and predicting the flexural capacity (see Appendix A); but it was also clear that new reinforcement approaches were needed to provide a global strengthening against dynamic loads and an overall anchorage preventing pulling apart. In fact the demand of new technologies to retrofit existing buildings to cope earthquakes and tornadoes hazard is becoming insistent all over the United States (see Figure 1.2). Additionally, all that had to be done respecting the original external look of the façades and considering applicability and durability issues.

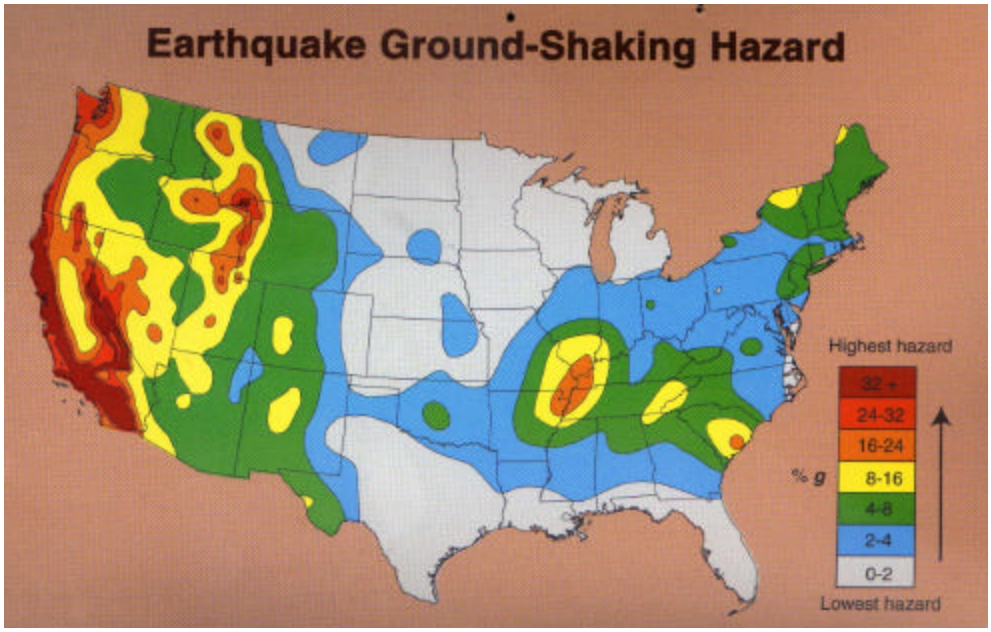

Figure 1.2: Distribution of seismic hazard on the United States.

It was this latter part of the research job that gradually led to the development of the new **"FRP Structural Repointing" System** (see Sections 1.3).
The first idea was immediately followed by an experimental evaluation program and modeling analysis (see Sections 4 and 5).

This project represents the beginning of the official collaboration between University of Missouri – Rolla (UMR) and University of Padua, Italy. Phases of the project were a preliminary overview of the main issues related with FRP strengthening, started in June 1999 in Padova, followed by the experimental and analytical program, between August 1999 and January 2000, performed at the Center for Infrastructure Engineering Studies (CIES) at UMR and a final numerical analysis, February and March 2000, conducted in Italy with the support of Co-FORCE - Italy.

1.3 DESCRIPTION OF THE FRP STRUCTURAL REPOINING TECHNOLOGY

This technology consists of embedding with suitable paste, continuous FRP rods in the horizontal joints of a wall previously grooved, reproducing the original form of the masonry. Color of mortar and workmanship of the joints can be accurately reproduced.

The masonry texture has to present continuous horizontal joints, with either running courses or stack bond. Obviously, in the latter case continuous embedded rods can be vertically applied, as well. The FRP Structural Repointing system includes also specially shaped FRP elements to mechanically connect running-courses with each other and tie multi-wythe walls together. Particular splicing and anchoring issues are addressed using FRP mechanical connections.

Before application, typical material characterization tests are recommended in order to determine the basic mechanical masonry properties to identify the best approach of installation and detailing design.

Except for special cases, functional collaboration between masonry and strengthening is based on the bond properties of the filling paste. Post failure behavior can also be entrusted to the paste-masonry interface friction in order to introduce energy dissipation mechanisms.

The paste has to perform an important role in bonding, anchoring and stress transferring, but workability, surface appearance and easiness of installation are also important issues to be considered. After a material characterization and a bond test program, a designed mix of epoxy resin, quartz sand and coloring pigments was selected as best suitable paste for the considered application. This "epoxy mortar", perfectly compatible with FRP materials, presented a very low ratio of void inclusions and when tested resulted to comply with the design requirements.

Preparation of the specimens for strengthening is a quick procedure consisting in removing with a grinder the outer part of the mortar joints to obtain grooves, whose depth

has to be related to the rod diameter as indicated in previous work on bonding characterization (De Lorenzis, 2000). Application on the specimens is performed injecting the epoxy mortar with a gun (see Figure 1.3); once the rods are embedded, making sure that no voids are left in the grooves, the profile of the joints is shaped using mason's tools and reproducing the original appearance of the wall texture.

Especially for rehabilitation application or post-damage repair, some injection or reconstitution of the substrate may be necessary. Also, a preliminary primer application can be considered when interface bonding needs to be improved.

Fig. 1.3: Operations of installation of the FRP Structural Repointing on masonry specimens for shear and flexural laboratory testing.

2. LITERATURE REVIEW

2.1 FRP OVERVIEW

Fiber reinforced polymers are a particular typology of composite materials, made of high resistance fibers impregnated with polymeric resins (see Fig. 2.1).
High tensile strength, lightness and corrosion insensitivity are the characteristics that make these materials particularly suitable for structural applications, especially in support or substitution of steel. Their function usually consists in adsorbing tensile stress due to shear and flexural actions. Often, among the reachable advantages are also the increase of the overall stiffness and ductility. When using FRP for confining increment of the load bearing capacity is obtainable, as well.

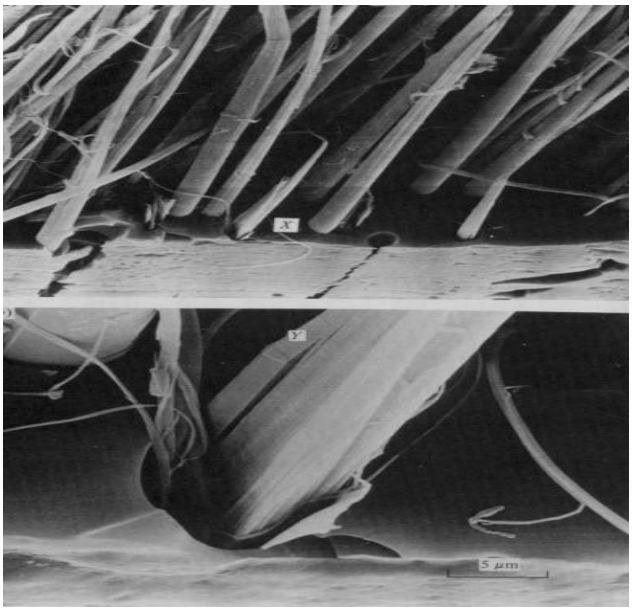

Figure 2.1: micro structure of FRP composite. Fibers and matrix are *failed under high tensile stress*

Due to their elevated cost of production and the non complete knowledge of their mechanical behavior, at the moment the use of FRP materials is limited to particular situations were steel applications are inadequate.
FRP applications are compatible with all the existing structural materials; the most investigated are the applications with concrete, but also masonry and wood have been combined with FRP. Steel structures are still excluded from this new strengthening approach, as at the moment it is easier to use a steel-steel combination instead of applying and hybrid system. In the next future is not excluded the some more confidence with FRP may lead to retrofitting application on steel structures.

New prospective are opened by the use of composites in both new constructions and retrofitting applications. For instance, the strength-lightness ratio of FRP raises the steel-bridges span theoretical barrier from 4.5 km to 11.5 km. But less sensational field applications have already demonstrated the effectiveness of these products. In fact, FRP retrofitting is increasing sensitively, involving also historically and architecturally remarkable buildings.

Without underlining the importance of a lower installation cost, the use of FRP composites possesses some advantages compared to traditional retrofitting methods. As an example, the disturbance of the occupants of the facility is minimal and there is no loss of valuable space. In addition, from the structural point of view, the dynamic properties of the structure remain unchanging because there is no addition of weight that would lead to increases in seismic forces.

FRP products are commercialized in different shapes: rods, tendons, laminates and three-dimensional components (see Figure 2.2).

Figure 2.2: Different FRP products

Nowadays, a few countries have proposed design guidelines for FRP structural use; Canada and Japan have already adopted codes referring to reinforced concrete with FRP rods, while the United States are in a preparatory phase (ACI committee 440, 1999. [53]).
Except for that, any other structural application involves an experimental approach, involving a preliminary material characterization and concluding with the identification of appropriate models and safety factors. These latter coefficients have to take into account particular phenomena and consider the possibility of brittle failure modes due to the typical linear elastic behavior of these materials.

The most important limit to the FRP use diffusion in Civil Engineering is represented by the high cost of production. Nevertheless, it must be noticed that in the structural strengthening field the materials affect only 20% of the total amount, while all the rest is related with design, transportation and labor costs. Furthermore, if in the cost of the work also site equipment and maintenance are included, FRP products may sometimes represent the most suitable alternative.

Another problem relative to the use of these products is the absence of standardization of a manufacturing level, which has, as consequence, that experimental results, preliminary to a certain application, obtained with a certain product cannot be automatically considered valid for other similar products from other manufacturers.

Durability issues are nowadays assuming relevant importance in many applications and especially for new materials as FRP it represent a fundamental requirement that cannot be ignored. Unfortunately, due to the relative short life of this technology and the complexity of the interfacing problems with other bonding materials, the reliability of available data on durability is not completely certain.

2.2 FRP BARS

Fiber-reinforced polymer bars are manufactured using different techniques, such as pultrusion, braiding and weaving. FRP rods are anisotropic, with the longitudinal axis being the major axis. Their mechanical properties can vary significantly from one manufacturer to another and within the same product. Factors, such as fiber volume, type of fiber, type of resin, fiber orientation, dimensional effects and manufacturing methods play a major role in establishing product characteristics. The relative volume of fibers and resin in the product affects the properties of FRP rods. A usual fiber volume is between 0.5 and 0.7. Furthermore, the mechanical properties of FRP bars, like all structural materials, are affected by such factors as loading history and duration, temperature and moisture.

FRP bars have a density ranging from four to six times smaller than that of steel. The reduced weight leads to lower transportation costs and decreased handling and installation time per bar on the job site.

Coefficient of thermal expansion. The coefficients of thermal expansion of FRP bars vary in the longitudinal and transverse directions depending on the types of fiber, resin and volume fraction fiber.
Table 2.1 lists the longitudinal and transverse coefficients of thermal expansion for typical FRP bars and steel bars.

Table 2.1: Typical coefficient of thermal expansion of reinforcing FRP bars ($x10^{-6}/C^{0}$).

Direction	Steel	GFRP	CFRP	AFRP
Long., a_L	11.7	6 to 10	-1 to 0	-2 to 6
Trans., a_T	11.7	21 to 23	22 to 23	60 to 80

Tensile behavior. Ultimate tensile strength of FRP bars is reached without exhibiting any plastic yielding. The relationship between stress and strain of FRP bars consisting of one type of fiber material can be represented as a straight line up to the point of maximum stress. Because the manufacturer can vary the volume fraction of fibers, strength variation is noted, even in identically appearing bars with the same types of constituents. The rate of curing, the manufacturing process and its quality control also affect the mechanical characteristics of the bar.

Unlike steel bars, some FRP bars exhibit a substantial size effect. Due to shear lag, fibers located near the center of the bar cross section are not subjected to as much stress as those fibers that are near the outer surface. This phenomenon results in reduced strength and efficiency in large diameter bars.

Determination of FRP bar strength is complicated because stress concentrations in the anchoring system during testing may lead to premature failure. Tensile properties of some commonly used FRP bars are summarized in Table 2.2.

Table 2.2: Typical tensile properties of reinforcing bars.

	Steel	GFRP	CFRP	AFRP
Strength (Mpa)	483-690 (yield 276-414)	483-1035	600-2900	1000-1400

Strength of bent FRP bars. FRP reinforcing bars can be made using one of two types of resins, thermosetting or thermoplastic. Cured FRP bars made of thermoplastic resins can be bent by applying heat and pressure. In this case, a strength reduction of 40 to 50% can occur due to fiber bending and stress concentration, compared to the axial tensile strength of a straight bar. The reduction depends on the bending technique and constituent material types.

Compressive behavior. Tests on FRP bars have shown that compressive strength is lower than tensile strength, and precisely of $0.55f_{fu}$, $0.78f_{fu}$ and $0.2f_{fu}$ for GFRP, CFRP and AFRP, respectively.

Compressive strengths are expected to be higher for bars with higher tensile strengths, except in the case of aramid FRP, where the fibers undergo ;yield-like behavior at a

relatively low stress. Unlike tensile modulus of elasticity, the FRP compressive modulus of elasticity varies with bar size, type, quality control in manufacturing and length-to-diameter ratio of the specimens. It is usually smaller than the correspondent tensile modulus of elasticity. According to reports, the compressive modulus of elasticity is approximately 80% for GFRP and 100% for AFRP of the tensile modulus of elasticity for the same product.

Shear behavior. The shear strength of FRP composites is low because it depends primarily on resin properties. This shortcoming can be overcome by orienting the FRP bars so that they resist the applied loads through axial tension. Orientation of the fibers in an off-axis direction will increase the shear resistance, depending upon the degree of offset. The strength in the main direction, however, will be reduced by the fiber offset.

Creep. The orientation and volume fraction of fibers in the composite have a significant influence on the creep performance of FRP bars. Studies report that the additional strain of a GFRP reinforcing bar caused by creep was estimated to be only 3% of the initial elastic strain.

Under adverse environmental conditions, FRP reinforcing bars subjected to the action of a constant load can suddenly fail after a time, referred to as the endurance time. This phenomenon, known as creep rupture, exists for almost all structural materials. As the ratio of the sustained tensile stress to the short-term strength of the FRP bar increases, endurance time decreases. Results of some tests indicated that a linear relationship exists between creep rupture strength and the logarithm of time for all load levels. The ratios of load level at rupture to the static strength of the GFRP, AFRP and CFRP bars after about 50 years were 0.3, 0.47 and 0.91, respectively. Environmental factors, such as moisture and temperature, can impair creep performance and result in shorter endurance time. Carbon fibers are least susceptible to creep rupture.

Fatigue. Of all types of current FRP composites for infrastructure applications, carbon FRP is generally thought to be the least prone to fatigue loading. An endurance limit of 60-60% of the initial static ultimate strength of CFRP in typical. For GFRP rods, more difficultly clear fatigue limit can be defined, as environmental factors can play an important role in the fatigue behavior of glass fibers due to their susceptibility to moisture, alkaline and acid solutions. In cases where fatigue of FRP bars in the longitudinal or transverse directions is likely, such as boned bars, the life-limiting mechanisms tend to shift from the fiber to the resin and possibly to the fiber-resin interface. Generalized comments on endurance limits are difficult to make due to the wide variation of results reported for different loadings modes and different material systems.

Bond behavior. Bond performance of an FRP bar is dependent on the design, manufacturing process, mechanical properties of the bar itself.
The bond force of an embedded FRP bar can be transferred by:

- Adhesion resistance of the interface, also known as chemical bond;
- Frictional resistance of the interface against slip;
- Mechanical interlock due to irregularities of the interface.

In order to improve the bond performance through mechanical interlock, the rods are produced by manufacturers in various types and with different deformation systems, including exterior wound fibers, sand coatings and separately formed deformations (see Figure 2.3).

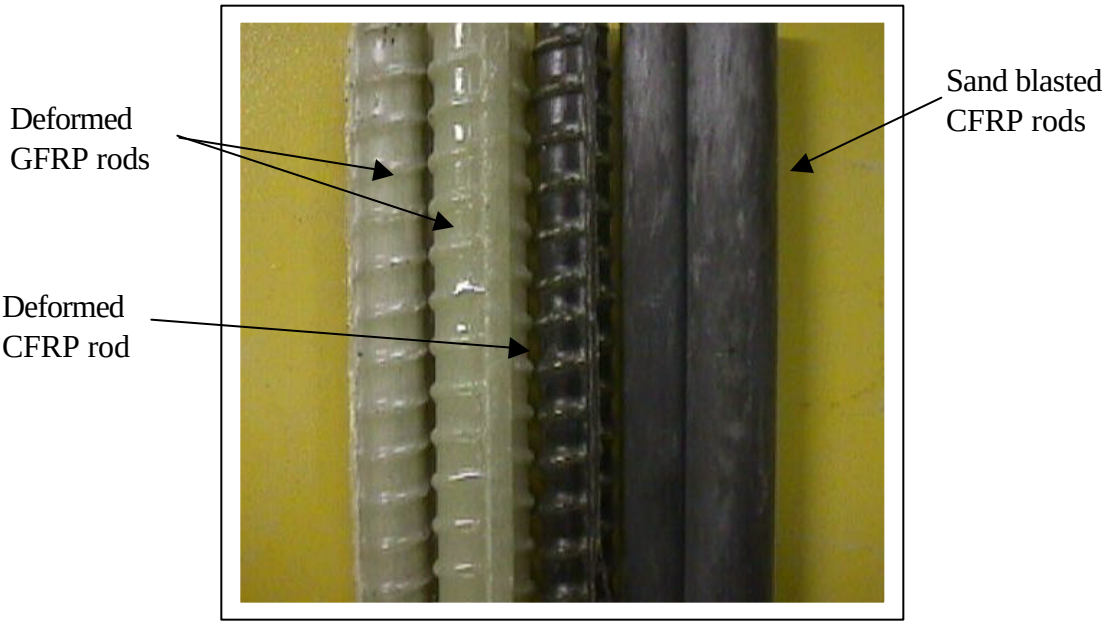

Fig. 2.3: Different superficial manufacturing of FRP bars.

Durability. Durability tests are conducted to determine the strength and stiffness reduction due to natural aging of FRP bars under service environments over 50 to 100 years of service life. Many researchers are establishing these reduction factors. These factors differ for each product, depending on the type of fiber, type of resin and bar size. In addition, the factors are affected by the environmental condition, such as surrounding solution media, temperature, pH, moisture and freeze-thaw cycles.

Fire resistance. The use of FRP reinforcement is not recommended for structures under high temperatures and for structures in which fire resistance is essential in order to maintain structural integrity. Because FRP reinforcement is embedded, the composite cannot burn due to the lack of oxygen; however, the polymers will soften. Locally, the effect of high temperature can result in increased crack widths and deflections. If the end regions of FRP reinforcing bars are kept cool and protected, the structure's safety should not be significantly affected. The temperature beyond which the elastic modulus of the polymers is significantly reduced is known as the glass transition temperature, T_g. The structure can collapse if the temperature rises well above T_g and the fibers start to degrade.

(Bars characteristics in Section 2.2 FRP are referenced from ACI committee 440 working document, 2000. [53]. The document is under discussion and upgrading process).

2.3 PREVIOUS WORKS ON FRP RODS

2.3.1 Introduction

Externally bonded FRP laminates have been successfully used to increase the flexural and/or the shear capacity (sometimes also the stiffness) of RC beams, to provide confinement to RC columns, to strengthen masonry walls subjected to out-of-plane as well as in-plane loading. A remarkable amount of experimental research has been carried out and is currently ongoing towards the characterization of RC and masonry structures strengthened with this technique. At the same time, many successful installations have covered the industrial, commercial, and public markets all over the world, so that strengthening with externally bonded FRP laminates can be considered close to achieve the status of mainstream technology.

A new FRP-based strengthening technique is now emerging as a valid alternative to externally bonded laminates. It consists in embedding FRP rods into grooves cut near the surface of the member to be reinforced. Embedment of the rods is achieved by grooving the surface of the member to be strengthened along the desired direction (De Lorenzis, 2000 [47]). The groove is filled half way with epoxy paste. The FRP rod is then placed in the groove and lightly pressed, so forcing the paste to flow around the bar and fill completely between the bar and the sides of the groove. The groove is then filled with more paste and the surface is leveled (see Figure 2.1).

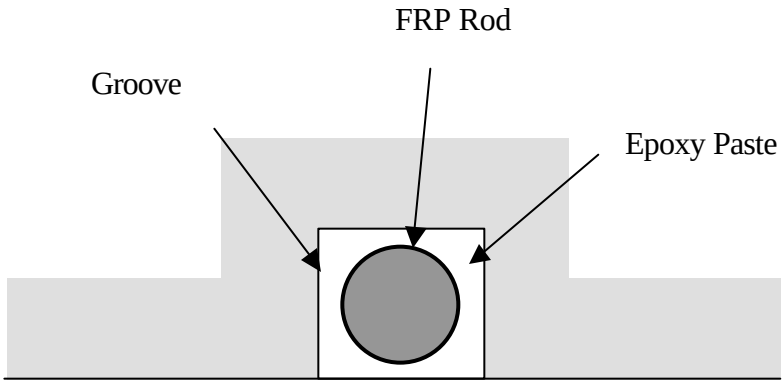

Figure 2.1: FRP rod insertion

In case of the Structural Repointing technique, the procedure involves a resin based mix with additives, as pigments, and fillers, as sand. Shaping of the paste profile is also required, while the exposed substrate surface is cleaned from paste stains when masking is not adopted.

The use of FRP rods is an attractive method for increasing the flexural and the shear strength of deficient RC members and masonry walls and, in certain cases, can be more convenient than using FRP laminates (De Lorenzis, 2000 [47]).

Due to the novelty of this technique, very limited literature is currently available on the use of external strengthening with rods. Although only a few experimental studies are documented to date, some significant field applications have been already carried out in the United States during the past two years. Laboratory studies and field projects are outlined in the following

2.3.2 Laboratory projects

In order of time, the last experimental work on the use of FRP bars as external post-reinforcement, called in that occasion Near Surface Mounted Rods (NSM) focused on RC shear and flexural strengthening (De Lorenzis, 2000 [47]). In that project bonding tests, involving also masonry concrete blocks, revealed different mechanisms of failure: splitting of the epoxy cover, cracking of the concrete surrounding the groove and pull-out of the FRP rod. In some cases, a combined failure mode (pull-out with some damage in the epoxy cover) was registered. It was also possible to derive the following observations.

The surface condition of the FRP rods influences the bond strength. Deformed rods appear to be more efficient than sandblasted rods from the standpoint of the bond performance; increasing the groove size, and thus the cover thickness, leads to higher bond strength when failure is controlled by splitting of the epoxy cover. Conversely, it does not have any effect when pull-out failure occurs. In the deformed-rod specimen with the largest value of the ratio cover thickness to rod diameter the splitting failure shifted from the bonding paste to the concrete surrounding the groove. When failure occurs by splitting of the epoxy cover or by pull-out of the rod, the ultimate load is expected to be independent from the concrete tensile strength. However, if the groove is deep enough to cause failure occur in the concrete, the concrete tensile strength becomes a significant parameter; from the experimental results involving different groove sizes, the optimum groove sizes appear to be 3/4 in. and 1 in. for embedment of NSM rods No. and No. 4, respectively. The distribution of bond stresses at ultimate is not uniform, except for the case of specimens with CFRP No. 3 deformed rods. Therefore, the development length has to be calculated by solving the differential equation of bond with the local bond stress – slip relationship of the NSM rods. The same failure modes were experienced during the bond tests of NSM rods in concrete masonry blocks: splitting for the specimens with GFRP deformed rods and pull-out for those with CFRP sandblasted rods; unlike in the case of NSM rods in concrete, a noticeable level of damage was induced in the portion of block surrounding the groove along with splitting of the epoxy cover, due to the lower tensile strength of the concrete masonry material.

The overall project allowed to characterize the tensile properties of the FRP materials and the bond behavior of NSM FRP rods embedded in concrete or in masonry units, using coupon-size specimens (sub-system level); investigate the structural behavior of RC beams strengthened in shear with NSM FRP rods using full-size specimens (structural member level); finally, develop a simplified design approach for shear strengthening of RC beams with NSM rods.

Experimental data on the bond between Carbon FRP (CFRP) rods and epoxy paste is reported in the Navy Special Publication SP-2046-SHR (Warren, 1998.[62]). Direct pull-out tests were conducted using smooth CFRP rods No. 3 (nominal diameter

3/8 in.) The surface of some of the rods was slightly sanded to improve the bond characteristics. The rods were embedded 4 in. (corresponding to 11 times the diameter). The test parameters were surface condition of the rods, type of epoxy and addition of sand to extend the epoxy volume. The addition of sand was found to provide less variation in results but also to slightly reduce the bond strength and the wetability of the epoxy.

Yan et al. (1999) [63] also performed experimental tests to characterize the bond strength of NSM FRP rods. The specimen used for this test consisted of two concrete blocks, two CFRP bars, and epoxy paste. The concrete strength was 5000 psi. The smooth CFRP rods had a diameter of 7/16 in. and were sandblasted prior to the test to improve the bond characteristics. The epoxy paste used was Concresive Paste LPL by Master Builders Technologies. The specimens differed for the value of the bonded length, which was equal to 2 in. (4.6 diameters), 4 in. (9.2 diameters) and 6 in. (13.7 diameters). The specimens were prepared by filling the groove with the epoxy paste and then placing the bar in the paste. The paste was allowed to cure for 14 days at room temperature before testing. The type of test performed was direct pull-out of the NSM FRP rods. Two types of failure mode occurred: the specimens with the two shorter bonded lengths failed by rupture of the concrete at the edge of the block, those with the 6 in. bonded length experienced failure at the rod-epoxy interface (pull-out). Load at onset of slip, ultimate load and free-end slip at ultimate were recorded.

Crasto et al. (1999) conducted experimental research on flexural strengthening of RC beams with NSM FRP rods. The materials used were CFRP rods manufactured by DFI Pultruded Composites, Inc. and a two-part epoxy by Dexter Hysol, Inc. The experimental program included the evaluation of the technique on 8.5-ft. RC beams, the scale-up to full-size (28-ft.) beams and the final application to deteriorated 34-ft. RC beams removed from a vehicular bridge after more than 80 years of service.

A number of tests was conducted on beams with varying ratios of steel/composite cross-sectional area. Rectangular grooves were machined into the tensile face of the beams to various depths, cleaned and dried. The CFRP rods were sanded, wiped clean with acetone and embedded in the epoxy within the grooves. The adhesive was then allowed to cure overnight under ambient conditions before the beams were tested under four-point bending.

All tests showed that the NSM composite reinforcement improved the flexural stiffness, the value of bending moment at which the steel yields and the ultimate moment of the beams.

2.3.3 Field projects

A strengthening project was carried out at the structural street level floor of Myriad Convention Center, Oklahoma City, OK (USA) in the summer of 1998 (Hogue et al., 1999.[65]). The floor required strengthening in order to increase its live load bearing capacity. The strengthening system implemented included a combination of externally bonded steel plates, CFRP sheets and NSM CFRP rods. The strengthening system sought to address both flexural and shear deficiencies. NSM rods were used in this case for

shear strengthening of one of the RC joists. Vertical grooves 1/2-in. wide and 3/4-in. deep with a total length of 20 in. were saw-cut along the side surfaces of the joist at such positions that existing stirrups were avoided (see Figure 2.2). CFRP No. 3 rods were then inserted in the epoxy-filled grooves.

Figure 2.2. Vertical Grooves for Shear Strengthening with NSM FRP Rods

NSM CFRP rods were used for strengthening of two RC circular structures in the United States in 1998. Longitudinal and transverse grooves 1/2-in. wide and 1/2-in. deep were cut on the surface of the structures (see Figure 2.3) and CFRP rods with a nominal diameter of 5/16 in. were embedded in the epoxy-filled grooves (see Figure 2.4).

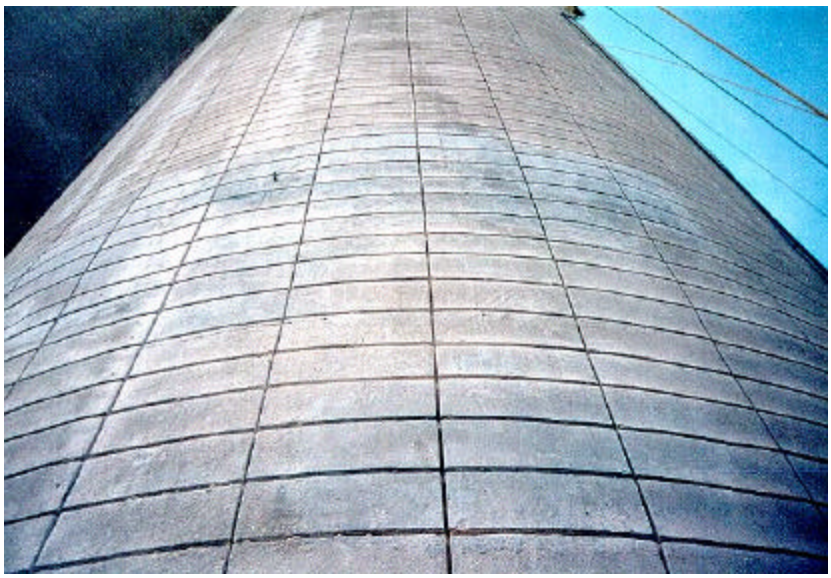

Figure 2.3. Grooves on the Surface of the Structure

Figure 2.4: Filling of Grooves with Epoxy Paste

Pier 12 at the Naval Station San Diego, CA (USA) was strengthened in November 1998 to meet demand of operational changes accompanied by higher vertical loads (Warren, 1998. [62]). NSM CFRP rods were used to increase the capacity of the deck slab in the negative moment regions. The surface area was primed with penetrating epoxy sealer/primer and allowed to cure overnight. Slots were saw-cut in the deck in the range of 7/8-in. deep and 5/8-in. to 3/4-in. wide. The slots were abrasive blasted to roughen the surface, air blasted to clean the concrete and primed before filling with epoxy encapsulate.

Carbon pultruded No. 3 rods were placed in sequence into the epoxy-filled slots and pressed to the bottom (see Figure 2.5). The slots were then filled up to within ¼ in. of the original concrete surface. After the epoxy was cured, the surface was abrasive blasted and a UV protective layer was added to the top of the slot. The surface was ready for use 24 hours after the installation.

Figure 2.5: Embedding CFRP Rods in the Top Surface of the Deck

After completion of the upgrade, some spans of the deck were tested using simulated outrigger loads. Strain gages attached to the CFRP rods allowed to monitor the performance of the strengthening system, which proved to be satisfactory. Half scale tests of the upgrade systems were also conducted. RC slabs strengthened with NSM CFRP rods were tested under three-point bending. The strengthened slabs showed significant gains in strength and ductility over the baseline slab, the failure mode being punching shear. Prior to ultimate load, some rods had begun to separate from the slab surface. There were no rod failures prior to ultimate load.

Bridge J-857 was located on Route 72 in Phelps County, MO (USA). It consisted of three solid RC decks simply supported by two bents. Each bent consisted of two piers connected at the top by an RC cap beam. Due to the realignment of Route 72, the bridge was decommissioned and scheduled for demolition. Therefore, it presented an excellent opportunity for in-situ testing to failure after strengthening with FRP composites (Alkhrdaji et al., 1999.[66]).

The bridge was strengthened in August of 1998 while in service. Two of the three decks were strengthened using two different FRP systems, namely, externally bonded FRP laminates and NSM FRP rods, while the third deck was left as a benchmark. The NSM reinforcement consisted of CFRP rods with 7/16-in. diameter and surface roughened by sandblasting to improve bond properties. Strengthening to about 30% of the nominal moment capacity was desirable to upgrade the bridge decks for HS20-modified truck load. The design called for 20 NSM CFRP rods spaced at 15 in. on-center. The rods were embedded in 20-ft long, 3/4-in. deep, and 9/16-in. wide grooves cut onto the soffit of the bridge deck parallel to its longitudinal axis, as shown in Figure 2.6. The grooves were sand blasted to remove dust and any loose materials that could interfere with the bond between epoxy paste and concrete. Strain gages and fiber optics

sensors were applied to concrete, steel reinforcement and FRP reinforcement to monitor strain during testing.

Each of the three decks was tested to failure by applying quasi-static load cycles. For the deck with NSM rods, failure was initiated by the rupture of some CFRP rods at the location of the widest crack. This deck showed the highest capacity with a failure load of 596 kips, corresponding to an increase in the moment capacity of 27% over the unstrengthened deck. At service levels (i.e., before the yielding of the steel reinforcement), both decks strengthened with FRP composites had higher stiffness than the unstrengthened deck.

Two columns were also strengthened with NSM CFRP rods to increase their flexural capacity (see Figure 2.7). The intended levels of flexural strengthening were such that two different failure modes would be achieved, one controlled by rupture of the CFRP reinforcement (6 rods, 3 on each face of the column) and one by crushing of concrete (14 rods, 7 on each face of the column). The rods were mounted on two opposite faces of the columns and fully anchored (minimum 15 in.) into the footings to ensure that the full capacity of the strengthened section is attained at the base of the column. The grooves and the drilled holes were filled with a viscous epoxy grout.

Figure 2.6. Installation of NSM CFRP Rods in the Bridge Deck

Figure 2.7: Columns Strengthened with NSM Rods

A strengthening and load-testing program at the decommissioned Malcolm Bliss Hospital in St. Louis, MO (USA) was conducted in 1999 (Tumialan et al., 1999.[49]). The building, a five-story RC-frame addition built in 1964, offered a unique opportunity for performing in-situ experimentation. Static load tests up to failure were carried out in order to validate strengthening of masonry walls and RC joists using externally bonded FRP laminates and NSM FRP rods.

The program on masonry walls strengthened with FRP composites included testing of unreinforced masonry walls subjected to out-of-plane loading and reinforced masonry walls under in-plane loading. Parameters such as the type of composite system, strip width, and FRP installation methods were evaluated. Figure 2.8 shows the installation of NSM FRP rods on a masonry wall to be strengthened for out-of-plane loading.

Figure 2.8: Installation of NSM FRP Rods on Masonry Walls

2.4 DIAGONAL TEST STRESS DISTRIBUTION

As demonstrated by many experimental investigations (see Bernardini et al., 1979.[42]), the diagonal compressive test is an easy and reliable method to obtain different parameters on the shear behavior of masonry assemblages. This test, performed on square panels, can be represented by a simplified scheme including two opposite external forces applied to the loaded corners and acting on the same direction coinciding with a diagonal.

Each of these forces can be decomposed in a vertical and a horizontal component (see Figure 2.9).

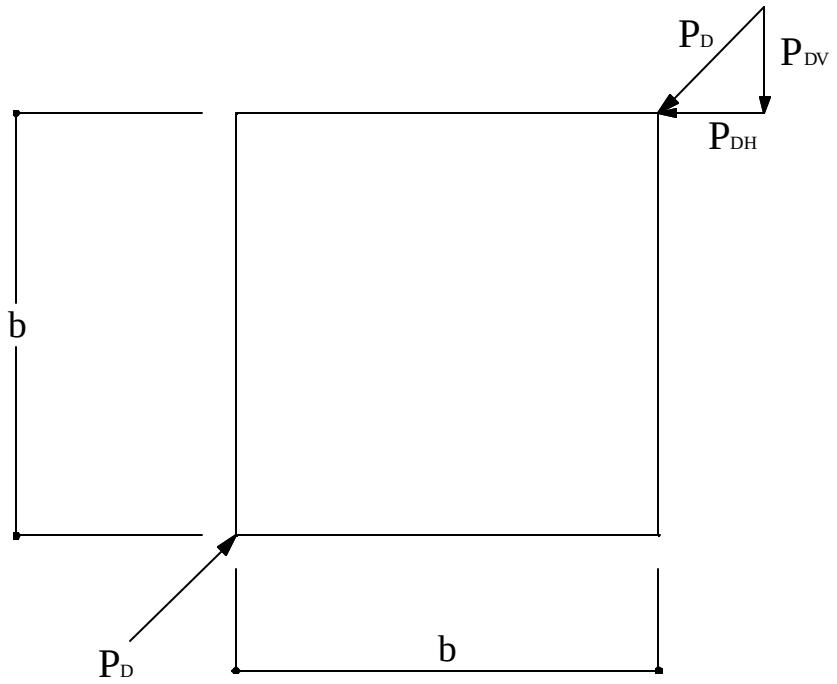

Figure 2.9: External forces on the diagonal test panel

The mentioned components are intended to simulate respectively the axial load and the shear force to which a structural member may be subjected. Clearly, limits of this shear test typology are due to the fact that both those actions are necessary distributed on the same surface area and have equal intensity.

Once the depth t of the panel is known, it is possible to define average values of shear and axial stresses generated:

Shear stress: $\tau' = P_{DO} / (b*t)$

Axial stress: $\sigma_y = P_{DV} / (b*t)$

In order to provide a qualitative description of the stress distribution into an unreinforced panel subject to diagonal compression, the masonry non-elastic orthotropic behavior is simplified with a linear elastic isotropic model.

The stress elastic distribution in a square plate diagonally loaded was calculated by Frocht, which found consistence of his results with the observations from a photoelastic model. Frocht simplified his equations assuming a Poisson ratio equal to zero.

In figure 2.10 the Frocht solution is compared with a Finite Element Analysis performed with different Poisson ratios. The influence of this latter parameter does not seem to affect remarkably the amplitude and stress distribution. In figure 2.10 axes refer to non-dimensional parameters and the following conventions are used:

σ_1= Principal tensile stress in the plane of the wall (along the diagonal not loaded).

σ_2= Principal tensile stress orthogonal the wall (it is assumed equal zero).

σ_3= Principal compressive stress in the plane of the wall (along the loaded diagonal).

Tensile stress is assumed as positive and compressive as negative, *t'* is positive.

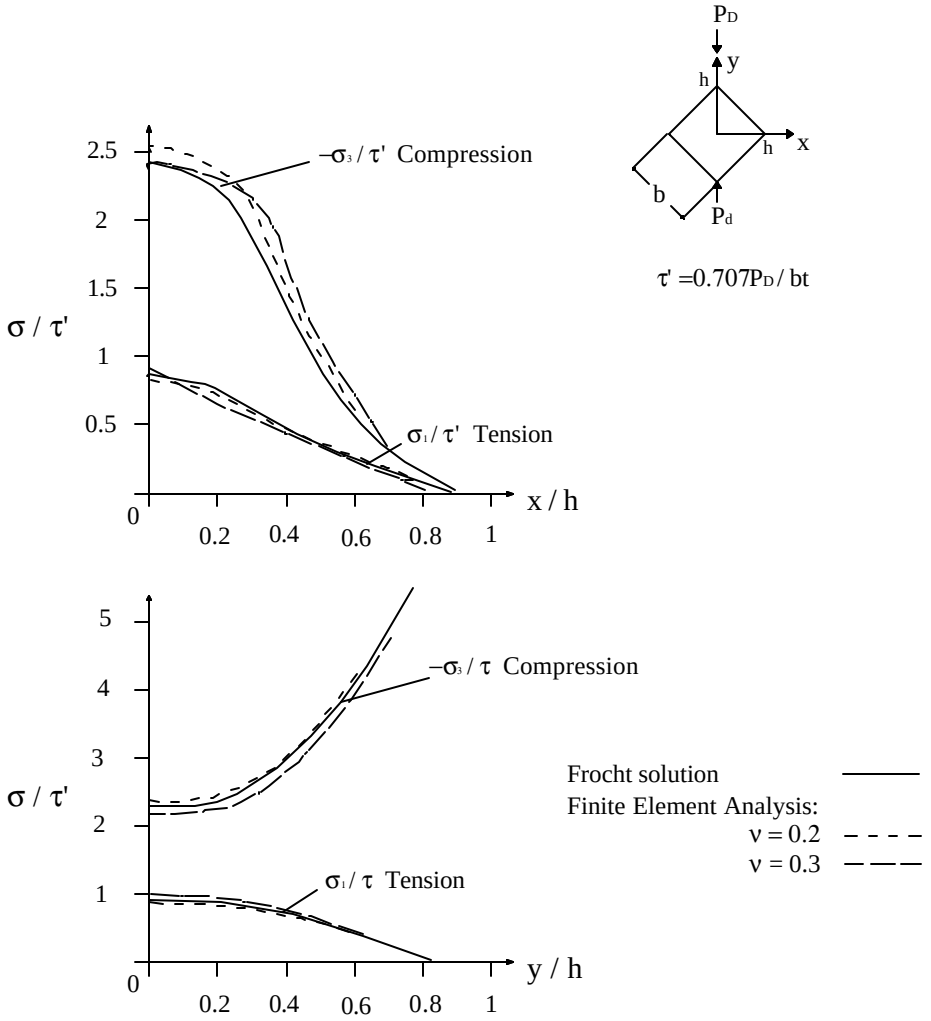

Figure 2.10: Diagonal test internal principal stress distribution

Frocht calculated the principal stresses in the middle of the panel of figure 2.10 as:

$$\sigma_1 = 0.7336\ \tau'$$
$$\sigma_3 = -2.38\ \tau'$$

Representing the Frocht solution with the Mohr circle it is possible to find the non-principal stress components in the middle of the panel (see Figure 2.11).

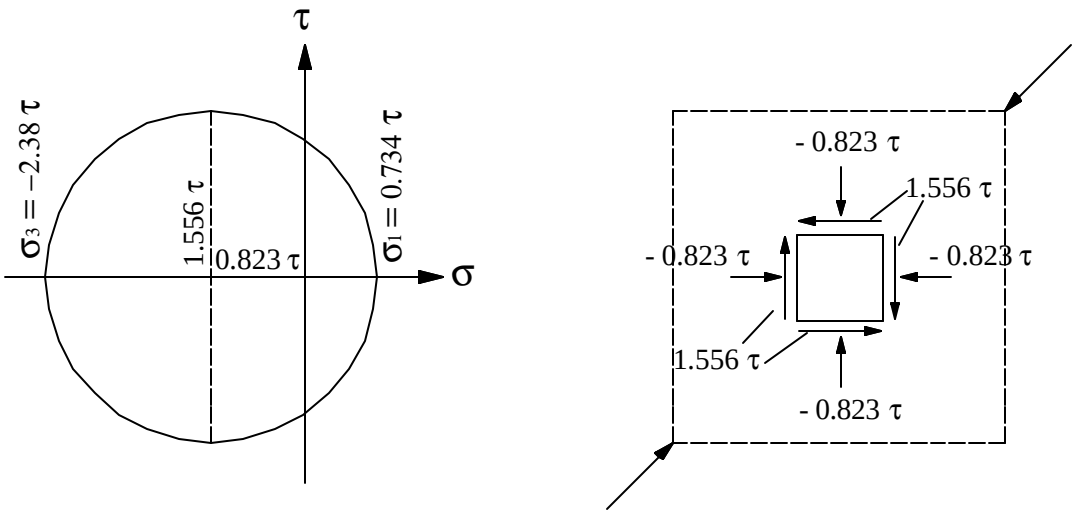

Figure 2.11: Diagonal test internal non-principal stress distribution

The value of shear stress equal to 1.556τ' is the maximum reached along a horizontal section, along which it is feasible to assume a parabolic distribution of shear stress; thus the average value is calculated as:

$$\tau = \frac{2}{3}\ 1.556\ \tau'$$

This theoretical value of the shear stress on a central bed joint plane of the masonry panel can be compared with the shear strength internal the joint. This latter can be calculated as friction stress in the brick-mortar interface by the Coulomb equation.
Obviously, at failure for sliding along a mortar joint shear stress and shear strength should be equal. This equality would be a validation of the approximation introduced by many codes, in which the shear capacity of unreinforced masonry panels is calculated as maximum friction force along a horizontal mortar joint.

From the experimental result, Wall 1 is the only specimen presenting failure due to sliding of the bed joint and its ultimate load was almost the same as the reference panels collapsed for diagonal joint sliding along a stepped pattern (see Section 4.4).

Thus, referring to Wall 1:

P_D= 72 kN

$\tau' = P_{DO} / (b*t)$=0.707*72kN / 542 cm^2 = 939 kPa

$\tau = \frac{2}{3}$ 1.556 τ'= 974 kPa *shear stress*

From Friction Test on mortar joints (see Section 4.2):

When σ < 200 psi (1.379 Mpa):

$\tau = \tau_0 + \mu\sigma$ = 407.6+0.6797σ = 1045.8 kpa *shear strength*

as in the diagonal test: $\sigma = P_{DV} / (b*t)$ = 939 kPa

The shear stress and strength, corresponding to sliding failure and calculated by the described simplified models, result to be acceptably similar and validate followed approach. The experimental results though reveal that the experimental shear strength obtained from tests triplets is slightly higher than the correspondent found from the test on the panels (see Appendix B, B3).

2.5 ROD-SUBSTRATE BOND FAILURE MECHANISMS

2.5.1 Background on Bond of Steel Rebars to Concrete

The importance of bond is that it is the means for the transfer of stress between the concrete and the reinforcement in order to develop composite action. The bond behavior has influence on the ultimate capacity of the reinforced element as well as on serviceability aspects such as crack width and crack spacing. Many researchers have studied the characteristics of bond between steel bars and concrete, which resulted in a full understanding of the related modes of failure.

In general, a smooth bar embedded in concrete develops bond with concrete through two mechanisms, adhesion between the concrete and the bar, and a small amount of friction. Both mechanisms are lost at higher levels of tension loads, particularly, because of the slight decrease in the cross sectional area due to Poisson's ratio.

Similar bond transfer mechanisms of adhesion and friction are present when deformed steel bars are loaded with small loads. As the load increases, these bond transfer mechanisms are lost, leaving the bond to be transferred through bearing stresses between concrete and the deformations on the bar.

The bond stress acting as shear between the reinforcing bar and the concrete gives rise to principal tensile and compressive stresses in the concrete. The lowest of the shear, principal tensile, or principal compressive strengths will be exceeded first, resulting in changes in the bond conditions. Three types of failure can be distinguished:

1. Shear failure along the perimeter of the bar. If the shear strength is the lowest, this will fail and result in bond failure along the perimeter of the bar which will be pulled out. This type of failure occurs in the case of smooth bars of large diameters.

2. Concrete cover splitting failure. If the shear strength is high enough so that the principal tensile stress exceeds first the tensile strength of the concrete, then cracks will appear transverse to the principal tensile stresses. These conclusions are supported by the findings of Goto (1971), Lutz and Gergely (1967), and Lutz (1970). The bond forces which radiate out from the reinforcing bar must be resisted by the surrounding concrete if immediate failure is to be avoided. Otherwise, the concrete will be split away by the pressure exerted by the anchored reinforcing bar. This type of bond action and failure is the most common in concrete structures reinforced with deformed bars.

3. Shear failure in concrete along the lugs of the bar. If the splitting resistance of the surrounding concrete is high enough, then bond failure in the case of a deformed bar also will occur as shear failure along the perimeter of the bar lugs. This bond strength is the maximum possible and is seldom reached.

Action of Splitting Forces on Concrete. The bond action between concrete and deformed steel bars has been experimentally shown by Goto (1971). The test specimens

were axially loaded tensile specimens, each a single bar embedded concentrically in a long concrete prism.

Cracks in the concrete were penetrated by ink from special injection holes. Afterwards the prisms were cut axially and the cracks colored by the ink became visible. The slopes of the internal cracks, from 45° to 80°, indicate the trajectories along which the compressive forces leave the ribs of the deformed bar and spread out into the concrete (see Figure 2.12).

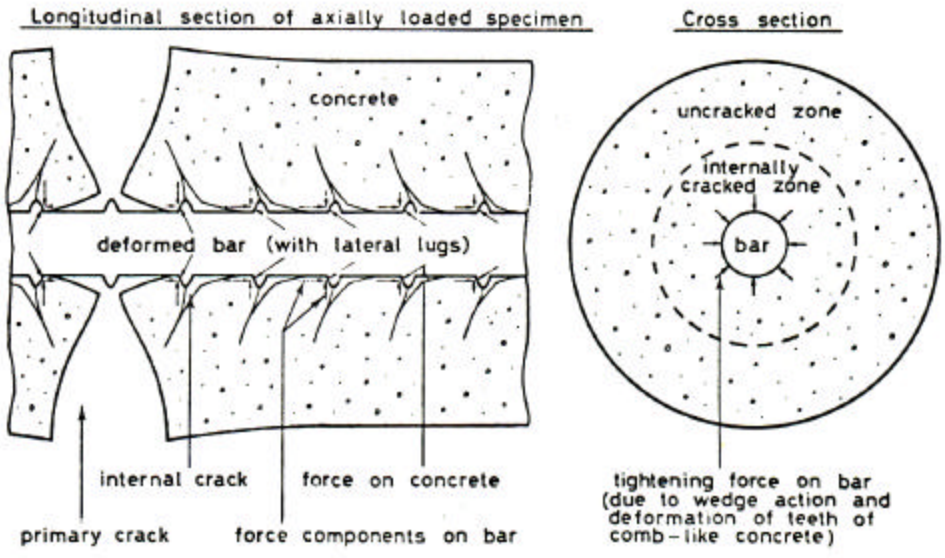

Figure 2.12. Internal Cracks Around Steel Deformed Bars (From Goto, 1971)

As stated before, when the load increases the bond is transferred through bearing stresses between the concrete and the deformations on the bar. When the principal tensile stress reaches the tensile strength of the concrete, it drops to zero. Therefore, after the formation of the principal tensile stress cracks, the bond forces between the concrete and a deformed reinforcing bar subtend an angle, α, with the bar axis. These bond forces or stresses can be resolved into radial and tangential components, the radial component being:

$$f_{br} = t_b \tan a$$

The radial stress, f_{br}, due to bond action on the concrete, can be regarded as a hydraulic pressure acting on a thick-walled concrete ring. This concrete ring approximately represents the effect of the surrounding concrete. The wall thickness of the ring is determined by the smallest possible dimension, that is, the least of the concrete covers. For normal concrete covers, the value of the bond stress at which the concrete over the bar cracks can be obtained as the average of the values applicable to the plastic and partly cracked elastic stages (Tepfers, 1979).

The radial components of the anchorage forces will be balanced by circumferential tensile stresses in the concrete cylinder (see Figure 2.12). When the cylinder is stressed to rupture, it fails at this point, and longitudinal cracks appear. The splitting cracks tend to develop along the shortest distance between the bar and the concrete surface (Orangun et al., 1977 and Jirsa et al., 1979). However, these cracks may start as internal longitudinal cracks which cannot be seen on the surface of the concrete before the ultimate load capacity of the ring is reached.

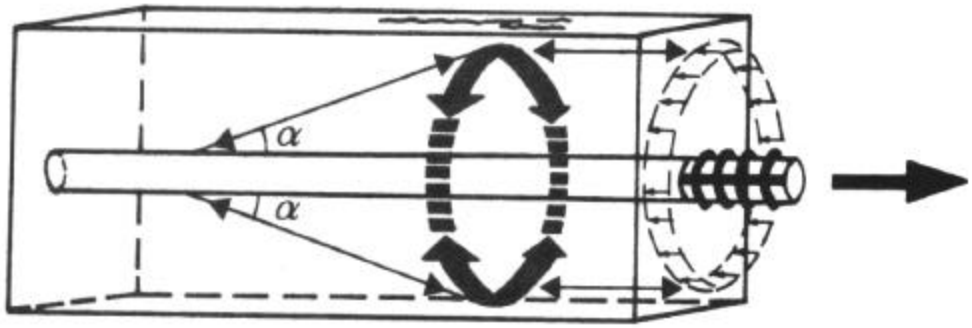

Figure 2.13. Schematic Representation of How the Radial Components of the Bond Forces are Balanced Against Tensile Stress Rings in the Concrete in an Anchorage Zone (From Tepfers, 1973)

When a longitudinal crack appears, displacement between the bar and the concrete increases considerably in comparison with that before cracking and leads to evenly distributed bond stresses along the cover cracked anchorage length.

The radial components of the anchorage force then impose a load on the concrete cantilevers (which are the remnants of the cracked concrete ring) surrounding the reinforcing bar. When these cantilevers are stressed to their ultimate capacity, they fail according to the minimum stressed surface failure pattern. This failure is explosive, and normally occurs without any warning of prior ductile deformation.

As a result of the mechanics of splitting failure, the load at which it develops is a function of:

- the minimum distance from the bar to the surface of the concrete or to the next bar. The smaller this distance, the smaller the splitting load.

- the tensile strength of the concrete.

- the average bond stress. As this increases, the splitting forces increase.

2.5.2 Background on Bond of FRP Rebars to Concrete

When characterizing the mechanics of load transfer between FRP rods and concrete, the anisotropic nature of the FRP materials makes it necessary to account for the mechanical and physical properties in the longitudinal and transverse direction. The FRP rods are considered to be transversely isotropic material. Their transverse elastic constants are largely dependent on the properties of the resin material.

Many researchers such as Al-Zahrani (1996) and Tighiouart et al. (1998) confirmed lower bond strength in FRP bars to concrete, which in turn was dependent on the diameter of the bar. Bakis et al. (1998) concluded that the bond between FRP bars and concrete is controlled by the properties of FRP bars. They investigated two types of bars, smooth and deformed. In the case of smooth FRP bars, they concluded that friction is the dominant bond mechanism and that the major factors that affect it are the longitudinal stiffness, transverse stiffness, and the major Poisson's ratio of the bar. For the case of lugged FRP bars, they observed that bond is governed by the sequential shearing of the FRP lugs and that the strength of concrete is of much less influence on the bond behavior.

Steel rebars, independent of type, have practically the same modulus of elasticity and surface hardness. This is not the case for FRP bars. The great variety of the FRP bars/rods results in many possibilities for bond resistance. In the following, bond influencing factors for FRP rods are outlined (Tepfers, 1998).

- Form of the transverse section. Round, flat rectangular or specially shaped – has importance for bond and anchorage of the rod.

- Surface condition. The size and type of lugs or surface deformations constituting the roughness of FRP rod are important for bond. Small dense surface deformations give a very intense bond transfer at low loads. However, for higher loads, when the rod becomes thinner due to Poisson effect or a splitting crack develops in concrete cover along the reinforcing rod, these small deformations may lose their grip in concrete very suddenly with bond failure as a result, while bigger ribs may still be active. Furthermore, it has importance for bond resistance if the rod lugs or surface deformations are made up of only resin, of resin mixed with special strengthening fiber reinforcement in the lugs or of resin containing some longitudinal continuous fibers in the surface deformations. This latter is achieved by braiding the fibers or by winding the rod by a separate fiber filament. When the longitudinal fibers are brought out of the direction of the bar axis by braiding or by press-deforming the longitudinal fibers (by winding a fiber bundle around) the axial modulus of elasticity of the rod decreases. If the shear resistance of the FRP rod lugs determines the ultimate load, an increase of the thickness of the lugs should raise the bond strength. The distance between the lugs can also influence the failure load.

  In the case of plain bars, the bond usually fails along the perimeter of the rod and the rod is pulled out from the concrete. The shear strength of the glue between the bar and the concrete or between the surface layer and the FRP bar is decisive.

- Poisson's ratio. The Poisson contraction of the rod, when tensioned, has influence on the bond. The Poisson's ratio is for most FRP materials about the same as for steel. However, as the modulus of elasticity is lower than for steel, the strain becomes bigger and consequently the transverse deformation.

- Elastic modulus. The modulus of elasticity of the bar has influence on the ultimate bond load. It has been observed that certain types of FRP bar with lugs give higher cover cracking resistance than corresponding steel rebars does. The cause for this is probably the fact that bars with modulus of elasticity magnitude like that of concrete at anchorage by lugs do not create as much stress concentrations in concrete as steel rebars do, because steel is much harder than concrete. This means that anchorage of steel reinforcement by lugs give local stress concentrations in concrete from which cracks develop.

- Coefficient of thermal expansion. Differences in thermal expansion between the FRP unit and concrete, especially in the transverse direction to the axis of the rod, might influence the bond. Too high transverse thermal elongation of the rod might give rise to splitting cracks in concrete surrounding the rod. However there are indications that the FRP rods are enough soft not to cause splitting off the concrete cover, when trying to expand.

- Environmental effects. Environmental influence on bond should be taken in consideration. Absorption of water leading to strength and modulus deterioration as well as expansion of the rod might influence the bond.

Failure Modes. Three different failure modes were experienced during the experimental tests (De Lorenzis, 2000.[47]):

- splitting of the epoxy cover (see Figure 2.14);

- cracking of the concrete surrounding the groove (see Figure 2.15);

- pull-out of the FRP rod (see Figure 2.16).

In some cases, a combined failure mode (pull-out with some damage in the epoxy cover) was registered.

The failure mode by splitting of the epoxy cover is similar in its mechanics to splitting of the concrete cover for reinforcing rods embedded in concrete. As already outlined in the previous background sections, bond stresses have a longitudinal and a radial component, with the latter causing circumferential tensile stresses in the material around the bar. When the maximum tensile stress reaches the tensile strength of the material, the cover splits parallel to the rod. The load at which splitting failure develops is influenced by the surface characteristics of the rods, the tensile strength of the cover

material and the thickness of the cover. Also the rod diameter has an influence on the splitting failure load: according to the model of the thick-walled cylinder for concrete, the significant parameter for the splitting strength is actually the ratio cover thickness to bar diameter (Tepfers, 1979). The cover thickness of NSM rods depends in turn on the depth of the groove in which the rods are embedded.

Epoxy has typically a much higher tensile strength than the concrete. However, the cover thickness of NSM reinforcement is very low compared to that of reinforcing bars in concrete, which makes this model of failure critical for NSM reinforcement.

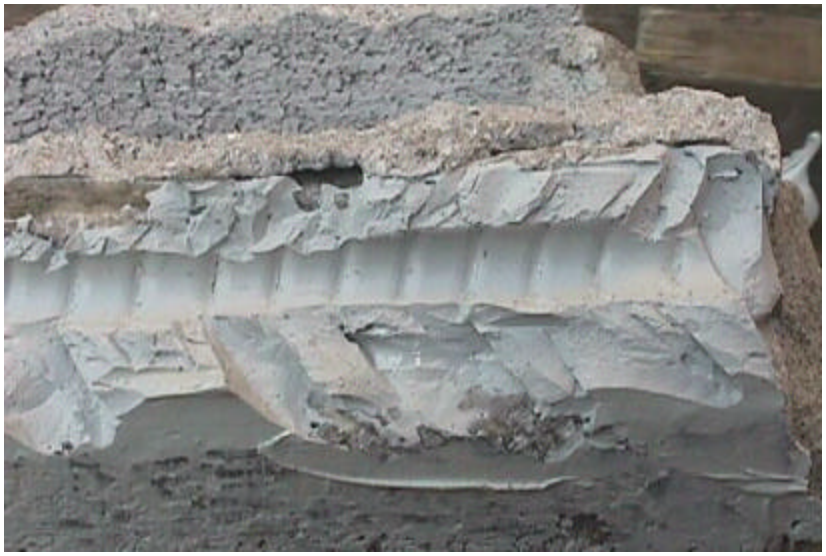

Figure 2.14: Bond failure due to splitting of epoxy paste

Must be noticed the complete correspondence between the cracks patterns of the epoxy paste in Figure 2.14 and the theoretical description represented in Figure 2.12.

In Figure 2.15 is also clearly visible the superficial crack due to the tensile failure of the epoxy paste ring, as previously described in Figure 2.13. The inclined cracks propagated also into concrete and the typical sudden splitting in this case involved also the substrate, as it presented the lowest tensile strength.

Figure 2.16 shows pull out failure of a deformed FRP rod; it is quite an unusual as the lags have to be sheared completely, as visible in the picture. This phenomenon is due to the absence of fiber reinforcement into small lugs, as curvature involved would be too sharp. Some manufacturers of deformed rods abandoned for this reason this kind of profile derived from steel rebars, to adopt different configurations based on longer pitch with curvature allowing introduction of fibers.

Figure 2.15: Bond failure due to cracking of the concrete substrate

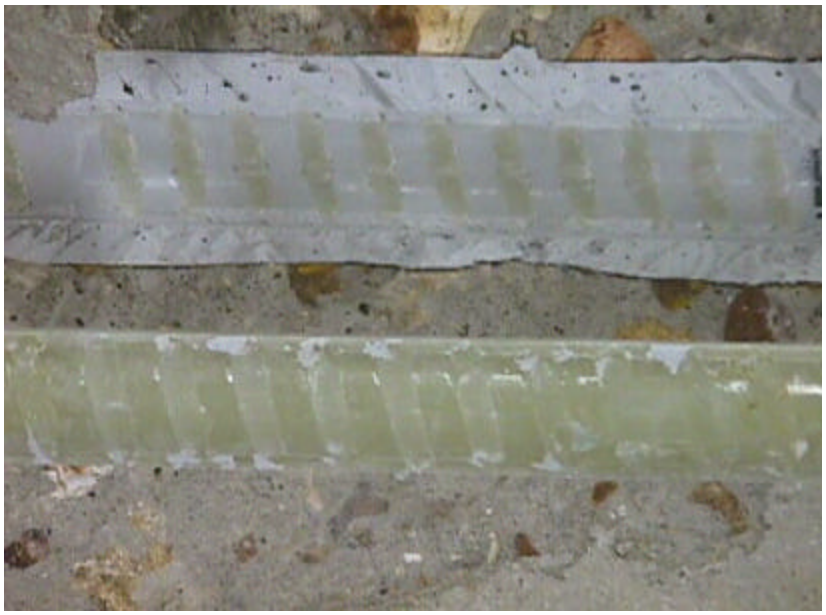

Figure 2.15: Bond failure due to pull out of the rod with shearing of lugs.

3 EXPERIMENTAL PROGRAM

3.1 MATERIALS USED IN THE EXPERIMENTAL PROGRAM

3.1.1 Introduction

This section deals with the properties of the materials used in the experimental program. These materials included mortar, clay bricks, concrete blocks, reinforcing GFRP rods and epoxy mixes. Units and assemblages behavior, bonding properties and interface interaction are investigated.

In order to represent in the tests some of the most typical masonry constructions of the Mid-America, hollow concrete blocks and two kinds of cored clay bricks were selected. Tests were performed to characterize epoxy paste and epoxy mortar mixes. For the composite rebars, the manufacturer provided the whole set of material properties.

A summary of the material characterization tests conducted on units and assemblages is here reported. The most relevant material properties are listed in Section 4.2. For a detailed description and further information see Appendix B.

3.1.2 Material Characterization Tests

Mortar used is available in bags in a dry premixed composition of masonry cement and sand, and is classified as Type N according to the standard ASTM C270 (see Appendix A). Standard tests on mortar samples revealed a compressive strength of 5.3 MPa and a tensile strength on the mortar-brick interface of 0.56 MPa.

Clay unit properties were controlled and the two different types of clay bricks presented properties as given below:

	Compressive strength	Tensile strength
Type 1	28.1 MPa	4.9 MPa
Type 2	22.3 MPa	3.7 MPa

Stock prism and RILEM compressive tests were performed on the three different masonry assemblages with the following results:

	Compressive strength	Modulus of Elasticity
Concrete Masonry	6.67 MPa	6.9 GPa
Clay Masonry Type 1	17.2 MPa	11.0 GPa
Clay Masonry Type 2	14.1 MPa	11.0 GPa

In order to identify the Coulomb friction equation related to the brick-mortar interface, twelve triplet tests were performed, considering different levels of orthogonal stress applied on the bed joints.

Epoxy mortar, obtained from a mixture of epoxy paste and pure quartz sand, was selected as the workable material with strong bond properties suitable to anchor GFRP rods. The salient properties of the epoxy mortar are obtained by friction tests on couplets, compressive and splitting tests on cylinders. Compressive and tensile strength were 21.5 and 4.7 MPa, respectively.

Bond characterization of GFRP rods embedded with epoxy paste into grooves cut in concrete blocks were conducted in previous works (De Lorenzis, 2000 [47]) and confirmed in the present experimentation. Those results indicate that a stable bond is achieved for anchoring lengths over 12 times the rod diameter, when the average bond strength on the anchoring surface settles at around 5 MPa.

The material characterization tests provided all the necessary data to compare the experimental results with the existing literature and to find analytical models describing the new mechanisms introduced.

3.2 FRP FLEXURAL STRENGTHENING

The flexural testing program consisted in four coupon masonry beams and three concrete block walls.

3.2.1 Concrete block walls

Concrete hollow blocks are typically used as both infill and load bearing masonry walls. Unfortunately in most applications they have not been reinforced during they construction and therefore they may result inadequate for mutated conditions involving elevate out-of-plane loads. In the case of infill walls into RC frames it is even impossible to perform grouting and reinforcing operation during their construction.

In all the mentioned cases it is necessary to introduce a retrofitting technique structurally effective and presenting unproblematic application, especially when the produced disturbance of the occupants is a fundamental issue.

From the experience of previous works on RC (De Lorenzis, 2000. [47]), a valid strengthening approach matching all the described requirements appeared to be the use of FRP Near Surface Mounted rods (NSM), and three specimen were prepared as following described.

The nominal dimensions of the three concrete walls were 60 x 120 x 19 cm, which resulted from a stack of six courses, one and a half block each course (see Figure 3.1).

One specimen was maintained unreinforced as control wall, while the other two concrete block walls were reinforced respectively with one and two 10-mm GFRP rods perpendicular to the bed joints, and were subjected to a typical four point flexural test.

The rods were positioned in the middle or on the thirds of the width respectively, embedded with epoxy paste into grooves cut on the surface of the blocks**.** During the construction, the bottom block row of both the reinforced walls was grouted with mortar, in order to control the effect of the grout on the cracks propagation (see Section 4.3.1).

Figure 3.1: Four point flexural test. Concrete wall with *grooves for* FRP rods embedding.

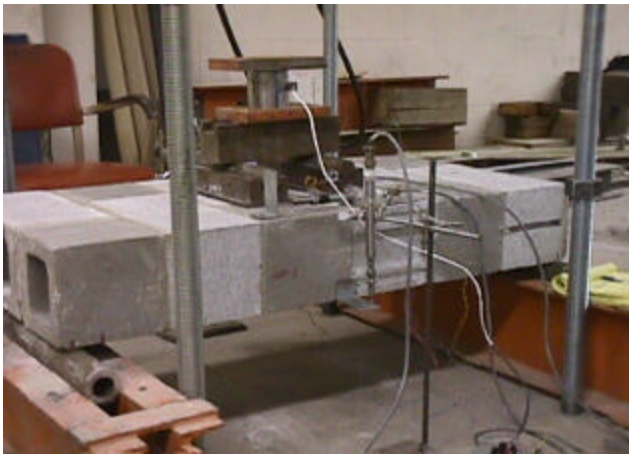

During the test (standard ASTM C 1390, [24]), concrete and mortar strain on the compressed side of the mid-span section, slip and strain in the rods and mid span deflection were measured.

3.2.2 Clay masonry beams

In order to investigate the potentiality of the FRP-"Structural Repointing" (SR) to be applied as flexural strengthening of masonry walls subjected to out-of-plane actions, and to explore the possibility of applying on those walls horizontal reinforcement, the following specimens were included in the test program.

Two masonry beams were 90 x 12.5 x 9 cm (see Figure 3.1) and built with running bond (i.e., discontinuous head joints) providing interlocking (see Figure 3.2); one of beams was reinforced with one 6-mm GFRP rod. In order to isolate the effect of interlocking on the flexural strength, two additional masonry beams were built 10 cm longer allowing in this way a stack bond (i.e., continuous head joints). Again, one of them was strengthened with one 6-mm GFRP rod. As comparison, another interlocked beam was built and reinforced with a 6-mm threaded steel rod. In all cases, the coupon beams reinforcement was longitudinally embedded with epoxy mortar into the continuous bed joint between the two brick courses, according with the newly introduced technique of FRP SR (see Section 1.3).

Bricks used in this test are typically used as veneer on concrete block infill panels, in both the typologies of barrier and cavity walls. As the block walls, also the masonry beams were subjected to a typical 4-point flexural test (standard ASTM C 1390, [24]), ensuring that the hinge supports did not provoke uncontrolled restraint of the rods. A reaction frame with a hydraulic jack and a load-controlled press were used to apply the

load during the tests (see Figure 3.3). During load-unload cycles mid-span deflection was recorded by means of an LVDT.

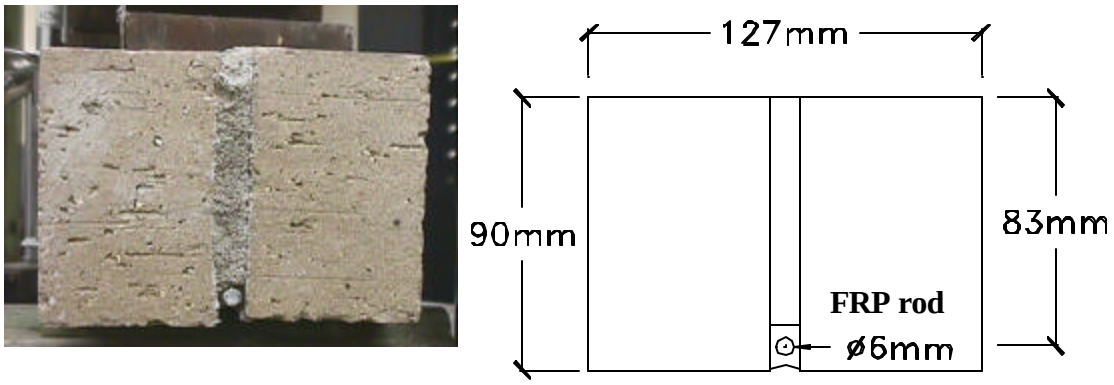

Figure 3.1: Masonry beams section.

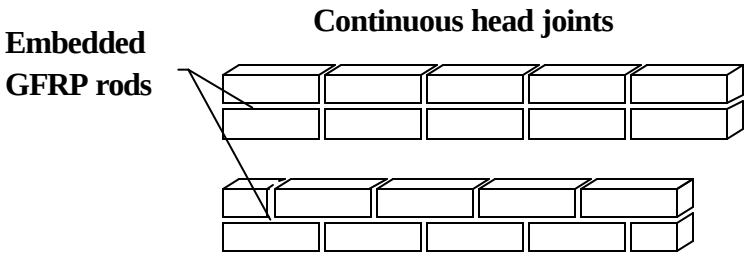

Figure 3.2: Masonry beams textures.

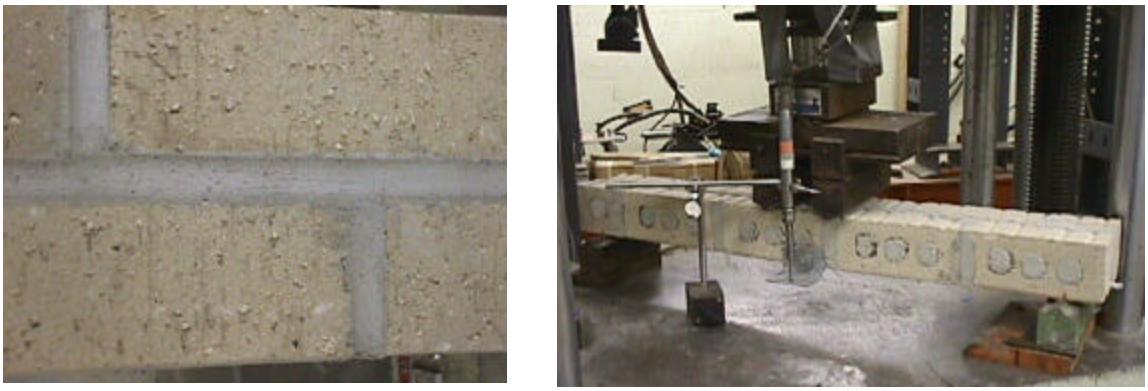

Figure 3.3: Detail of the SR reinforcement look. Flexural test set up.

3.3 FRP SHEAR STRENGTHENING

Different laboratory test methods are used to determine the shear resistance of a masonry wall, each of them offers characteristics that can result suitable to investigate particular aspects of the complex phenomenon (Bernardini et al., [42]). In this project, the diagonal compression test (standard ASTM E519, [23]) was considered to be the most suitable for panels reinforced with FRP-Structural Repointing, as the first experimental investigation was thought to be as conservative as possible. In fact, this new strengthening system in most cases relies on friction developed into the brick-paste interface (see Section 4.4), and the proposed shear test presents a relatively very localized and limited load component orthogonal to the mentioned friction interface. Vice versa, when FRP Structural Repointing is applied to a full-scale wall subjected at least to its own weight, friction increases and therefore the effectiveness of the reinforcement raises (see Section 5.3). Obviously, for consistency the same procedure was maintained to test the panels strengthened with laminates, even though the presence of axial load does not exert any influence on the reinforcement performance.

During the test, consisting in quasi-static load-unload cycles, deformations and displacements were recorded along the loaded and the splitting diagonals on both sides. Special supports were designed to avoid crushing of the loaded corners (*see Figure 3.4*).

Figure 3.4: Designed corner supports: fixed part and removable base (gray color). Compressive diagonal test set up (aside).

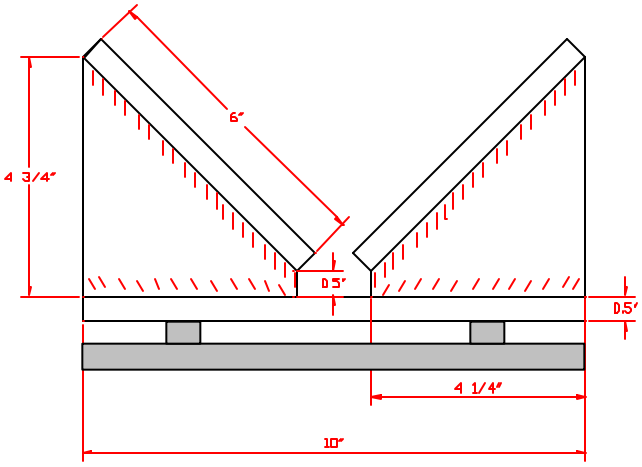

The nominal dimensions of the clay masonry panels were 60 x 59 x 9 (or 19) cm; 11 of them were single-wythe (or leaf) and the remaining three were double-wythe (see Figure 3.5). One double-leaf and two single-leaf unreinforced wallettes were the reference. The rest of the specimens were strengthened applying different configurations of GFRP laminates and rods on the façade and, in some cases, on the back (see Figure 3.6).

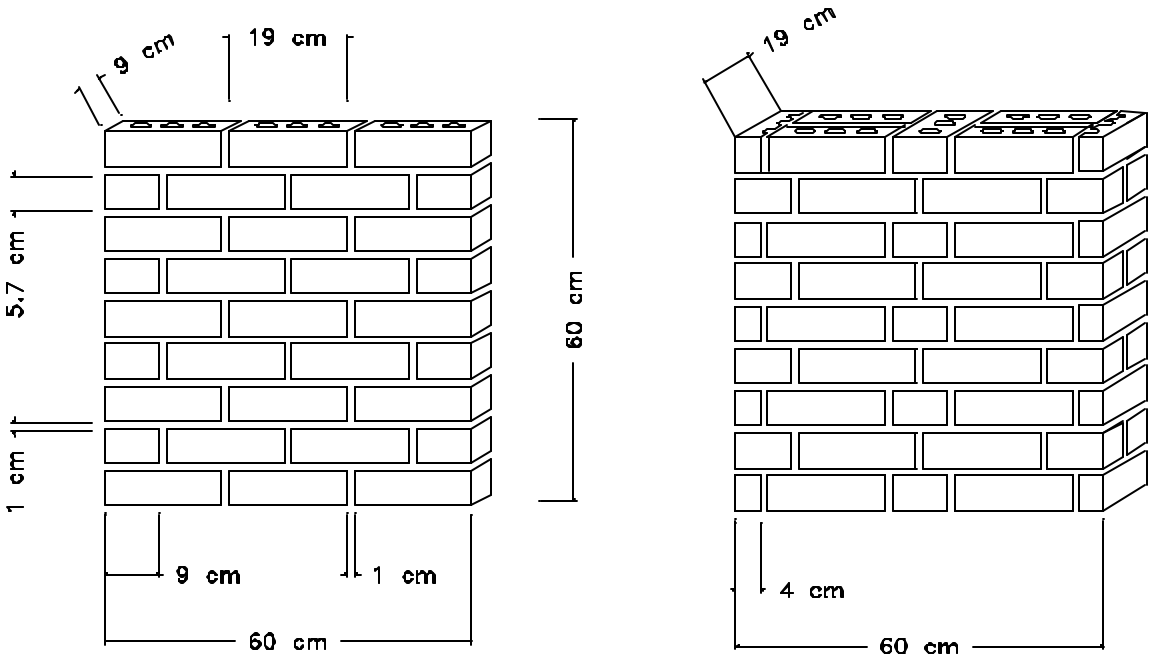

Figure 3.5: Clay masonry wallettes geometry.

Figure 3.6: Some of the FRP strengthening configurations: vertical narrow strips (with additional mechanical anchoring), crossed large strips, vertical large strips, vertical rods and FRP-Structural Repointing (each joint).

As on the coupon masonry beams tested for flexural analysis, also with some of these shear wallettes the SR method for strengthening was introduced.

Six single-wythe wallettes were reinforced only on one side and the different strengthening approaches involved the following configurations of rods and laminates: SR each second bed joint, SR each joint (see Figure 3.7), vertical rods into grooves, vertical strips, vertical and horizontal crossed strips (see Figure 3.8). On three additional single-wythe panels, SR was used in the façade, while on the back vertical rods, large strips and narrow strips, respectively, were applied (see Figure 3.9). Finally, a double-wythe wall was reinforced with SR on both sides and the last one with SR and strips on the opposite sides (see Figure 3.10).

WALL 1

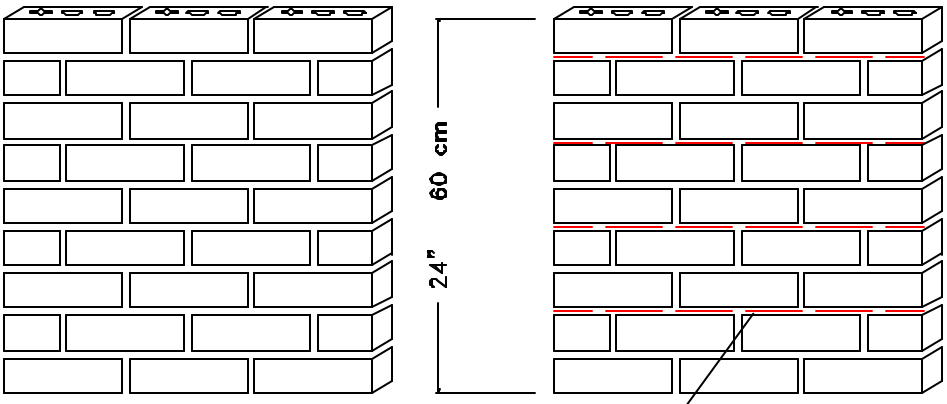

WALLS 2 and 3

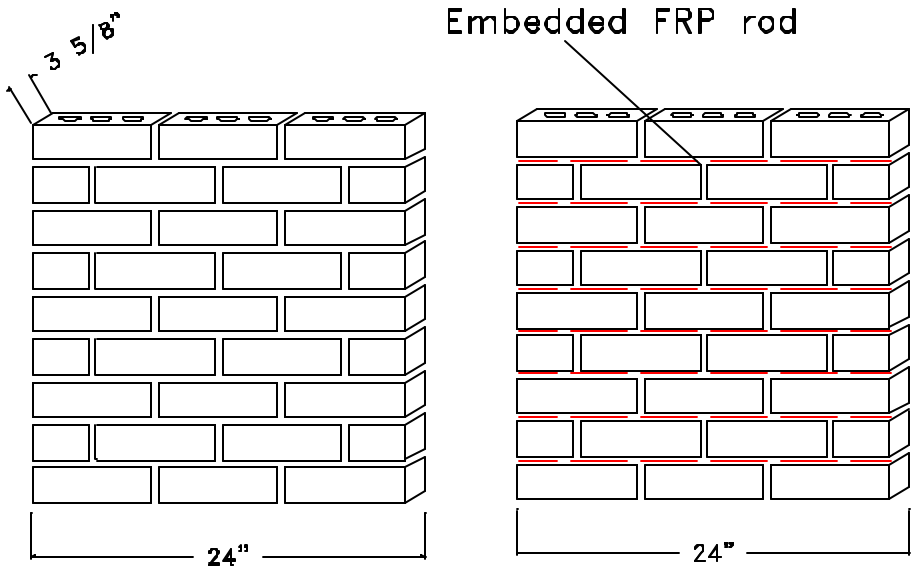

Figure 3.7: Structural Repointing on the façade: each second bed joint and each bed joint.

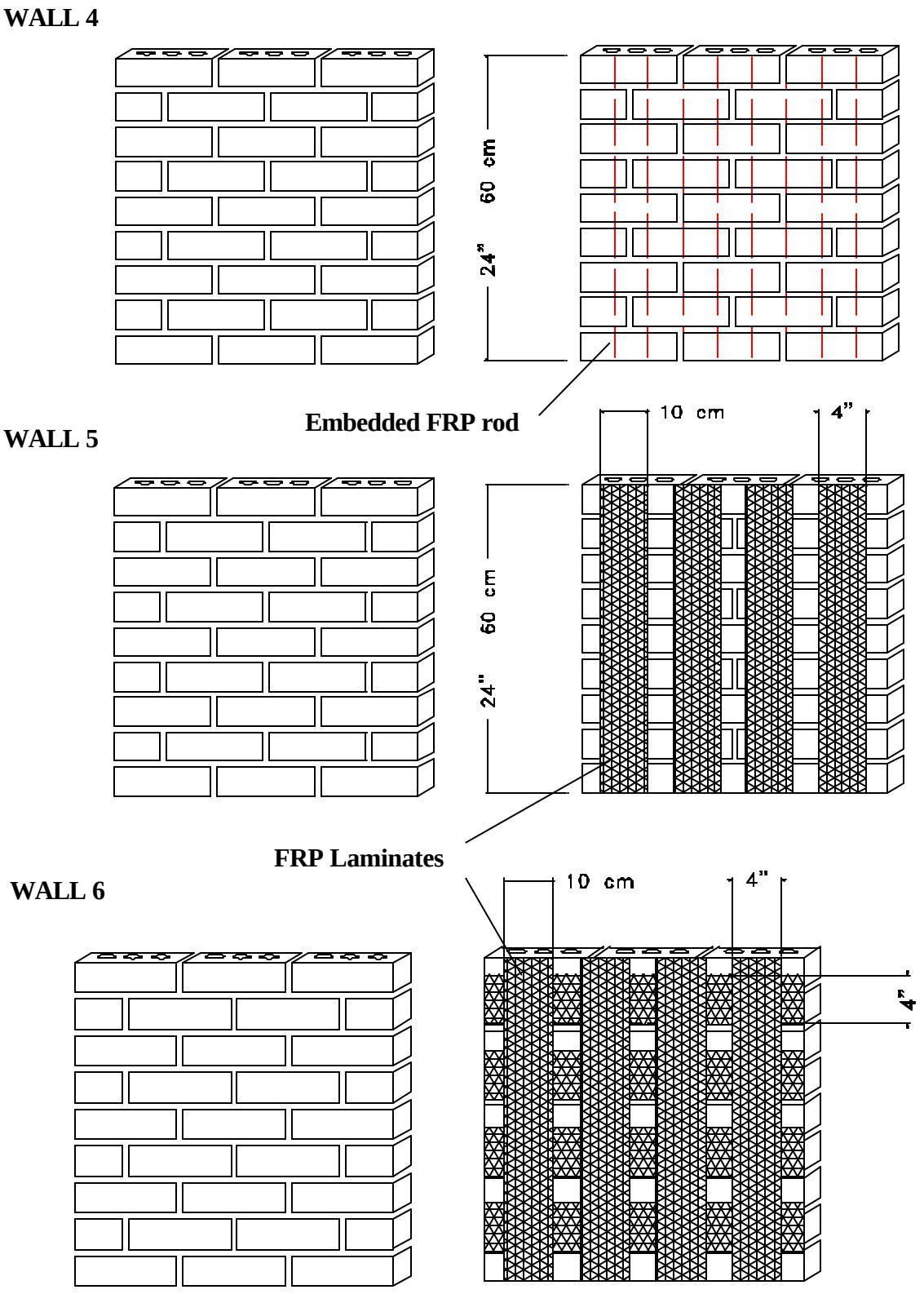

Figure3.8:FRP strengthening on the façade: vertical rods, vertical strips and crossed strips.

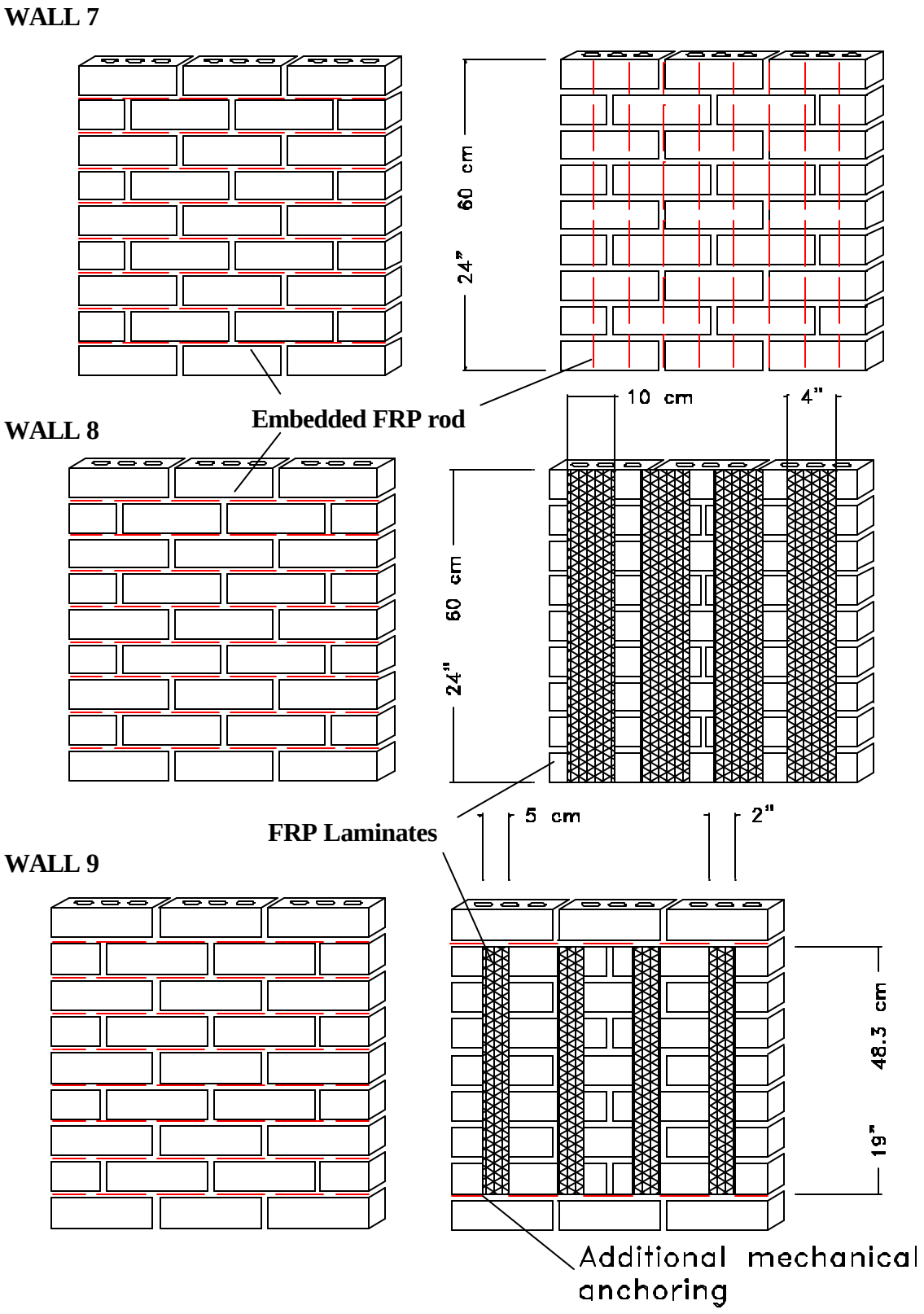

Figure 3.9: FRP strengthening on both sides. On the façade SR and on the back-side: vertical rods into grooves, large vertical strips and narrow vertical strips (two plies).

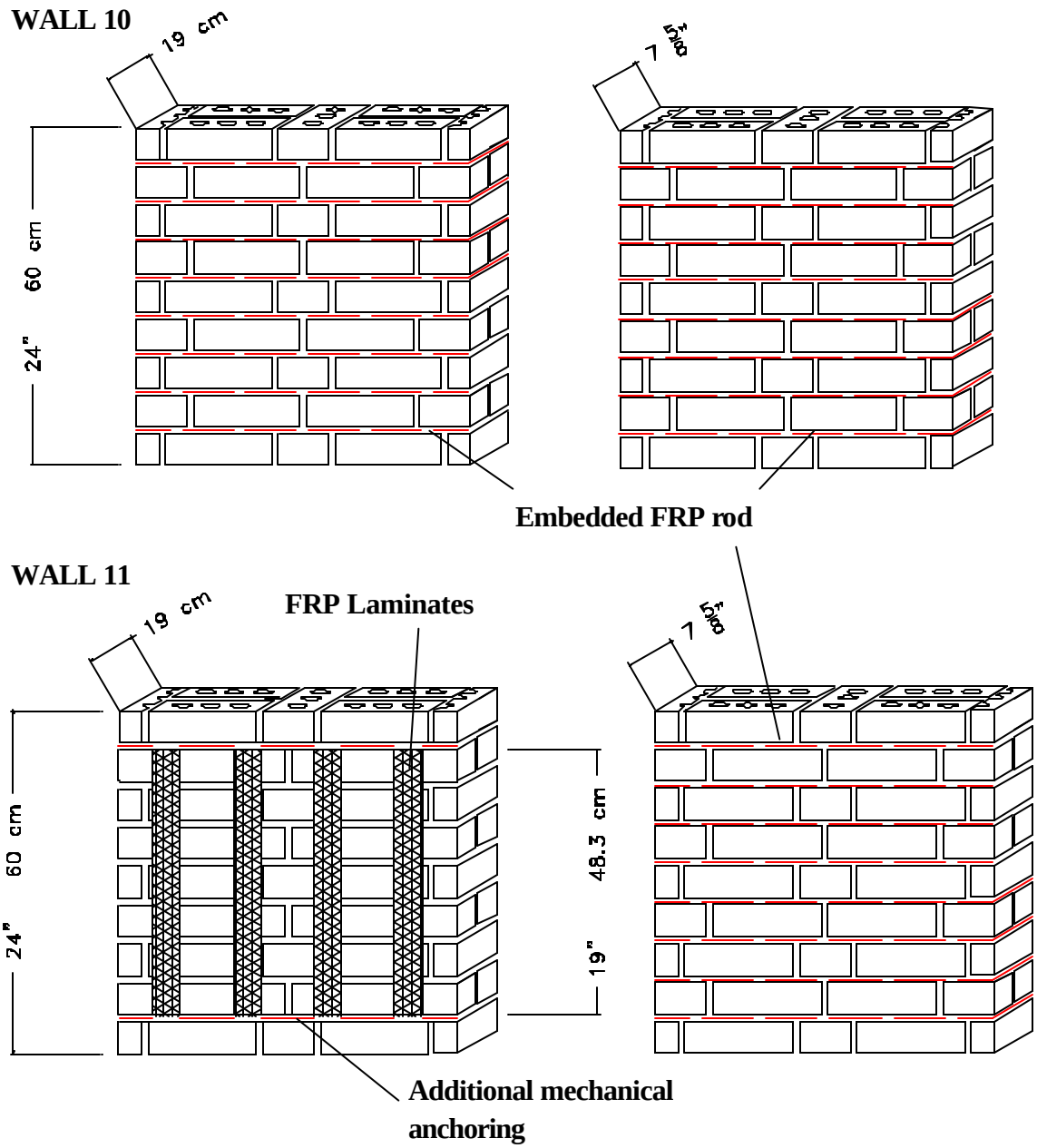

Figure 3.10: FRP strengthening on both sides of double-wythe walls. SR on both sides, narrow vertical strips (two plies) and SR.

Dimensions of the described wallettes are a half of the requirements from the standard guidelines. These dimensions were chosen considering the problems of handling bigger specimens in the laboratory but also considering the limited detrimental effect that the reduced scale could have provoked on the final results. Fortunately this choice revealed to be adequate as the limited confinement effect at the corners due to the test setup did not affect the quality of the research program.

For what concerns the SR, the criterion applied to design the reinforcing amount was imposed by geometrical restrictions. In fact, from the test result on Wall 1 (see Section 4.4) it was clear the necessity of applying SR in each joint and, in order to embed a rod in a one-centimeter groove it was necessary to use the smallest FRP rod available on the market: a GFRP six-millimeter rod.

When using laminates it was decided to maintain the same mechanical amount of reinforcement as the one provided by the rods, hence the product of the reinforcement ratio by the ultimate tensile strength was constant for both the systems:

$$r_{rods}\, f_{fu,rods} = r_{strips}\, f_{fu,strips}$$

Only, for each application, the distribution *d* factor is changing (see Table 4.1). The distribution factor is the parameter that indicates the impact, in terms of area, of the strengthening system over the face of the wallette considered. It is calculated as amount of the area covered by the reinforcement divided by the area of the side of the panel on which the mentioned reinforcement is applied.

In the anchoring areas of some configurations excessive stress levels were expected, so the following solution were introduced. In order to prevent debonding of the strips, a mechanical anchor was provided in turning the sheet up around a GFRP rod embedded into a groove (Gose, Nanni, 2000. [57]) (see Figure 3.11). In another instance, FRP bent rebars substituted the straight ones to avoid pull out or when a confinement effect was required (see Figure 3.12).

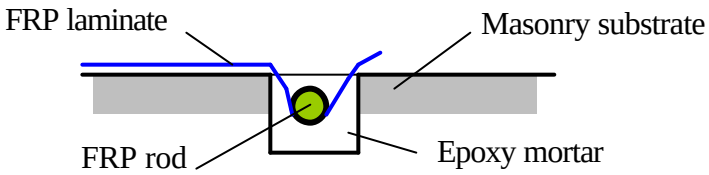

Figure 3.11: Masonry "U-anchoring" into a grooved joint.

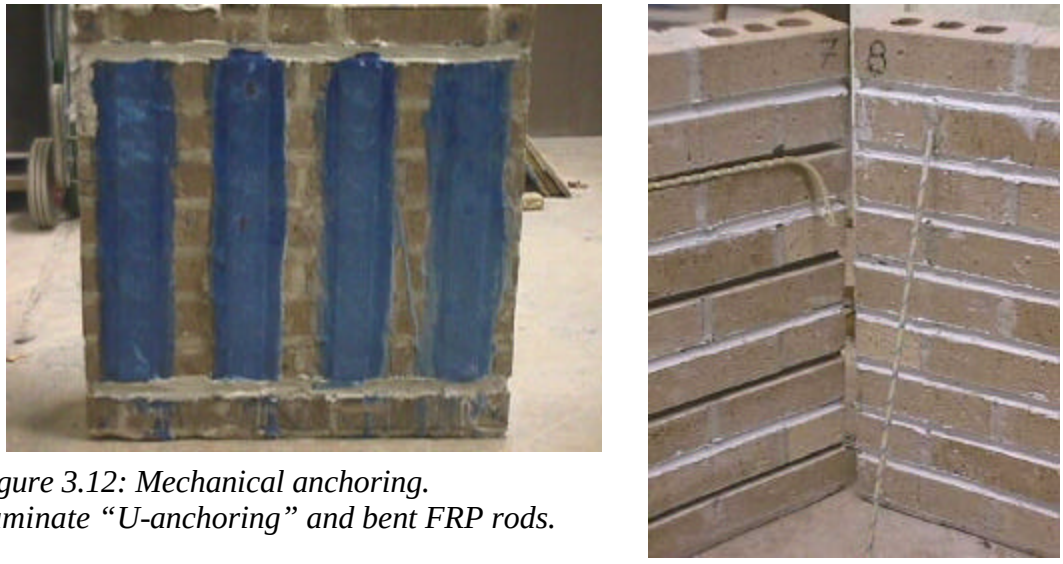

Figure 3.12: Mechanical anchoring. Laminate "U-anchoring" and bent FRP rods.

In order to evaluate the capacity of FRP reinforced walls to resist cyclic actions even if highly damaging, some specimens were subjected to load-unload cycles on both diagonals, simply overturning the panel of ninety degrees.

Thus, the same set up and procedure was planned to be used to test up to failure the second diagonal of Walls 7,8 and 9, once the first one was failed. During this second turn of shear tests also the level of damage introduced was controlled by limiting the splitting displacement, in order to related at a later date this latter parameter with the residual load bearing capacity under axial loading test.

3.4 AXIAL LOADING TEST

Walls reinforced with the aim to be able to survive a seismic event must have as basic requisite the capacity of maintain an adequate level of load bearing capacity, even after some damage has been provoked by the necessary presence of energy dissipative mechanisms. In fact, this post-failure behavior is the second performance required to load bearing masonry walls, once they have adsorbed part of the dynamic energy by internal plastic deformations of the materials or of the overall system.

In order to evaluate the confining effect of the FRP strengthening methods used on damaged masonry under axial load, further test, as described below, were planned on some clay brick wallettes.

A load-controlled press was used to find the residual load bearing capacity of Walls 7,8,9 and 11. These walls were subjected to monotonic or cyclic axial load, after being cracked under cyclic shear actions during the preliminary diagonal tests (see Figure 3.13). Load-displacement relations were recorded and compared with the undamaged condition.

Figure 3.13: FRP-Structural Repointing reinforced double-wythe wall subjected to diagonal and axial load testing.

4. TEST RESULTS

4.1 ABSTRACT

From the envelopes of the flexural tests, the dramatic increase of the flexural capacity and the ultimate deformation is evident. Load cycles on both kinds of masonry assemblage revealed an elastic behavior until debonding of the reinforcement occurred.

Compressive diagonal tests have demonstrated how FRP strengthening completely changes the failure mode of shear walls, preventing any detrimental sliding of the mortar joints and forcing tensile splitting. Progression and width of the cracks are limited by the reinforcement effect, which causes a spread-out cracking pattern; obtaining higher capacity, damage progression control, ductile behaviors and energy dissipation.

Axial load tests were carried out on panels previously submitted to up to failure load cycles in both diagonals, revealing excellent residual load bearing capacity; which suggests the validity of this retrofitting approach for seismic strengthening.

4.2 MATERIAL PROPERTIES LIST

A summary of the fundamental structural properties of the materials is reported.

Assemblages:

Compressive tests on concrete block prisms:
f'_m = 967 psi (6.67 Mpa) (gross area)
f'_m = 1934 psi (13.33 Mpa) (mortared area)
Modulus of Elasticity: E_m= 1000 ksi (6.9 Gpa) (estimated)

Compressive tests on brick prisms:
Type 1(light bricks): f'_m = 2500 psi (17.2 Mpa)
Type 2 (dark bricks): f'_m = 2050 psi (14.1 Mpa) Ratio: 82%
Modulus of Elasticity: E_m= 1600 ksi (11 Gpa)
Poisson Ratio = 0.18 (from reference)

Blocks:

Percent solid: 50%
f'_m = 1600 psi (11.03 Mpa) (gross area)
f'_m = 3200 psi (22.06 Mpa) (net area)
E_b=1760 ksi (12.14 Gpa) (reference)
Poisson Ratio ν=0.28 (reference)

Bricks:

Compressive tests:
Type 1(light bricks): f'_b = 4070 psi (28.06 Mpa)
Type 2 (dark bricks): f'_b = 3239 psi (22.27 Mpa)
E_b=1380 ksi (9.52 Gpa)
Poisson Ratio ν=0.14 (typical 0.15)

Tensile:
Type 1(light bricks): f_t = 716 psi (4.9 Mpa)
Type 2 (dark bricks): f_t = 536 psi (3.7 Mpa) Ratio: 75%

Mortar

Compressive tests (mortar type N>750 psi)**:**
f'_{mor}= 768 psi (5.3 Mpa)
E_{mor}= 247 ksi (1.7 Gpa) (from reference)
Poisson Ratio ν=0.21 (from reference)

Tensile:
f_t= 465 psi (3.2 Mpa) (mortar prism)
f_t= 81.6 psi (0.56 Mpa) (mortar-brick interface)

GFRP rods #2 (6 mm):

Cross sectional area: A_f=0.054 in^2 (34.84 mm)
Tensile strength: $f_{f,u}$ =130 ksi (900 Mpa)
Tensile modulus of elasticity: E_f = 5920 ksi (40.8 Gpa)
Ultimate strain: $\varepsilon_{f,u}$ = 2.2%

GFRP laminates:

Thickness: 0.0139 in (0.353 mm)
Tensile strength (ultimate): $f_{f,u}$ =251 ksi (1730 Mpa)
Tensile modulus of elasticity: E_f = 10500 ksi (72.4 Gpa)
Ultimate strain: $\varepsilon_{f,u}$ = 2.4%

LPL epoxy paste:

f'_{ep} = 2548 psi (17.57 Mpa) (cylinder)
f_t= 699 psi (4.82 Mpa) (cylinder)
bond strength >577 psi (3.98 Mpa)

manufacturer data:
f'_{ep} = 8000 psi (55.2 Mpa)
E_{ep}= 400 ksi (2.8 Gpa)
f_t= 2000psi (13.8 Mpa)
bond strength 1500 psi (10.3 Mpa)

Epoxy mortar (epoxy paste, quartz sand, pigments):

f'_{em} = 3125 psi (21,55 Mpa) (cylinder)
f_t= 675 psi (4.65 Mpa) (cylinder)

Friction Test on mortar joint:

When σ < 200 psi (1.379 Mpa):

$\tau = \tau_0 + \mu\sigma$ = 59+0.6797σ psi (407.6+0.6797σ kpa)

Friction Test on epoxy paste joint:

$\tau = \tau_0 + \mu\sigma$ = 116.4+0.4932σ psi (802.6+0.4932σ kpa)

4.3 FLEXURAL PERFORMANCE

4.3.1 Concrete Block Walls

On the concrete block walls reinforced with FRP NSM, the improvement of the nominal flexural capacity with the one-rod and two-rods strengthening is respectively 7 times and 15.7 times the capacity of the unreinforced case (see Figure 4.1).

The mechanism of failure of both specimens consisted in splitting of the epoxy cover, which presents analogies with splitting of the concrete cover of reinforcing rods embedded in concrete (see Section 2.4).

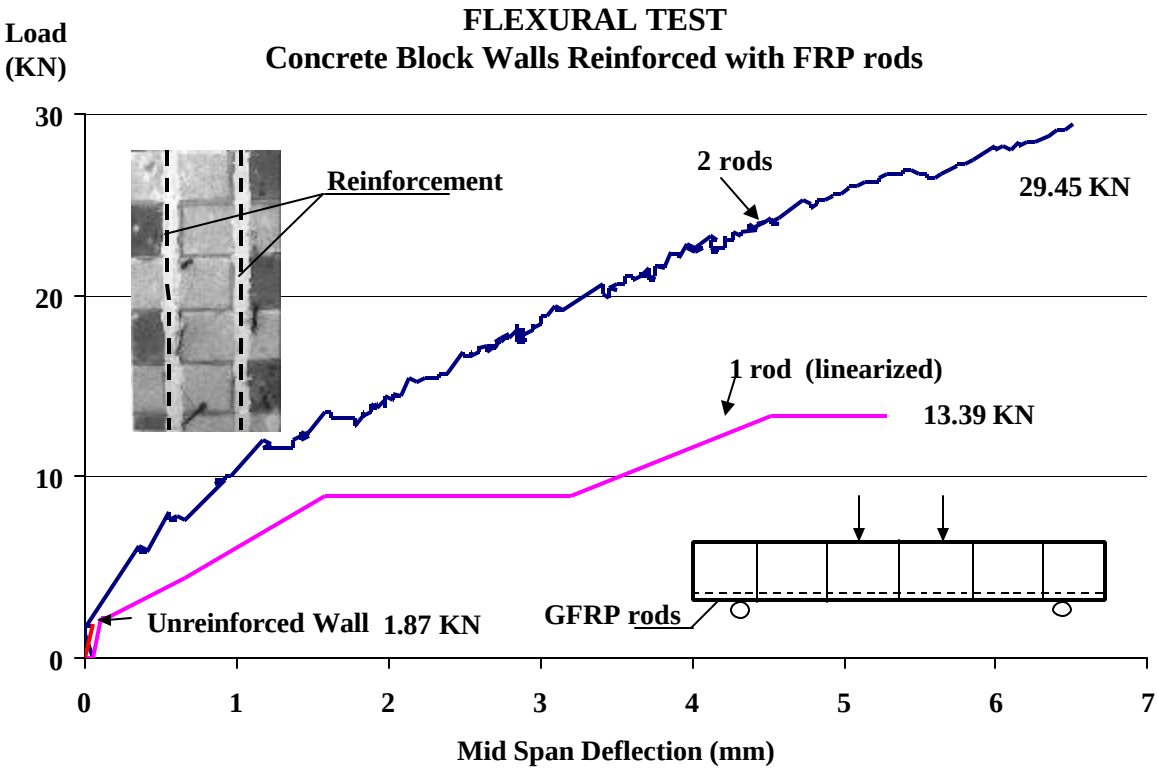

Figure 4.1: (above) Load vs. mid-span deflection of block walls strengthened with FRP rods. (aside) Flexural test set up.

This typology of failure clearly indicates a deficiency of tensile strength in the epoxy paste, while, as some residual paste remained on the rod, bonding between the two materials resulted to be adequate (see Figure 4.2, *a* and *b*).

a *b*

Figure 4.2 Splitting section and residual adhesion of paste on the rod surface.

However, between the two specimens there were some difference on the point of onset of splitting and the modality this failure propagated.

In the one-rod reinforced wall, flexural cracks opened in correspondence of each joint, thus portions of rebar crossing those crack were subjected to hi levels of tensile tresses. When the principal tensile stress reached the tensile strength of the paste and of concrete, inclined cracks opened. After that, bonding forces relied on the splitting tensile strength of the paste (see Section 2.4). Increasing the load, the splitting crack appeared on the surface of the paste or on the concrete-paste interface (see cracks 3 of Figure 4.3), depending on which, in the specific position, presented the lowest tensile strength and the shortest distance from the rod. Once splitting was triggered in correspondence of the mid span section, it suddenly spread along the groove toward the support at the non-grouted end (see Section 3.2.1) and the collapse was immediate. Before the total expulsion of the rod happened, it was observed that concrete on the bottom of the groove was already cracked (see Figure 4.4), and the collapse indicated also the longitudinal division of the part of wall involved by splitting (see Figure 4.5). Supposedly, this latter phenomenon should be absent with mortar-grouted blocks.

In the block wall reinforced with two FRP rods the same flexural cracks appeared at the opening of each joint, but splitting was triggered in a different point in each rebar. In fact, while a rod was complete expel from the mid-span joint to the grouted end, following the same pattern as the previous case; in the second rod paste splitting occurred in the bed joint close to the support at the non-grouted end (see Figure 4.6). The rod was completely expulsed for exactly the length of a block. A wide crack immediately connected trough some mortar joints the two points of onset of the failure (see Figure 4.7), but the total collapse of the wall did not occur as each section of the wall still had at least one rebar collaborating.

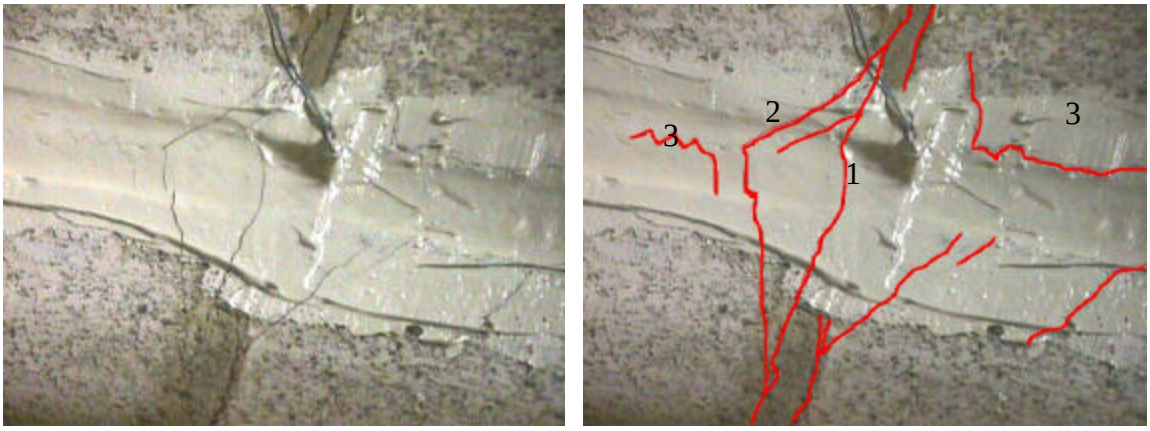

Figure 4.3: Mid-span joint with flexural cracks (1), crack due to principle tensile stress in the paste and in concrete (2), splitting cracks due to tensile failure of the paste or of the concrete-paste interface (3).

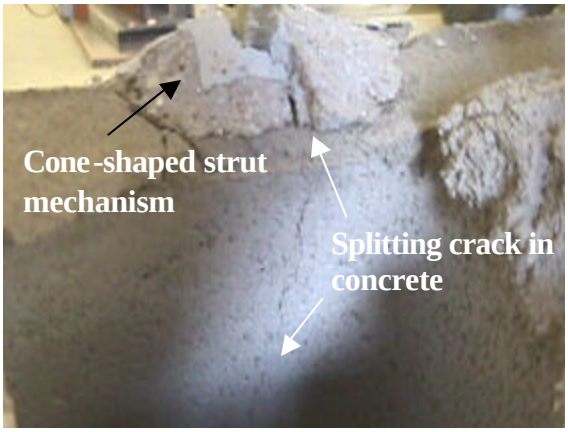

Fig. 4.4: Concrete splitting failure.

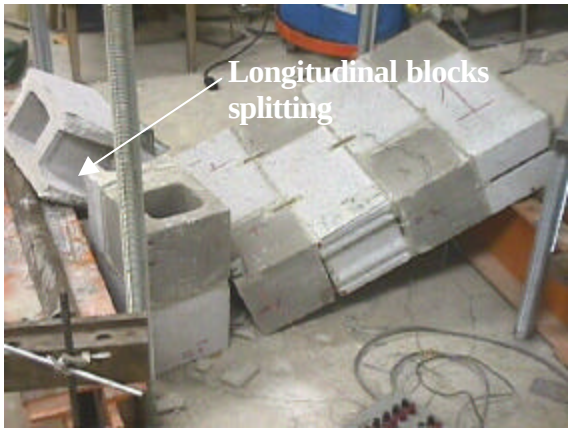

Fig. 4.5: Collapsed wall.

Fig. 4.6: Splitting at the end of the rod.

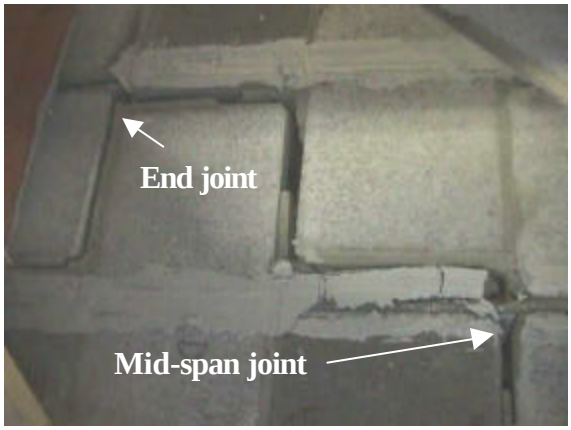

Fig. 4.7: Joint crack at failure.

Fig.4.8: Concrete block plitting crack.

Fig. 4.9: Compressive crushing.

Also in this case splitting of concrete anticipated the expulsion of the rod. In fact, due to its lower tensile strength and the same layer thickness as the paste, concrete necessary reaches earlier tensile failure (see Figure 4.8).

At failure, as the rod was debonded, the block over the support was free to rotate; as a consequence, two adjacent blocks and the included bed joint crushed (see Figure 4.9).

From the exposed failure modes, appears that splitting can start at any bed joint of a masonry wall subjected to the described test set up (see Section 3.2.1). Shear, and consequently the dowel action of the rebar was subjected to, may play and important role in triggering splitting in a lateral joint instead of a mid-span joint. Further considerations could be allowed only having the availability of a larger number of samples, that the encouraging results of the present experimentation suggest.

4.3.2 Clay Masonry Beams

The masonry beams with running bond and stack bond texture, reinforced with one GFRP rod, recorded a flexural capacity 5 and 7 times higher than the respective reference specimens (see Figure 4.10). Failure was due to the loss of bonding between masonry and epoxy mortar. In fact, once shear transferred in the masonry-reinforcement interface reached the typical shear strength characterizing the couple of materials, sliding occurred. This mechanism does not involve brittle failure, as sudden and complete loss of collaboration is prevented by friction in the interface (see Figures 4.14 and 4.15). As a consequence, mid-span displacement increased with load, and as the phenomenon is related also to local interlock due to the roughness between masonry and epoxy mortar, the progression of the displacement was irregular.

The reference masonry beam with stack bond (i.e., continuous head joints) recorded the poorest capacity, as the mid-span joint opened suddenly once it tensile strength was reached. The correspondent reinforced beam showed the highest capacity because of the indentation created at each joint on both sides of the sliding epoxy mortar; in fact those

irregularities may cause the epoxy mortar prism to be forced to slide through a slightly smaller section. This observation was confirmed by the fact that, after some sliding, the reinforcement remained locked into the groove (touching only the corners of a joint) until of masonry crushed in the compressed side of the beam. At this point also a certain shear sliding occurred along the head joint (see Figure 4.11). Load dropped to a lower value where it remained constant as displacement increased till complete failure occurred (see Figure 4.10).

Must be noticed that in the experimental diagram of the stack bond reinforced beam, the first part of the curve corresponding to the uncracked range is missing. In fact, this part of the curve should present a higher steep, as the section is not reduced yet. Unfortunately, most likely due to inaccurate handling operations on the beam, pre-cracking of the mid-span section was provoked before the testing session.

The unreinforced running bond (i.e., discontinuous head joints) masonry beam presented a higher capacity than the unreinforced stack bond beam. This was due to the interlocking effect of the texture, as discussed in section 5.1.1. The failure mode consisted in rotation of the mid-span section and the consequent opening of a crack through head and bed joints (see Figure 4.12).

In the reinforced case, cracking of the mid-span section at a higher level of load, as the brick modulus of rupture had to be overcome. The opening of the crack was accompanied by a sudden noise (see Figure 4.13) and identifies of the graph a remarkable decrease of stiffness (see Figure 4.10).

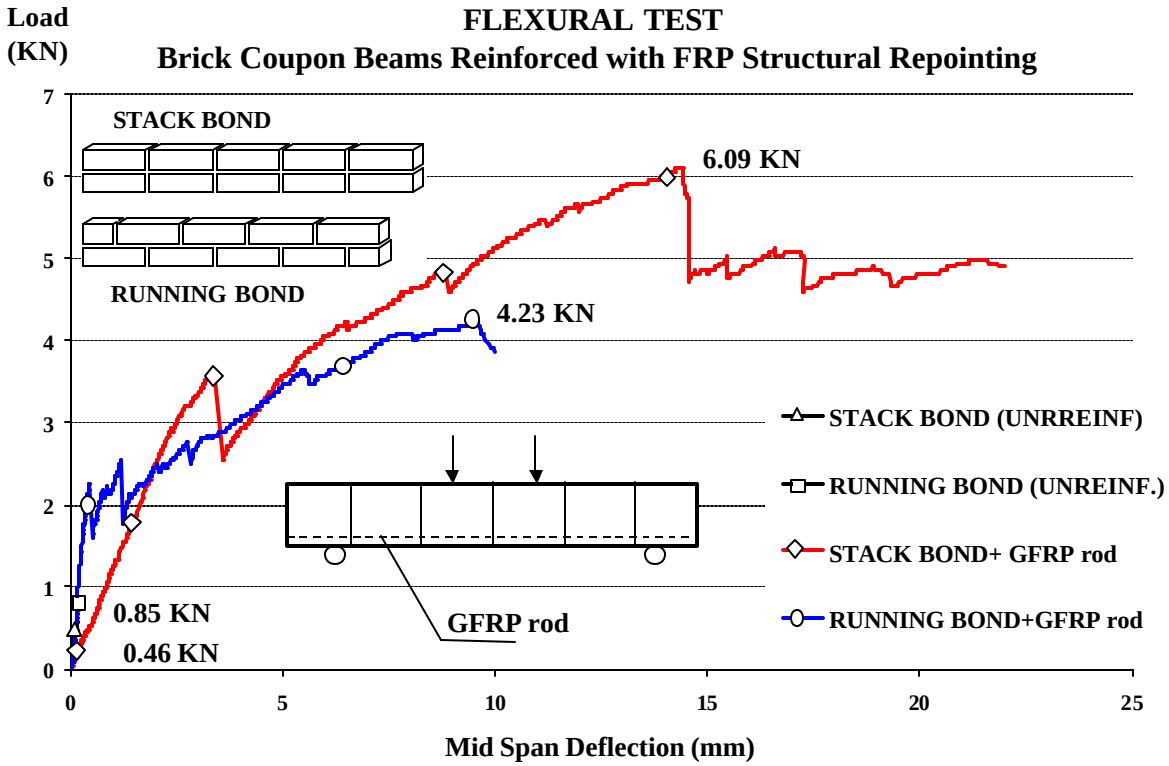

Fig. 4.10: Load vs. mid-span deflection of masonry beams strengthened with FRP rods.

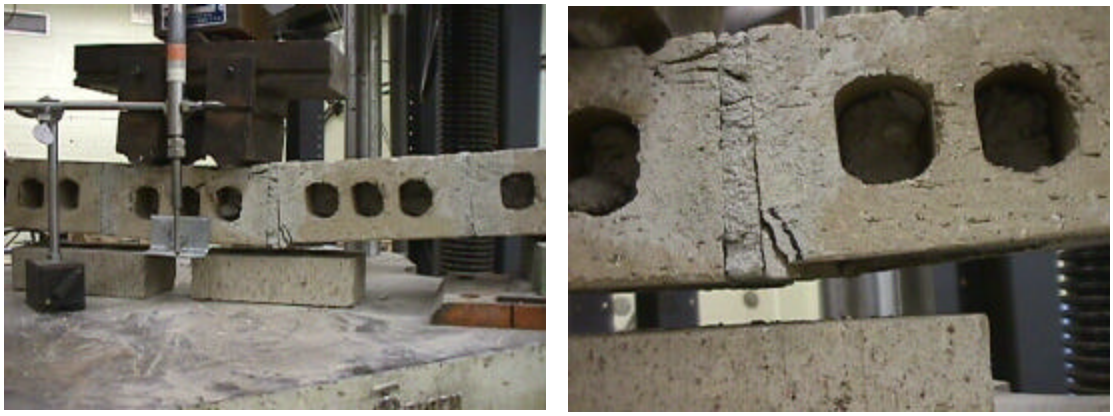

Figure 4.11: Crushing of masonry in the compressed side of the stack bond beam.

Fig. 4.12: Unreinforced beam failure

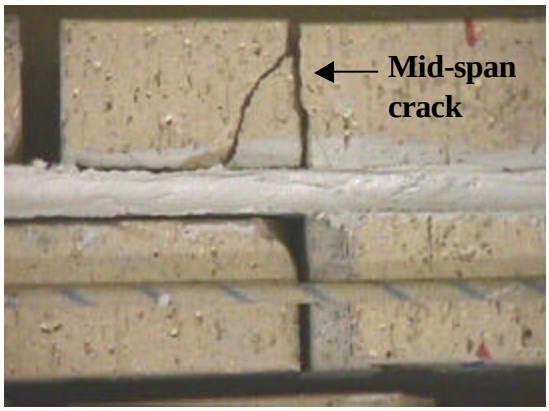

Fig. 4.13: Reinforced beam failure

Fig. 4.14: Sliding in stack bond texture.

Fig. 4.15: Sliding in running bond texture.

Load cycles on both kinds of masonry beams revealed an elastic behavior until the sliding of the reinforcement into the grooves occurred. After this limit, an inelastic range began and energy dissipation was developed by friction accompanying the larger deformations of the beams. For the proposed analytical models see also Section 5.1. For further details on the experimental results see also Appendix C.

4.4 SHEAR PERFORMANCE

Shear wallettes results are summarized in Table 4.1, while strengthening configurations are presented in Section 3.3.

The failure mode characterizing the sudden collapse of the unreinforced panels consisted of the joint sliding along the compressed diagonal, following a stepped pattern (see Figure 4.16). Similarly, but less brittle than the reference cases, the sliding in Wall 1 was forced to occur all along a central bed joint, although benefit for the shear capacity was not significant (see Figure 4.17).

Differently, Wall 2 and Wall 3 reached a mean shear capacity 45% higher than the reference walls. The failure mode was changed as joint sliding was prevented and shear capacity improved. Diagonal splitting of the panel triggered the crisis, but once cracks crossed a rod any propagation was prevented and new cracks were forced to open in a different position; their spreading on the compressed diagonal direction (see Figure 4.18) lead to a progressive degradation of the stiffness, accompanied by increase of deformations. The limit of this phenomenon was the sliding of the masonry-paste interface (see Figure 4.19) occurring once the anchoring length of the rod was shorter than the minimal development length associated to the force carried by the rod. As result of that was the loss of collaboration between masonry and reinforcement. This post peak different mechanism allowed larger deformations and dissipation of energy due to friction between the paste and bricks. Total collapse eventually occurred once the level of friction gradually decreased, due to the interface becoming smoother, and sliding of the mortar-brick interface took place along one of the central bed joints (see Figure 4.20).

This latter phenomenon could be avoided if reinforcement was placed in the direction orthogonal to the bed joints. For this reason Wall 4 was strengthened, only in one side, with Near Surface Mounted Rods (De Lorenzis, 2000. [47]). It was expected that the provided dowel action could improve also the shear performance and not only to prevent final collapse. The test result revealed instead the same shear capacity as the average of Walls 2 and 3, reinforced with SR. This result means that the controlling mechanism is only the debonding of the reinforcement, without any relation with the pin action of vertical reinforcement. Debonding occurs when the shear transferred through the masonry-epoxy mortar interface reaches the ultimate strength. Therefore, provided a sufficient bond of the reinforcement, the effectiveness of strengthening installed in the bed joint direction is the same as when operating in the orthogonal direction. This latter result is completely new respect the traditional strengthening approaches based on vertical or sub-vertical steel rebars anchored by cemetitius mixes.

Wall 4 revealed a diagonal splitting along the original joints and the grooves, showing less effectiveness in spreading the damage (see Figure 4.21). However, as foreseeable, complete loss of capacity was achieved at smaller splitting deformation than the SR case.

Fig. 4.16: Unreinforces wall. Typical stepped-sliding failure.

Fig 4.17: Wall reinforced with Structural Repointing each second joint. Sliding is forced along an unreinforced bed joint.

Fig. 4.18:FRP Structural Repointing reinforcement forces the spreading of the cracks.

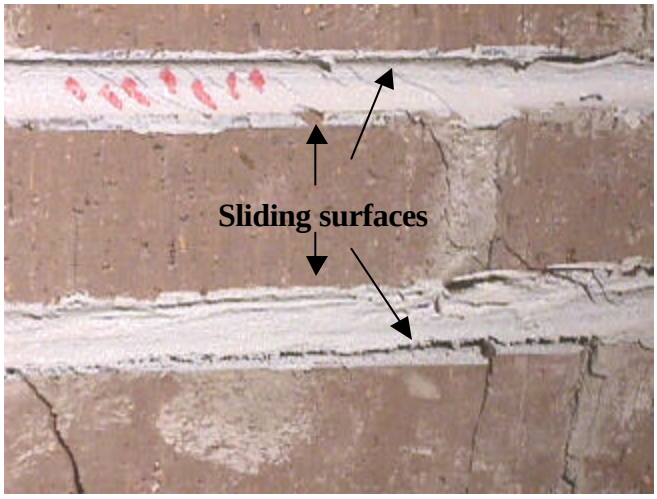

Fig. 4.19: Advanced phase of sliding of the reinforcement into the grooves.

Fig. 4.20: Post-failure final collapse, due to loss of the original friction in the masonry-reinforcement interface.

Fig. 4.21: Splitting pattern of the wallette reinforced with rods orthogonal to the bed joints.

Unfortunately some specimens were built using a weaker type of bricks and, in order to compare the test result excluding this inconsistence, a method of homogenization of the wallettes performances had to be found. Bricks with the superior mechanical properties are called Type 1, while the other are Type 2. Those latter are distinguishable in the pictures as their color is darker.

As the failure of the reinforced panels is triggered by the tensile splitting of masonry, which in turn is affected by the tensile strength of the bricks, the shear capacity of panels built with bricks Type 2 is increased by the modulus of rupture ratio of the two kinds of bricks (see values into brackets in table 4.1). This simplification is necessary also to formulate an analytical model predicting the behavior of the strengthened wallettes (see Section 5.2.2).

In order to compare the different effect of a laminate-based reinforcement respect the previously tested rod systems, Wall 5 was strengthened with vertical large strips (see Section 3.3). The rectified result reported in Table 4.1 into brackets, attests that a better increase of capacity is obtainable using systems involving a larger portion of the panel surface; that is obviously due to the fact that stresses are lower since are better redistributed. On the reinforced side, cracks were very limited in number and size (see Figure 4.22), while on the opposite side the absence of any reinforcement provoked the developing of a deep crack pattern caused by both shear splitting and flexural cracks (see Figure 4.23). In fact, the remarkable difference of stiffness on the opposite faces of the panel caused on the unreinforced side much more splitting than on the other; provoking the bending of the panel on the horizontal plane in which the splitting diagonal lies (see Figure 4.24). At failure, splitting of the reinforced side increased, as strips were delaminating from the panel (see Figure 4.25).

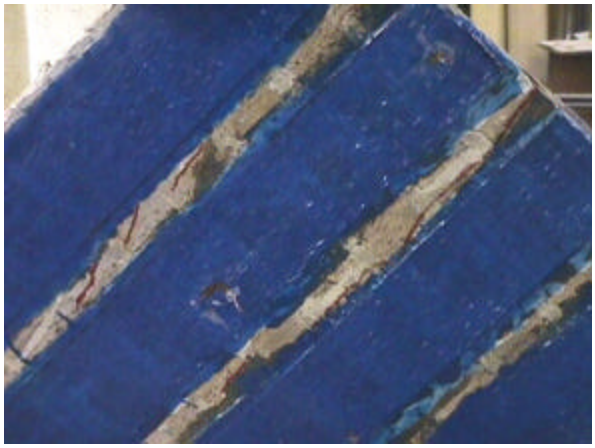

Fig. 4.22: Crack on the reinforce side of Wall 5

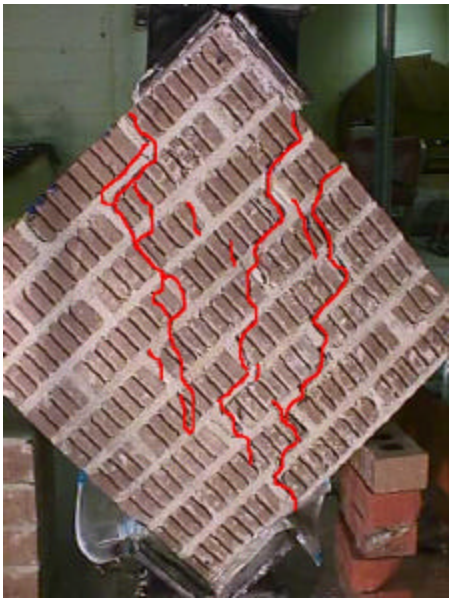

Fig. 4.23:(right) Wall 5, unreinforced side.

Fig. 4.24: Bending of Wall 5 under shear test.

Fig. 4.25: Splitting and delamination.

In order to further investigate the bending behavior due to asymmetrical laminate reinforcement, in Wall 6 was doubled the reinforcement amount and divided along the direction parallel to the bed joints and along the orthogonal one(see Figure 4.26). In this panel the phenomena previously observed were amplified: a higher shear capacity was obtained with few narrow cracks on the reinforced side, while a wide crack pattern on the opposite side caused, greater than before, bending deformation (see Figure 4.27).

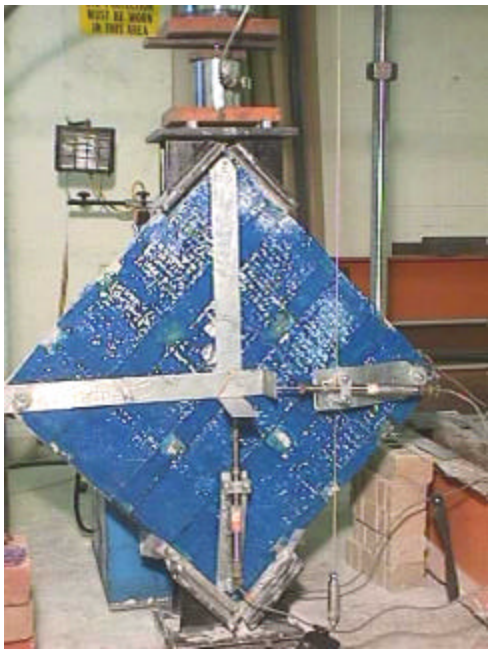

Fig. 4.26: Wall 6 crossed strips configuration *Fig. 4.27: Crack pattern of Wall 6*

In this case, presence of further reinforcement distributed along orthogonal directions caused also bending in the vertical plane, and as the lower support could no move, this deformation was traduced in eccentricity of the load. This particular behavior, due to reinforcement asymmetry, had encouraged to further investigate the phenomena as it had never been assessed in previous researches.
In real applications the bending effect may represent a static problem; particularly in case of load bearing walls, even if the bending could be limited by the panel constrains it would represent a detrimental event as small eccentricities easily cause instabilities non counterbalanced by any reinforcement. In this way, a limited bending on the vertical plane would lead the member to collapse.

In order to evaluate the effect of symmetrical reinforcement another specimen with rods on both sides was prepared. As the previous tests demonstrated that vertical or horizontal rods reinforcement have the same effect and as the number of specimen had to be limited, in Wall 7 was considering the insertion of rods in two orthogonal directions, one each side (see Section 3.3). Accompanied with a remarkable shear capacity, a diffused crack pattern testified the effectiveness of this strengthening configuration (see Figure 4.28).

A typical use of the FRP strengthening on masonry walls would expectedly consist in SR on the outer part and laminate reinforcement in the inner part, where most likely a plaster layer can cover the application. Wall 8 was designed to represent this approach, and can also shows the effect of combining the reinforcement used in Walls 2 and 5.

The shear capacity recorded was the higher of the one-with walls, while the number of diagonal cracks was limited by the effect of the FRP strips (see Figure 4.29).

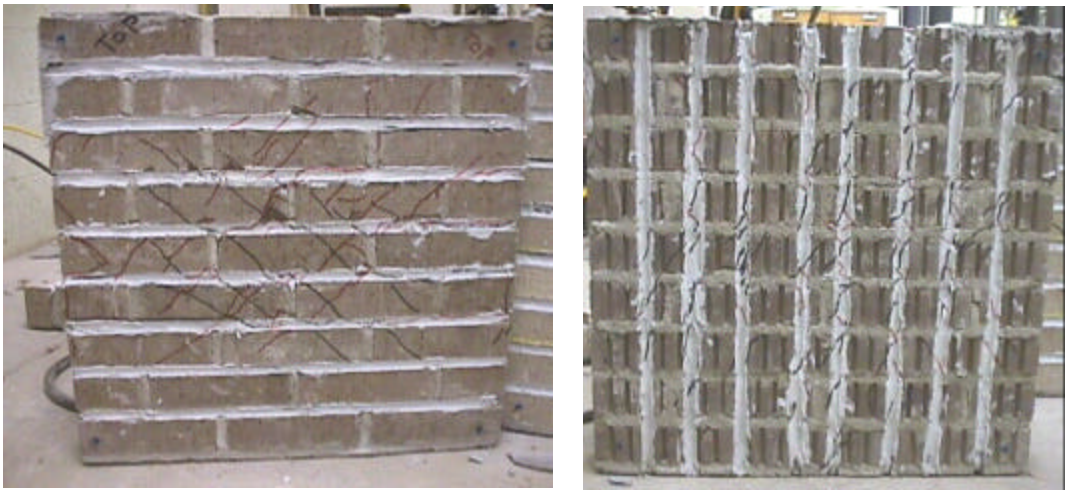

Fig. 4.28: SR and NSM rods are applied on opposite sides of Wall 7.
Crack patterns after both diagonal have failed under alternate shear actions.

Fig. 4.29: Wall 8 diagonal cracks

A variation respect the last case was introduced in Wall 9, where the same amount of FRP laminate was distributed in two plies, therefore the strips were narrower. In order to prevent delamination due to the inferior area of bonding, a special mechanical anchoring system was introduced (see Section 3.3). The ultimate shear capacity was slightly lower than the previous case and the crack patterns on the two sides were very similar each other, demonstrating that the same amount of reinforcement distributed on a lower area diminishes effectiveness. Therefore, it is also proved that when strips are narrow,

relatively the reinforced panel dimension, their advantage over embedded rods is reduced and can be even inferior if debonding is not prevented (see Figure 4.30).

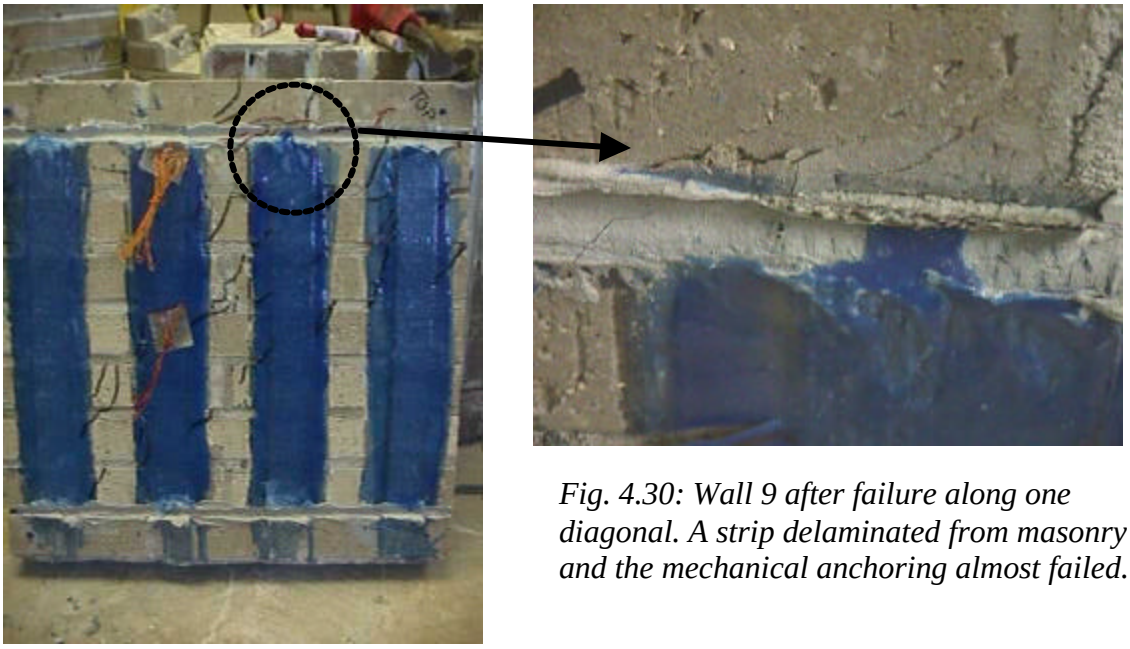

Fig. 4.30: Wall 9 after failure along one diagonal. A strip delaminated from masonry and the mechanical anchoring almost failed.

In order to simulate the damage provoked by bi-directional shear actions such a seismic event, after failure of the first diagonal, Wall 7, Wall 8 and Wall 9 were subjected to the same shear test also on the opposite diagonal (see Figure 4.28, 4.29 and 4.30), with load cycles up to failure. During this second series of tests shear capacities at least still over 60% of the reference value were recorded (see Table 4.1).

Two wythes walls were built with the scope of investigating the effect of different aspect ratios. In fact, while the depth of these walls has doubled, the amount of reinforcement, the grooves depth and the number of laminate plies have remained the same as in previous tests on one-wythe walls.

Wall 10, with structural repointing on both sides, demonstrated an overall behavior similar to Walls 2 and 3: shear capacity improvement, cracks diffusion, sliding into the grooves of the reinforcement and final mortar joint sliding along a central course of bricks (see Figure 4.31). The fact that the number of crack was limited once sliding occurred, reveals that Wall 10 encountered premature failure before the compressive masonry resistance could be completely exploited. Definitely, horizontal reinforcement provided noticeable benefits, but still the presence of vertical strengthening, as well, could have limited splitting displacements that provoked the premature failure.

In order to avoid splitting in the middle plane between the two wythes of the panel, bent rods were used for the SR. In this way, on each side, a short piece of rod was embedded in the bed joint in the depth direction of the wallette.

Wall 11 was reinforced with SR and narrow strips on the opposite sides and in orthogonal directions. Strips were mechanically anchored at the end parts. This set up was chosen as narrow strips allow a crack pattern similar to embedded rods and, in the same time, due to the special anchoring they provide reinforcement effectiveness beyond the sliding of the SR on the opposite side.

This last effect could also be realized by means of specially anchored vertical rods, as bent rods, but the grooving operation would have been too onerous. Instead, bent rods were used in the SR reinforcement and for the mechanical anchoring of the strips; the fact that those rods were inserted into mortar joints did not present any application difficulty. The reason of using bent rods in Wall 11 consisted on providing confinement on the depth direction of the wallette, to avoid separation of the two wythes due to splitting in the plane of the panel.

Performance of Wall 11 was extraordinary, as a remarkable shear capacity increase was obtained exploiting completely the compressive masonry potential along the loaded diagonal. That was due to the fact that cracks were maintained narrow and splitting was contained by the laminate reinforcement, which was maintained active by the mechanical anchoring beyond delamination of the strips (see Figure 4.32).

Wall 10 and Wall 11 did not seem to suffer from the unfavorable geometrical condition of the reinforcement. In fact, even if SR and FRP strips are superficial reinforcement systems, their effectiveness has been proved also in double-wythe panels. Especially for SR, there is the opportunity of embedding the rods deeper in the joint, and it is also possible doubling the rods. In this way the SR strengthening system, combined with laminates or not, can be effective also in multi-layered walls. In fact, as applications of steel-based repointing in multi-layered walls have already been successfully performed (Binda et al., 1999. [46]), it is feasible to aspect the same development also for the FRP SR.

Load – splitting displacement graphs of all the panels are reported below (see Figure 4.33, 4.34 and 4.35). As for some panels splitting was remarkably different on the opposite sides, both the displacements are recorded and distinguished. Different parenthesis symbols help to identify which side of each panel was reinforced and which side is represented by a curve. The kind of reinforcement is also specified.

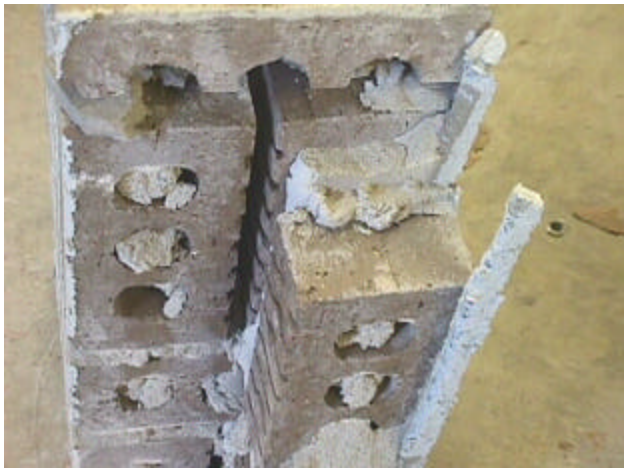

Fig. 4.31: Wall 10. Sliding of the central mortar joint determined the final collapse. Detail of the embedded rods slid along the grooves (above).

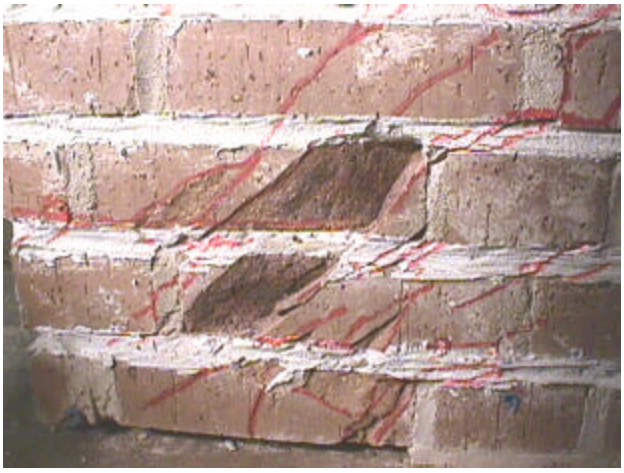

Fig. 4.32: Wall 11. Cracks concentration due to compressive failure of the loaded diagonal. Mechanical anchoring maintains delaminated strips effective

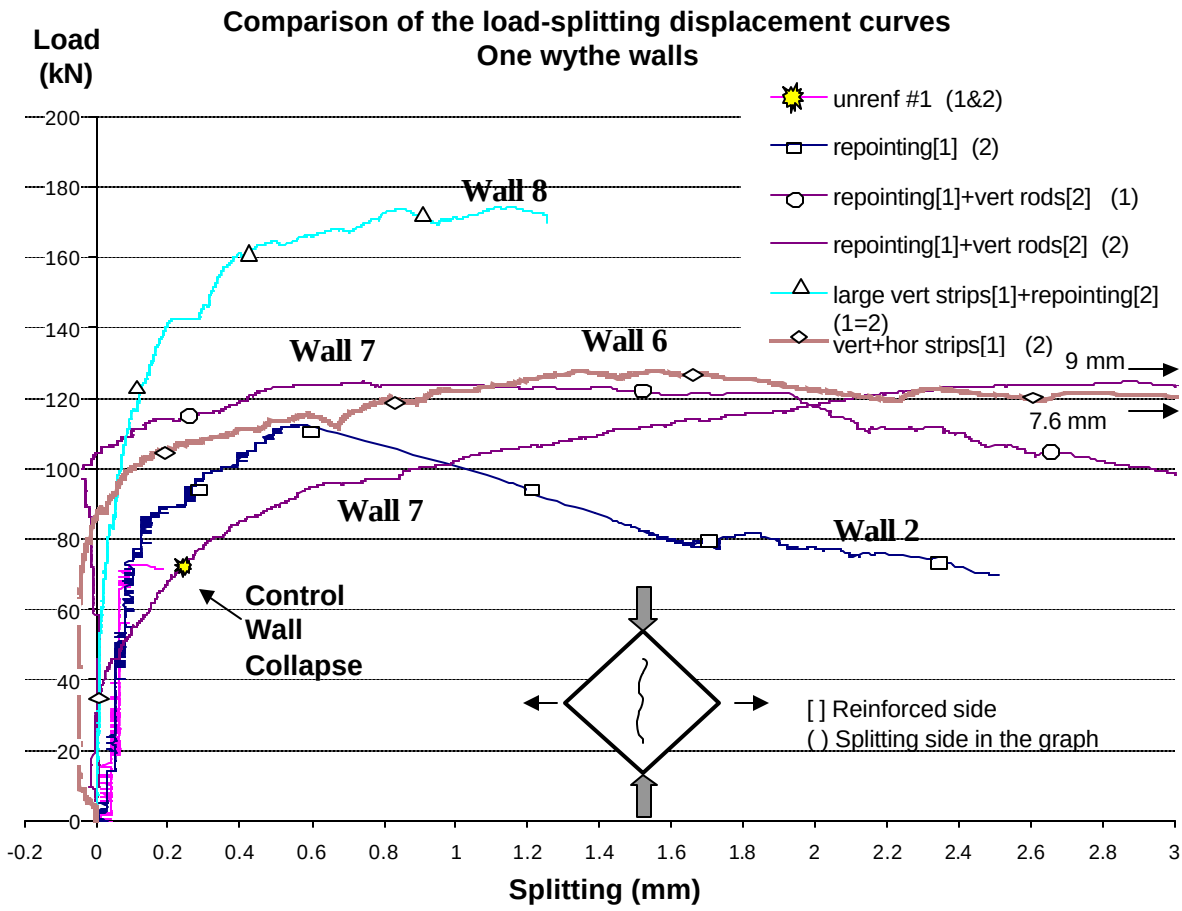
Comparison of the load-splitting displacement curves
One wythe walls
Load (kN)
unrenf #1 (1&2)
repointing[1] (2)
repointing[1]+vert rods[2] (1)
repointing[1]+vert rods[2] (2)
large vert strips[1]+repointing[2] (1=2)
vert+hor strips[1] (2)
Wall 8
Wall 7
Wall 6
Wall 7
Wall 2
9 mm
7.6 mm
Control Wall Collapse
[ ] Reinforced side
( ) Splitting side in the graph
Splitting (mm)
200
180
160
140
120
100
80
60
40
20
0
-0.2
0
0.2
0.4
0.6
0.8
1
1.2
1.4
1.6
1.8
2
2.2
2.4
2.6
2.8
3

Figure 4.33

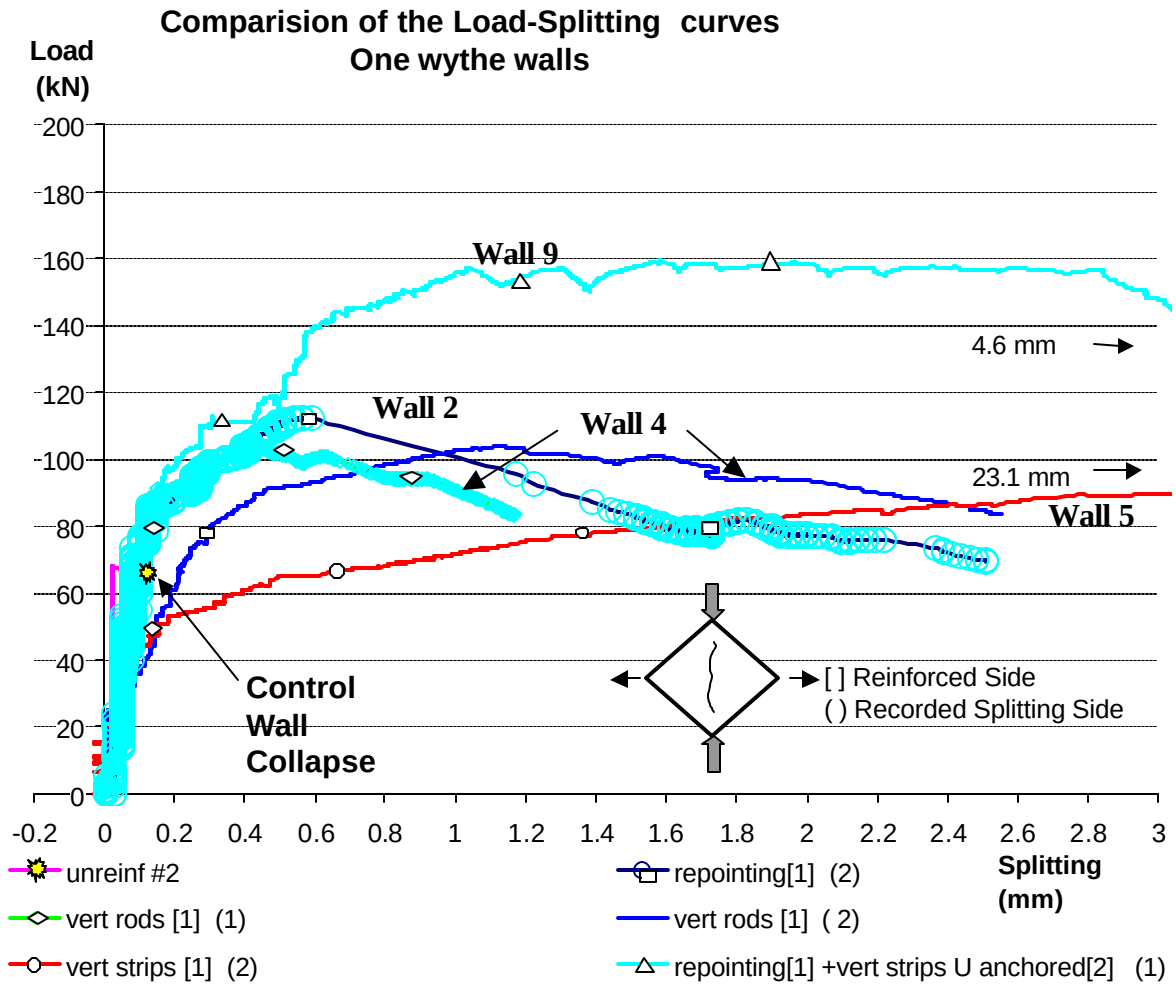
Comparision of the Load-Splitting curves
One wythe walls
Load (kN)
200
180
160
140
120
100
80
60
40
20
0
-0.2
0
0.2
0.4
0.6
0.8
1
1.2
1.4
1.6
1.8
2
2.2
2.4
2.6
2.8
3
Splitting (mm)
Wall 9
Wall 2
Wall 4
Wall 5
4.6 mm
23.1 mm
Control Wall Collapse
[ ] Reinforced Side
( ) Recorded Splitting Side
unreinf #2
vert rods [1] (1)
vert strips [1] (2)
repointing[1] (2)
vert rods [1] (2)
repointing[1] +vert strips U anchored[2] (1)

Figure. 4.34.

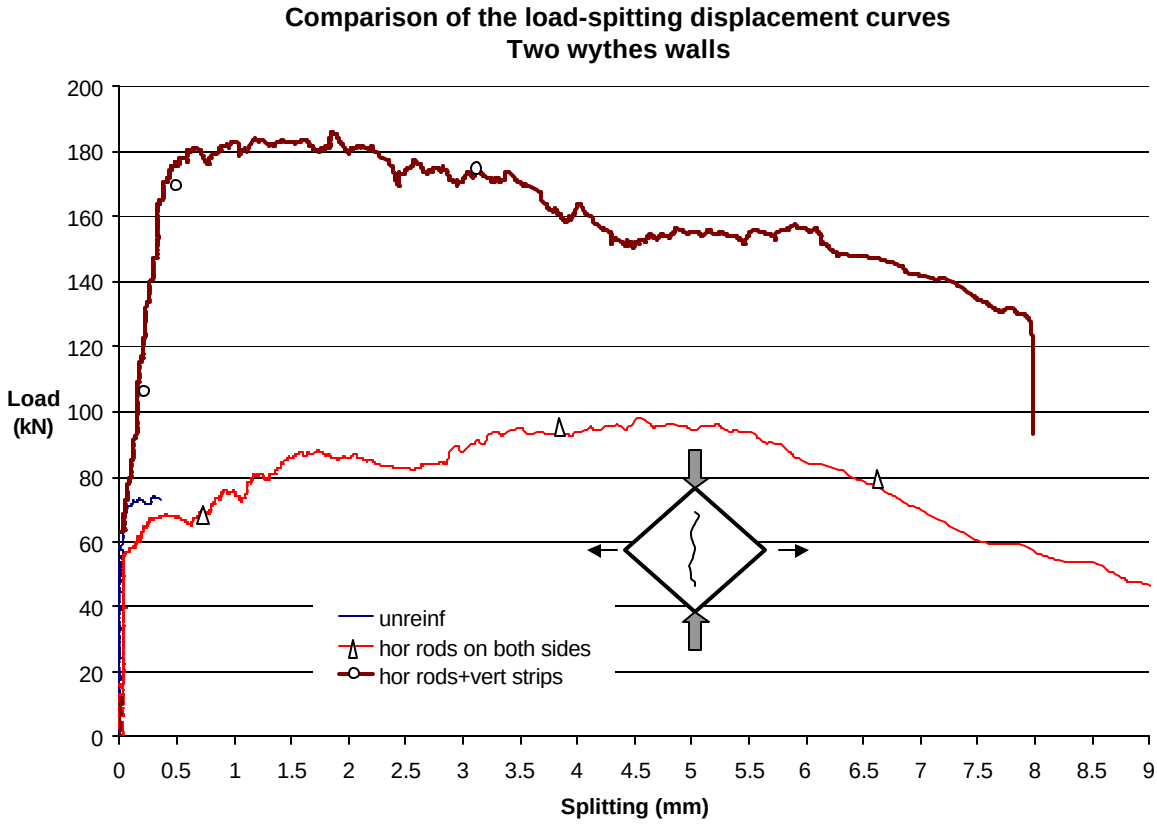

Figure 4.35.

During the diagonal shear tests, strain in the FRP reinforcement, was recorder by means of strain gauges attached directly on both strips and rods. Data from those measurements allowed to better understand the stress redistribution inside the panel in the elastic range. In addition, in the inelastic range once a crack crossed a rod in correspondence of the gauge, it was possible to see the local stretching of the reinforcement reacting.

On this concern, it is interesting to notice that during the diagonal test, in the elastic range, the reinforcement on the vertical and horizontal directions is in compression. In fact, only the not loaded diagonal is interested by the tensile stress. As explained in Section 2.4, the diagonals are the directions of the principal stresses, which are compressive and tensile stresses in the loaded and not loaded diagonal, respectively. Therefore, the presence of reinforcement applied on the non-principal direction became effective only when the plastic range occur, which coincide with the appearing of the first splitting crack.

Strain gauges applied to the rods of Wall 2, reinforced with SR, demonstrate, respect the middle horizontal axes, a symmetric strain distribution in the rods. Particularly, strain increased in the rods closer to the middle of the panel, and in each rod the point of maximum strain was on the splitting diagonal. After cracking, the point of maximum strain on each rod depended on where the crack crossed the rod. In Figure 4.39 are

represented the load-strain curves of the upper four rods of Wall 2; strains in the graph were recorded along the splitting diagonal. The numeration of the rods starts from the upper rod toward the middle of the panel.

Strain measurements were also useful to observe the maximum strain the laminate could bear before debonding occurred; but after that limit, strain measurement revealed the contribution of mechanical anchoring at the ends of the FRP strip.

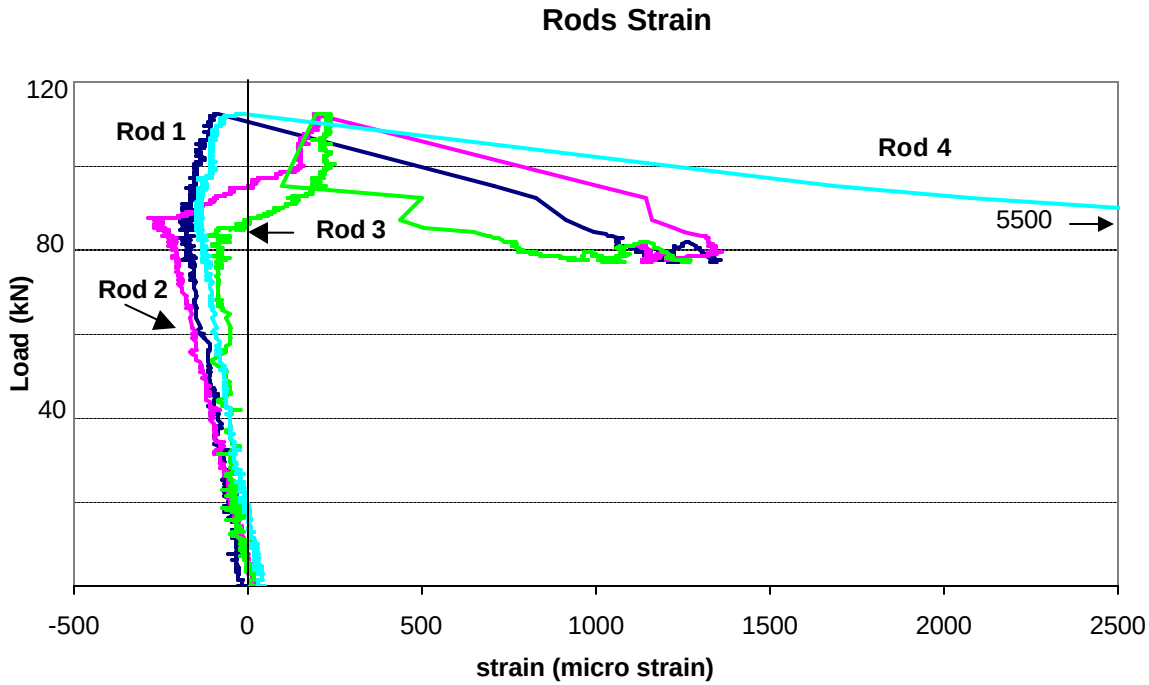

Fig 4.39: Load-strain relations of FRP rods applied to Wall 2.

4.5 POST DAMAGE PERFORMANCE

A fundamental characteristic of load bearing walls is to sufficiently maintain their function even after a damaging event, especially when the cause of damage is a short-term action as a seismic event.

Evaluation of the post-damage load bearing capacity could be done on the available specimens by means of axial loading tests, once shear failure was already occurred on one or both diagonals. The residual capacity obtained from the tests was compared with the theoretical capacity of the unreinforced wall obtained from the compressive strength the RILEM and stack bond prisms reached (see Section B3).

Obviously the level of damage introduced by the shear tests can be described in terms of cracks progression and therefore can be associated to the diagonal splitting displacement. Therefore, the level of shear capacity recorded by a specimen is not directly connected to the level of residual load bearing capacity, as most depend on how much during the diagonal test the cracks were allowed to extend. In fact, in order to

obtain graphs showing the semi-ductile behavior of the reinforced panels, during some diagonal tests the load was maintained to increase the splitting deformation. For this reason at the moment it is not possible to relate the result of the axial tests with the specific reinforcement configuration (see Figure 4.36). Certainly, the fact that large stripes of laminate limited the cracks width and diffusion during shear testing, granted those walls a better starting condition for the successive compressive tests.

After failure of the second diagonal, Walls 7,8 and 9 were tested under monotonic axial force to determine the residual load bearing capacity (see Figure 4.37). Recorded values, still noticeable, were related to the damage introduced in terms of splitting deformation during the previous shear tests.

Wall 11 was subjected to compressive test after shear failure of only one diagonal. The performance in terms of load bearing capacity was encouraging, especially considering the elevate level of damage previously introduced by the shear test. During the compression phase rods confined the façade of the wall, therefore compressive cracks opened on the opposite side were FRP strips were already delaminated (see Figure 4.38) and in the plane between the two wythes.

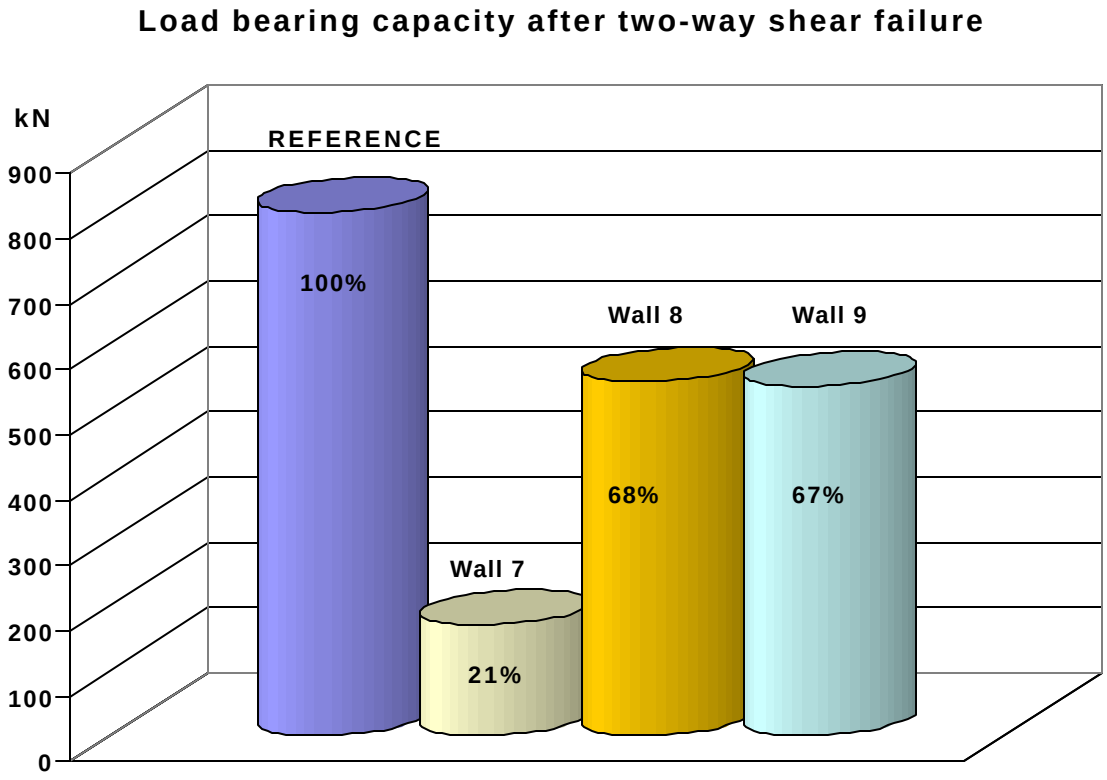

Fig. 4.36: Comparison of the original and the post-damage load bearing capacity.

Fig. 4.37: Wall 7 and Wall 8 under axial load. Both panels already failed under shear test.

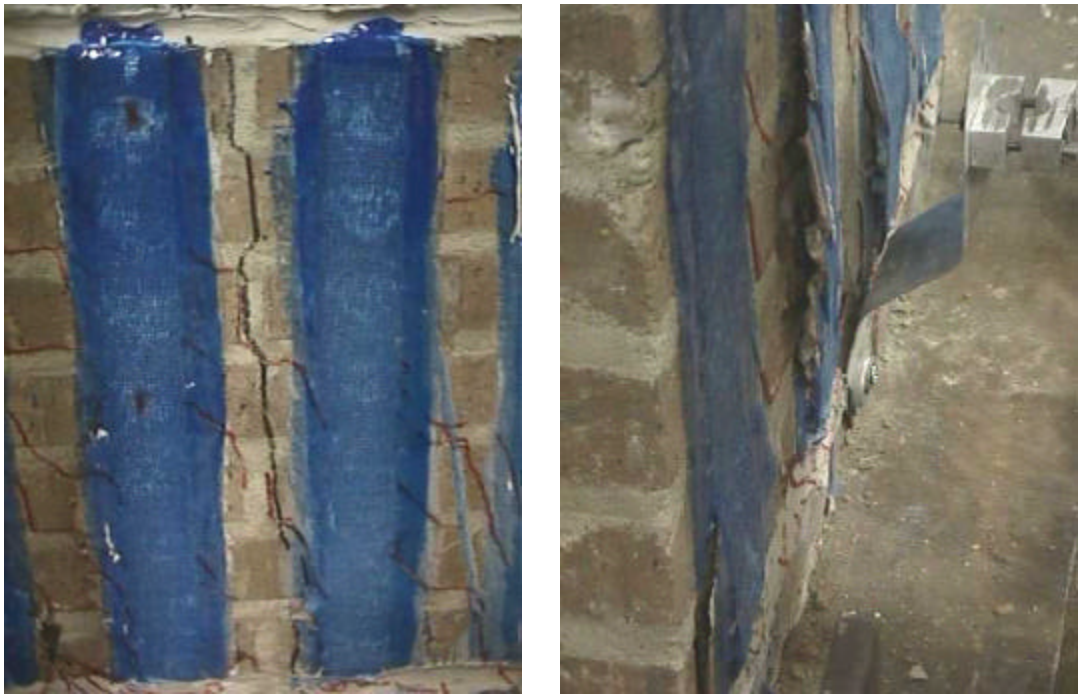

Fig. 4.38: Wall 11. Compressive crack between two anchoring rods and two strips (left). Strips of laminate completely detached from the diagonal failure (right).

Table 4.1: *Shear Wallettes Results*

Diagonal compression test (ASTM E519) on clay masonry wallettes

Identifier	Wall Type $\rho=A_{FRP}/A_m$	Reinforcement set up $d=A_{reinf}/A_{race}$ 1st side	2nd side	Tests performed & max load (KN) 1st diagonal		2nd diagonal (1st diag. failed)	Axial compression (both diagonals failed)	
REFERENCE	One wythe	Unreinforced		73.2	Average 70.8 KN 0%			Percentile referred to the uncracked theoretical compressive capacity
REFERENCE	One wythe	Unreinforced		68.5				
WALL 1	One wythe ρ=0.257%	Repointing (each 2nd joint) d=6.25%	Unreinforced	72	+1.5%			
WALL 2	One wythe ρ=0.514%	Repointing d=12.5%	Unreinforced	112.2	Average 102.4 KN +45%			
WALL 3	One wythe ρ=0.514%	Repointing d=12.5%	Unreinforced	92.6				
WALL 4	One wythe ρ=0.514%	Vertical rods d=12.5%	Unreinforced	103.7	+46%			
WALL 5	One wythe (type 2 bricks) ρ=0.265%	Vertical strips (one ply) d=66.7%	Unreinforced	93 (116.3)	+31% (+64%)			
WALL 6	One wythe ρ=0.530%	Vertical and horizontal strips (one ply) d=66.9%	Unreinforced	127.6	+80%			
WALL 7	One wythe (type 2 bricks) ρ=1.028%	Vertical rods d=12.5%	Repointing d=12.5%	124.6 (155.7)	+76% (+120%)	113.4 +60% (141.2 +100%)	168.9	21% (26%)
WALL 8	One wythe ρ=0.779%	Vertical strips (one ply) d=66.7%	Repointing d=12.5%	174.3	+146%	135.5 +91%	540.7	68%
WALL 9	One wythe ρ=0.779%	Vertical narrow strips U-anchored d=29.5%	Repointing d=12.5%	159.3	+125%	127.7 +80%	533.8	67%
REFERENCE	Two wythes (type 2 bricks)	Unreinforced		73.4	0%			
WALL 10	Two wythes (type 2 bricks) ρ=0.514%	Repointing d=12.5%	Repointing d=12.5%	95.8 (119.8)	+30% (+62%)			
WALL 11	Two wythes (type 2 bricks) ρ=0.368%	Vertical 2" strips U-anchored d=29.5%	Repointing d=12.5%	186 (232.5)	+152% (+215%)		1034.2	65% (79%)

Cross Sections:

$A_v=b_xt$= 542 cm^2

$A_{GFRPstrip}$ =0.3587 cm^2

$A_{GFRP\ rod}$ (ϕ 6)=0.3484 cm^2

Material properties

$E_{GFRP\ strip}$=72400 Mpa

$E_{GFRP\ rod}$=40800 Mpa

$E_{GFRP\ rod}/E_{GFRP\ strips}$=1.77

d=distridution factor

which is calculated as:

area covered by the reinforcement divided by the panel face area

Values into brachets take into account that type 2 briks have a 25% lower modulus of rupture

5. ANALYTICAL STUDY

5.1 DESIGN APPROACH FOR FRP-STRUCTURAL REPOINTING FLEXURAL STRENGTHENING OF MASONRY COUPON BEAMS

Test Scheme And Cross Sectional Area:
Following the four point flexural scheme, the cross sectional area and the principal characteristics of the reinforced masonry beams are represented (see Figure 1).

L=81cm
l=10cm

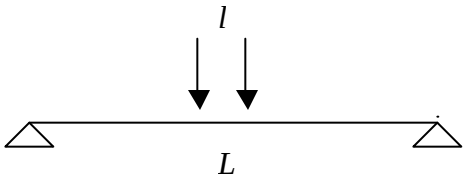

b=127mm
h=90mm
$A_m = b \times h = 11430 mm^2$
$A_f = 34.84 mm^2$
$r = 0.00305$
$E_m = 11 Gpa$
$E_f = 40.8 Gpa$
$n = E_f / E_m = 3.7$
$f'_m = 17.2 Mpa$
$f_t = 0.56 Mpa$
$f_{f,u} = 900 Mpa$
d=83mm

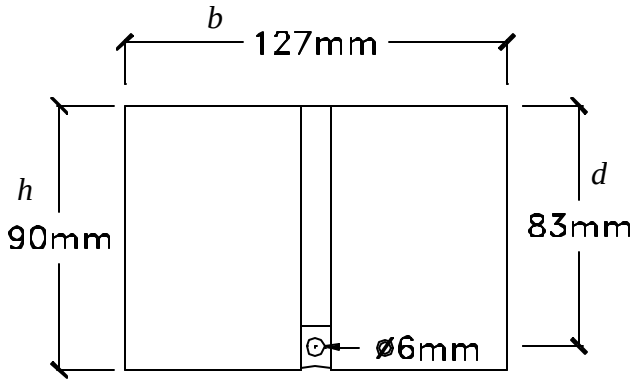

Figure 5.1: Beam cross sectional area.

5.1.1 UNREINFORCED BEAMS

Free-joints beam
The theoretical capacity of the free-joints unreinforced beam can be calculated assuming a linear elastic distribution of stress. Introducing the tensile strength obtained from the material characterization, the ultimate moment in the section is:

$M_{u,TOT} = f_t \, b \, h^2/6 = 0.56*127*90^2/6 = 96012 \, Nmm$

In order to find the maximum load that can be applied under a four point flexural test, the contribution of the dead load has to be taken into account removing the moment generated by dead loads from the ultimate moment calculated. The dead load is assumed to be 150N.

$M_{u,LL} = M_{u,TOT} - M_{u,DL} = 96012 - 15000 = 81012 \, Nmm$

Therefore this moment is generated by a load of 0.456 kN; this value is very close to the load of 0.460 kN experimentally found (see Figure 5.4).

Interlocked-joints beam

Failure consists in rotation of the mid-span bed joint portion included between two brick halves. The effect of friction in the brick-mortar interfaces is opposed to that rotation. This mechanism was described by Royen and the analytical form is obtained by the membrane analogy (Sven Sahlin,1971.[1]). Assuming that the shear stress over the area d x z (see Fig.5.2) never exceeds the friction stress τ (in this case it is τ_o, as normal stress is not applied to the bed joint), the maximum moment carried by such area is:

$M_{tot} = (t_o\, d^2/2\,)\,(z\text{-}d/3)$

Where: z=9.5 cm
d=9 cm
t_o=407.56 kpa

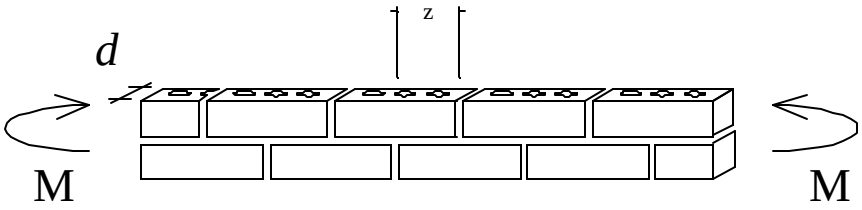

Figure 5.2: Interlocking area in running bond texure.

Otaining:

M_{tot} =107.29kNmm

Taking off the dead load contribution as shown before, the live load obtained is 520N, which is considerably lower than 850N experimentally found (see Figure 5.4).
A reason for this discrepancy is due to the fact that the introduced model does not consider the opposition action of vertical mortar joints against rotation, and therefore the friction area results over stressed.

5.1.2 REINFORCED BEAMS

Free-joints beam

The typical assumptions of RC members, plus some related to FRP material, are proposed:

- Plane sections before loading remain plane after loading.
- Perfect bond exist between concrete and FRP reinforcement.
- Tensile strength of concrete (in the specific case is mortar) is ignored.
- The maximum usable strain at the extreme concrete compression fiber is assumed to be 0.003 mm/mm, provided that the specified FRP ultimate design strain does not occur first.

- The compressive stress distribution in the concrete at ultimate is represented by the equivalent rectangular compressive stress block, provided that the strain at the extreme concrete compression fiber reaches a value of 0.003.
- The stress strain curve of FRP is linear elastic up to failure, with the maximum stress equal to the specified ultimate design strength.

The cracking moment correspondent to a the tensile failure of the mid-span mortar joint can be calculated as in a RC section, using the tensile strength from the material tests:

$$c = \frac{(bh/2) + A_f (n-1)d}{bh + A_f (n-1)} = 45.67\text{mm}$$

$I_{tr}=bh^3/12+bh(h/2-c)^2+A_f(n-1)(d-c)^2=835.95cm^4$

$M_{cr}=f_t\, I_{tr}/(h-c)=105.6\ kN\ mm$

Subtracting the dead load contribution as done before, the load causing the cracking of the section is:
Cracking Load=510.4N
The mid-span immediate deflection reached at this point can be approximated using the elasticity theory:

$D_{cr}=M_{cr}\, L^2/12\, E_m\, I_{tr}=0.063mm$

As the FRP rods do not present any yielding phenomena, the failure mode controlled by the rupture of FRP bars is brittle and therefore undesirable. For this reason, members reinforced with FRP should be proportioned to ensure a compression failure. It is recommended (Nanni, 1993. [55]) for FRP reinforced concrete members to refer to a failure mode based on crushing of concrete. The proposed ratio of FRP reinforcement in tension is $r_f > 1.33\ r_{f,b}$ (ACI committee 440, 1999. [53]). The immediate deflection under serviceable loads has to be particularly controlled when designing FRP reinforced members; for this reason a reasonable reinforcement ratio is included between 2 and 4 times the balanced value. In order to evaluate the ultimate capacity of steel reinforced masonry beams, many authors (Drysdale et al., 1994 [3]) refer to the same Whitney stress block introduced for RC sections; where the coefficient β_1 is assumed to be equal to 0.85 (see Figure 5.3). From these considerations it is now possible to calculate the balanced condition of the examined case is:

$$r_{f,b} = 0.85\ b_1\ \frac{f'_m}{f_{f,u}} \frac{E_f e_{cu}}{E_f e_{cu} + f_{f,u}} = 0.165\%$$

The actual reinforcement ratio is:

$r_f = A_f / A_m = 0.305\%$; $r_f = 1.85\ r_{f,b}$; $r_f > 1.33\ r_{f,b}$ is satisfied.

Note: in presence of a steel rod of the same diameter, the section would be even more over-reinforced.

Therefore, unless different mechanisms occur, crushing of the mortar joint controls the failure mode of the free-joint masonry beam. Following the aforementioned studies the model proposed for the mid-span cross section is:

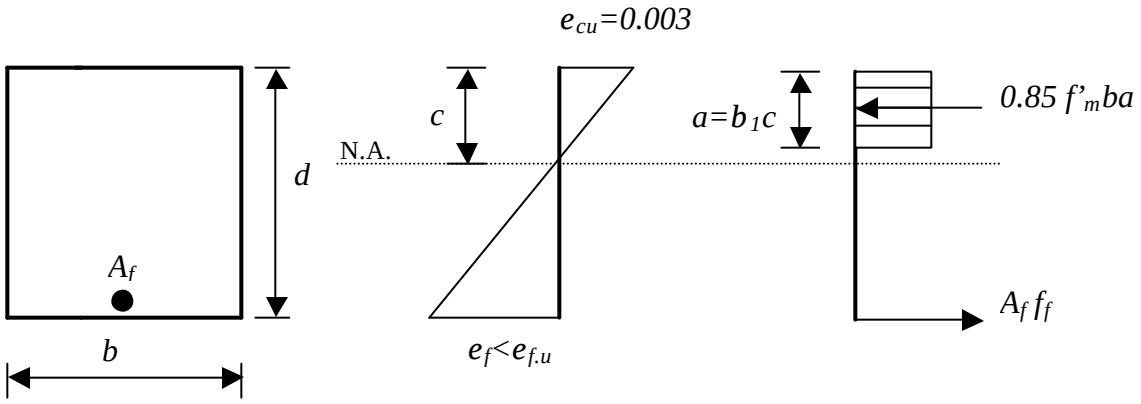

Figure 5.3: Stress and strain distribution of FRP-reinforced sections at ultimate strength

Based on equilibrium of forces and strain compatibility shown in Fig.5.3, the following can be written:

(1) $A_f f_f = 0.85\ f'_c\ ba$

(2) $M_n = A_f f_f\ (d - a/2)$

(3) $f_f = E_f e_{cu}\ (b_1 d - a)/a$

Substituting a from Eq. 1 into Eq. 2 and taking $A_f = r\ b\ d$ results in the following expression:

(4) $M_n = r\ f_f\ (1 - 0.59\ r\ f_f / f'_m)\ bd^2$

Substituting a from Eq. 1 into Eq. 3 and solving for f_f results in:

(5) $$f_f = \sqrt{\frac{(E_f e_{cu})^2}{4} + \frac{0.85 b_1 f'_m}{r_f} E_f e_{cu}} - 0.5 E_f e_{cu}$$

Introducing the correspondent values into equation (5) and (4) the following results are obtained:

f_f =647.6Mpa (72% of ultimate; e_f = 1.59%)

M_n=1610.9 kN mm

Subtracting the dead load contribution as done before, the ultimate load causing the crushing of the mortar joint is:

Ultimate Load= 8.991 kN

The mid-span immediate deflection corresponding to the ultimate condition can be approximated using the elasticity theory and the effective moment of inertia (ACI committee 440, 1999. [53]):

$$I_e=\left(\frac{M_{cr}}{M_a}\right)^3 bI_g+\left[1-\left(\frac{M_{cr}}{M_a}\right)^3\right]I_{cr}\le I_g$$

Where M_a is the applied moment and b is a reduction coefficient estimated as :

$$b = a\left[\frac{E_f}{E_s}+1\right]=0.602$$

The coefficient a depends on the characteristics of bond between rods and substrate. Available results from experimentations on GFRP rods embedded into concrete, found this value to be equal to 0.5. Certainly this subject needs further experimental investigation and must be treated considering the uncertainties, especially as in the analyzed case the critical bonding interface is between masonry and epoxy mortar.

Calculating the other factors:

$I_g=bh^3/12=$ 771.5 cm^4

$I_{cr}=bd^3/3\,k^3+ nA_f d^2(1-k)^2=$ 88.9 cm^4

with: $k=\sqrt{2r_f n_f+(r_f n_f)^2}-r_f n_f$ is obtained:

I_e=89 cm^4

Assuming that the cracked masonry beam deflection could be approximated as dealing with a cracked equivalent concrete beam subjected to a localized load at mid-span, at ultimate load condition:

$D_u=M_n L^2/12\,E_m\,I_e=$ 9mm

Comparing the theoretical analysis described above with the experimental results appears that the ultimate displacement D_u is over estimated; in fact the load-displacement theoretical curve in the cracked range would result to have a smaller inclination than the experimental case. This discrepancy is due to the fact that the deflection of the masonry beam is due to rotation of only joint sections; while the model considered refers to concrete beams where each section is subject to rotation. Assuming then for the theoretical diagram the same inclination as the experimental case, the displacement obtained is:

D'_u=6.78mm

It is now possible to obtain a curve that better represents the free-joint reinforced masonry beam behavior in absence of premature failure modes. (see Figure 5.4).

Must be noticed that in the stack bond reinforced beam experimental diagram the first part of the curve corresponding to the uncracked range is missing. As described in Section 4.3.2, this is due to a pre-cracking of the mid-span section before the testing session; that could be due to inaccurate handling operations on the beam.

The theoretical curve gives a benchmark of the increase of capacity that could be obtained if sliding of the reinforcement is prevented. Certainly, the theoretical model is based on assumption related to RC that should be confirmed from experimentations when applied to masonry assemblages.

In the theoretical approach above described, the assumptions introduced refer to the UBC guidelines. When referring to the European Code for Masonry Structures, the EC6, some assumptions change, as a different ductility philosophy is involved. Here are reported different values associated to some parameters from the two codes (see Table 5.1).

Table 5.1

		Whitney stress block:	
Code	*Ultimate masonry strain*	*Reduction factor*	*Stress*
EC6	e_{cu} *=0.0035*	b_1*=0.8*	*0.59 f'm*
UBC	e_{cu} *=0.003*	b_1*=0.85*	*0.85 f'm*

Clearly, the nominal performances of a structural member are slightly affected from these differences:

f_f*(UBC)=647.6Mpa*	f_f*(EC6)=548.3Mpa*	*(-15.2%)*
M_n*(UBC)=1610.9 kN mm*	M_n*(EC6)=1378.9 kN mm*	*(-14.4%)*

Interlocked-joints beam

The presence of reinforcement prevents the failure due to rotation into the bed joint, as described in the unreinforced case. Similarly to the free-joints beam, a cracking of the mid-span section appears when the its maximum tensile strength value is reached. The cross sectional area at mid-span consists of brick, for a half, and of a head joint for the rest. Excluding the tensile contribution of mortar and assuming the whole section composed of brick, the cracking moment can be approximated as:

$M_{cr}=f_{t,brick}\, I_{tr}/\,(h\text{-}c) = 924\ kN\ mm$

Where $f_{t,brick}$ is equal to 4.9Mpa, as found in the material characterization.

This approximated value, once the contribution of the self-weight is removed, gives a cracking load of *2.56 kN*, which is very close to the value experimentally found of *2.27 kN*.

After the crack of the section occurs, since the sliding of reinforcement takes place immediately, the behavior of the reinforced beam is similar to the previous case with open joints (see Figure 5.4).

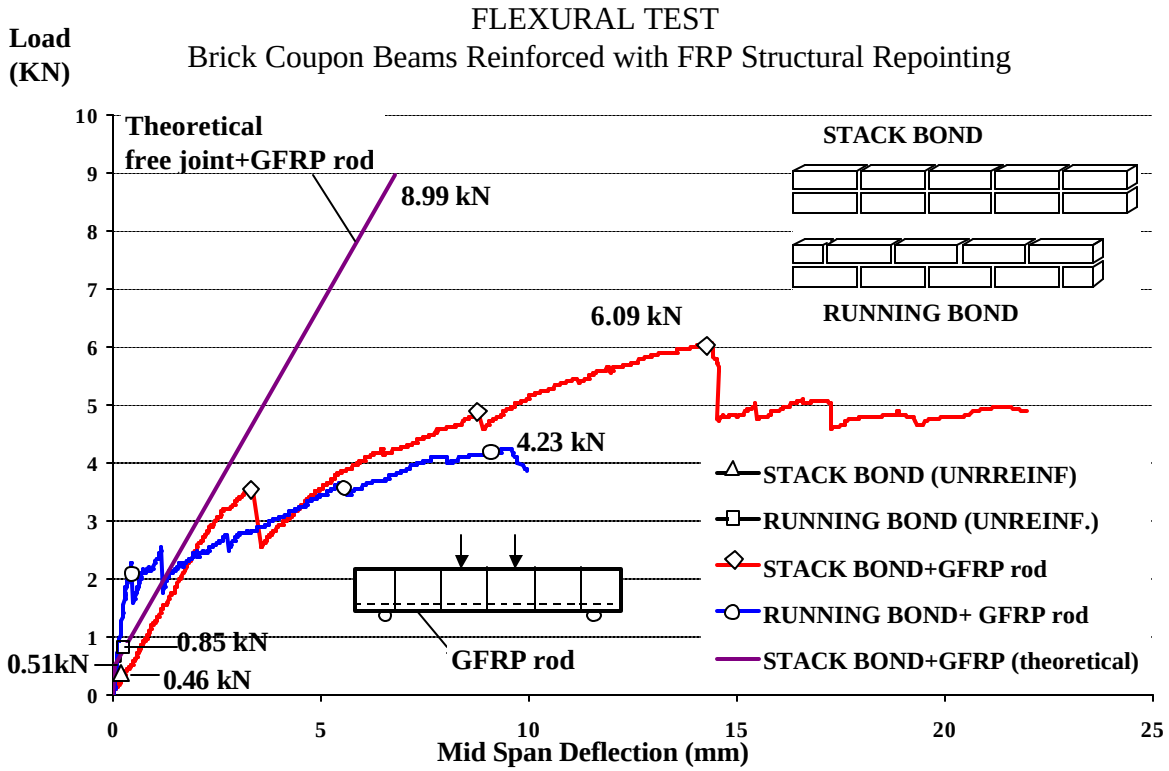

Figure 5.4: Load-deflection graph of the FRP reinforced masonry beams, experimental and theoretical curves.

NOTE: The described theory, applied to the reinforced masonry beams, has the basic assumption of complete collaboration, up to failure, between masonry and reinforcement. The discrepancy with the experimental results is due to the fact that this collaboration is lost once bond failure, in the specific case due to sliding, occurs. Therefore, is fundamental to perform a preliminary characterization of the bond properties with a successive identification of the bond failure mode expected (see Section 2.4), obtained by computing the stress in each cross section at different load levels, and comparing it with the maximum strength of materials and interfaces involved. In this procedure, on the ends of the rod a proper length has to be accounted as necessary anchoring.
For detailed calculations on the bond failure mechanisms between FRP rods and embedding paste see the methods proposed on section 5.3.5.

5.2 General Analitical Model for Shear Strengthening of Masonry Walls

5.2.1 VALIDATION OF THE EXPERIMENTAL PROGRAM

Some previous experimentations involving FRP laminates on masonry, carried out at Universities of Missouri-Rolla and Padua, demonstrated that delamination, consisting in failure of the outer part of the masonry support, is the controlling factor that still need to be addressed in new analytical models and prevented in applications. Related to this aspect is obviously the width of the strips and their anchoring length. Evidently, debonding phenomena like the mentioned delamination or the peeling-off due to interface failure, are the result of a geometrical reinforcement distribution that affects not only the failure mode but also, and first of all, determines the shear capacity.

The limits of the existing analytical approaches are due to the fact that they refer to design of new structures; hence specific issues introduced by retrofitting applications, as eccentric reinforcement, are not contemplated. On the other hand, it is clear that different restrictions can prevent from the use of a symmetrical strengthening, and in order to describe the influence on shear capacity of the reinforcement position, a first distinction has to be done between double or single side retrofitting.

On this concern, previous works (Marchetti, 1999. [45]) demonstrated the detrimental effect of reinforcement eccentricities on shear capacity of masonry panels, and the discrepancy with nominal shear strength calculated through models not including parameters connected with reinforcement distribution.

Also constrain boundary conditions have a decisive impact on the effect of eccentric reinforcement. That can be described with a common situation: on the edges of an infill wall under horizontal action into a stiff frame, a total restrain condition can be applied; on the contrary, only two corners are constrained if the frame is deformable and the result would be an amplification of the eccentricity effect, as the unloaded diagonal is free to bend. After these considerations, the choice of the shear testing method to be used was simplified: the diagonal test simulates the worst condition, as the supports can provide localized confinement only on the loaded corners of the panel.

5.2.2 ANALYTICAL MODEL PROPOSAL FOR MASONRY SHEAR STRENGTHENING WITH FRP LAMINATES AND RODS.

In order to obtain a qualitative model describing the shear test results, they need to be preliminary homogenized in terms of masonry properties. In this way the substrate material is not affecting the model, thus other parameters connected with the reinforcement can be easily isolated. As the failure of the reinforced panels is triggered by the tensile splitting of masonry, which in turn is affected by the tensile strength of the bricks, the shear capacity of panels built with bricks type 2 is increased by the modulus of rupture ratio of the two kinds of bricks (see values into brackets in table 5.2). Therefore,

as the mentioned ratio is equal to 75% (see section 4.2), the shear capacity of the panels made of bricks type 2 are to be increased of a 25%.

Referring to the corrected values (without at the moment discuss if the most suitable method has been used) is now possible to introduce a first model that considers the strengthening distribution factor. It is based on superposition of masonry and reinforcement contributions (see section 5.3.2).

$V_n = V_m + V_F$

$V_n = r\, A_m\, (f_{vk}/g_M) + A_m\, K \sum_i (r_i\, f_{fu,i}/\gamma_{FRP,i})$

Where:

r reduction coefficient that should include the irregular friction distribution caused by relevant bending moments

A_m masonry cross sectional area

f_{vk} masonry shear strength, which can be calculated referring to the mortar-brick interface friction, as $f_{vk} = (f_{vk,o} + m s_n)$

g_M material safety factor for masonry

r_i reinforcement ratio of the FRP material type i (different types can be present) If appropriate bonding is provided, both vertical and horizontal reinforced are included

$f_{fu,i}$ design ultimate tensile strength of the FRP material type i

$\gamma_{FRP,i}$ material safety factor for the FRP material type i

K strengthening configuration factor. It is defined as:

$K = 0.07d + 0.15$ in case of double side reinforcement

$K = 0.11d + 0.11$ in case of single side reinforcement with $d < 0.667$

$K = -0.31d + 0.39$ in case of single side reinforcement with $d \geq 0.667$

Where d is the distribution factor, calculated as area covered by the reinforcement on the considered face, divided by the total area of the face.

The strengthening configuration factor is obtained by interpolating the experimental results (see Figure 5.5). The introduced model perfectly predict the shear capacity of the test results of the present research and offers an acceptable approximations of the results obtained from previous works (Marchetti, 1999. [45]).

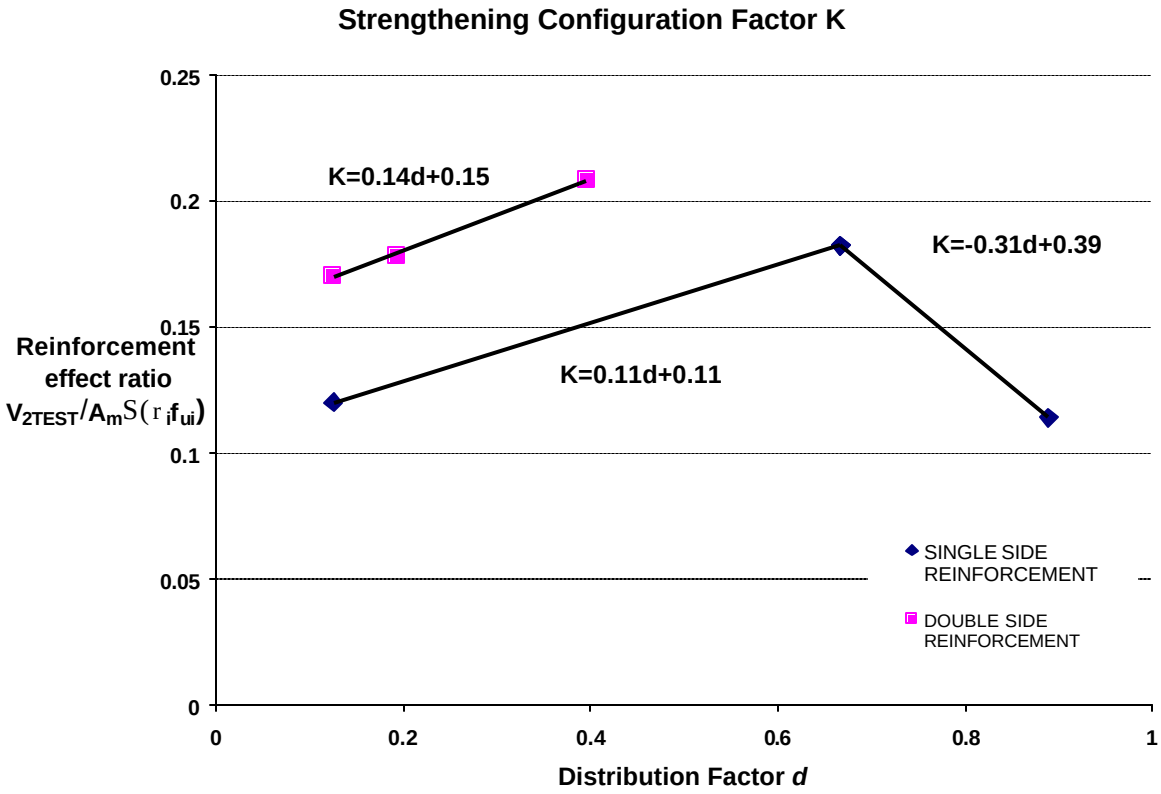

Figure5.5: Experimental over theoretical reinforcement effect vs. distribution factor.

The graph offers a qualitative idea of the effect of eccentricity and of the reinforcement distribution: for contained values of *d*, increasing the area covered by the reinforcement both single-side and double-side strengthening have proportional benefits. When the single-side reinforcement covers a major part of a panel, the stiffness difference between the two opposite faces determines a dramatic increase of the crack width in the unreinforced face. As result a capacity lower than the equivalent double-side strengthening case is obtained.

Certainly, the tests performed cover a vast range of FRP reinforcing systems that cannot be precisely described with a few data. Presumably each technique presents its own curve for single or double-side application, which may also depend on the degree of eccentricity. Never the less, the foreseeable tendency indicated from the graph of figure 5.5 gives a rough representation of a phenomenon that is usually underestimated and therefore dangerously ignored by code provisions, analytical models and designers.

In order to obtain a more precise model a wider experimental program is necessary. Hopefully, a more accurate analytical investigation should distinguish among the different failure modes of the FRP reinforcement systems.

Table 5.2: Diagonal test results

Identifier	Wall Type $r=A_{FRP}/A_m$	Reinforcement set up $d=A_{reinf}/A_{face}$		Diagonal Test ASTM E519 (kN)	
		1st side	2nd side		
REFERENCE	One wythe	Unreinforced		73.2	Average 70.8 KN 0%
REFERENCE	One wythe	Unreinforced		68.5	
WALL 1	One wythe r=0.257%	Repointing (each 2nd joint) d=6.25%	Unreinforced	72	+1.5%
WALL 2	One wythe r=0.514%	Repointing d=12.5%	Unreinforced	112.2	Average 102.4 KN +45%
WALL 3	One wythe r=0.514%	Repointing d=12.5%	Unreinforced	92.6	
WALL 4	One wythe r=0.514%	Vertical rods d=12.5%	Unreinforced	103.7	+46%
WALL 5	One wythe (dark bricks) r=0.265%	Vertical strips (one ply) d=66.7%	Unreinforced	93 (116.3)	+31% (+64%)
WALL 6	One wythe r=0.530%	Vertical and horizontal strips (one ply) d=88.9%	Unreinforced	127.6	+80%
WALL 7	One wythe (dark bricks) r=1.028%	Vertical rods d=12.5%	Repointing d=12.5%	124.6 (155.7)	+76% (+120%)
WALL 8	One wythe r=0.779%	Vertical strips (one ply) d=66.7%	Repointing d=12.5%	174.3	+146%
WALL 9	One wythe r=0.779%	Vertical 2" strips U-anchored d=29.5%	Repointing d=12.5%	159.3	+125%
REFERENCE	Two wythes (dark bricks)	Unreinforced		73.4	0%
WALL 10	Two wythes (dark bricks) r=0.514%	Repointing d=12.5%	Repointing d=12.5%	95.8 (119.8)	+30% (+62%)

5.3 Design Approach For FRP-Structural Repointing Shear Strengthening Of Masonry Walls

5.3.1 INTRODUCTORY CONSIDERATIONS

Investigations of FRP near surface mounted rods (NSM) on RC members were carried out in previous works (De Lorenzis, 2000. [47]), but a little is available on masonry applications. The present work represents the first attempt of technical approach to the use of rods for masonry strengthening, and also introduces for the first time the FRP Structural Repointing technique.
Due to the novelty of both the mentioned technologies, the experimental background is not sufficient to precisely identify the numerical values of coefficients introduced, but still the experience acquired allows isolating the most significant parameters affecting the test results.

When masonry walls, retrofitted according with the structural repointing method, are subjected to in-plane loading, three controlling failure mechanism are possible. The first mechanism of failure is related to local crushing of the masonry assemblage. The second one is associated with rupture of the rod. Finally, the bond failure can occur causing the loss of collaboration between masonry and reinforcement.

5.3.2 BACKGROUND

Either in codes or research proposals, the current approaches to calculate the shear capacity of reinforced masonry walls are based on the superposition of the contributions from the unreinforced masonry and the effect of reinforcement. Therefore the analytical models proposed are basically expressed as:

$$V = V_1 + V_2$$

As the typical failure mode of unreinforced walls under shear action consists in sliding of the joints following a diagonal or sub-horizontal step pattern, the contribution of the unreinforced condition is conservatively evaluated starting from the friction characteristics of the mortar joints. No considerations are related to the fact that, ones the panel is reinforced, the failure mode tends to change and splitting becomes the controlling factor better than a sliding mechanism. Due to the difficulties of predicting these combined phenomena, the aforementioned approach attributes the increased shear capacity consequent the reinforcement to the physical properties (typically cross sectional area and tensile strength) of the reinforcement itself; the final result is eventually adjusted with some reduction factor obtained from experimental experience.

Obviously this model represents a quick solution for the problem of managing masonry, a composite material itself, with some kind of reinforcement included. In fact the variable parameters in reinforced masonry are to many to be introduced in a general model; therefore aspects like bonding, anchoring and local crisis due to excessive stress concentrations are supposedly included in material safety factors and reduction factors.

The biggest limit of this simplified approach is related to the fact that it is inspired to the traditional strengthening based on the use of steel rods bonded with typical grouting materials as mortar or concrete.

Ones new materials with different constitutive law, stiffness, strength and bonding properties are introduced as reinforcement, aspects previously discarded from the analytical models need to be considered. For example, the modulus of elasticity, never introduced in the common models as the use of steel is assumed, may be taken into account when non-standardized new materials are involved. Another factor that has to be considered is the distribution of the reinforcement. In fact, using FRP laminates or rods determine different redistributions of stresses close to the covered area: a strip causes a stress spreading much more uniform than the localized effect due to a rod. To confirm this, the different crack patterns of masonry panels reinforced with rods or laminates subjected to shear tests.

Another example of the limits of the current models is the fact that only vertical reinforcement is considered when calculating the capacity of a strengthened wall, as the horizontal reinforcement is included into the bed joint courses and do not prevent sliding along the brick-mortar interface. On the contrary, the results of the present study demonstrate how, ones materials offering a stronger bond are used, rods embedded into bed joints can be as effective as vertical reinforcement systems.

5.3.3 EXISTING CODES PROVISIONS

Eurocode 6:

This code presents the discussed model approach, in which the determination of the masonry contributions is based on the preliminary evaluation of the unreinforced masonry shear strength. This latter is related to the axial compressive stress through the Coulomb Friction equation. The effectiveness of the reinforcement, intended as steel rods, is related to the angle it forms with the horizontal, and it must to be included between 0 and 45 degrees.

Also the distribution of the reinforcement into the section is taken into account by the spacing factor *s*.

$V_{Rd}=V_{Rd1}+V_{Rd2}$

$V_{Rd}=(f_{vk}/\gamma_M)\, b\, d + 0.9\, d\, (A_{sw}/s)\, (f_{yk}/\gamma_S)\, (1+\cot\alpha)\, \sin\alpha$ $\qquad f_{vk} = (f_{vk0} + \sigma_n)$

Uniform Building Code:

According to the basic equation presented in the 1997 UBC, also this model presents the effects superposition pattern, but in this case the unreinforced masonry contribution is defined from the compressive strength f'_m and depends also on a geometrical coefficient C_d (see Figure 5.6 and 5.7). The reinforcement is taken into

account only with horizontal configuration and its contribute is equal to the yielding strength.

$V_n = V_m + V_s$

$V_m = C_d A_{mv} \sqrt{f_m'}$ [C_d is a geometrical aspect factor, see Figure 5.6 and 5.7]

$V_s = A_{mv} r_n f_y$

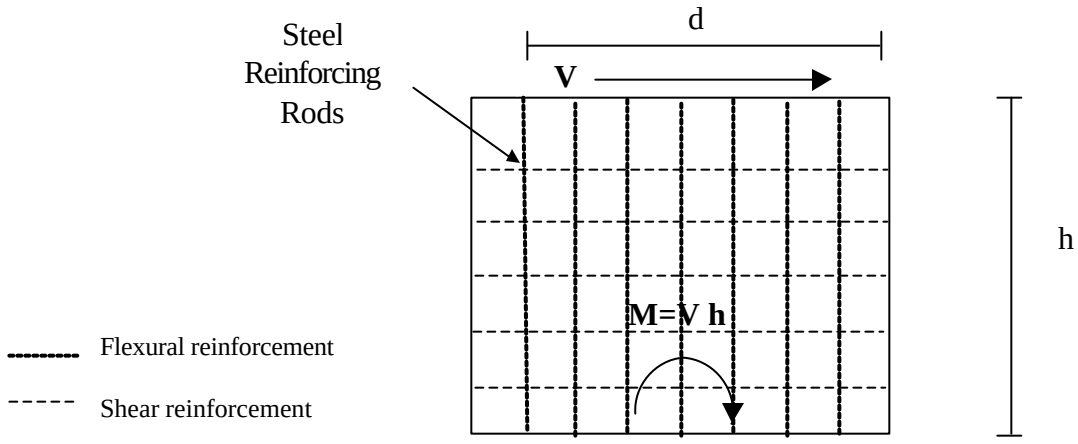

Figure 5.6: Definition of aspect ratio M/Vd

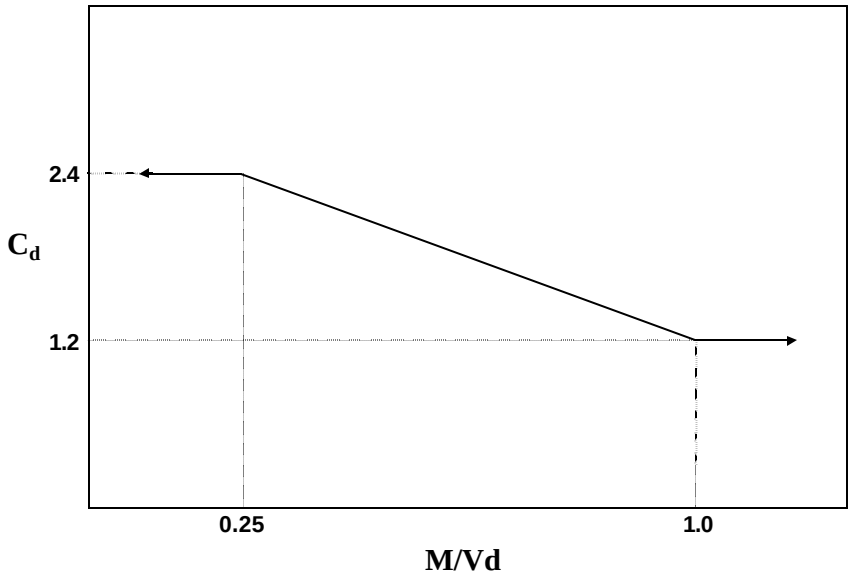

Figure 5.7: Computation of C_d

5.3.4 RESEARCH APPROACHES

Here are presented some models proposed by different authors as result of their research works on masonry shear strengthening. The purpose of reporting those models is to demonstrate how alternative approaches can be considered and developed.

M. Tomazevic Theory

This research approach introduces an alternative way to the Coulomb Friction to calculate the unreinforced masonry contribution: it is more correctly inspired to splitting instead of a sliding mechanism. However the model suffers of the fact that it is still designed for steel reinforcement.

$$V_{Rd1} = 0.9*b*l*\frac{f_{vk0}}{b}\sqrt{1+\frac{s_0}{f_{vk0}}} = 0.9*b*l*\frac{f_{vk0}}{1.5}\sqrt{1+\frac{V_{Rd1}}{t*l*f_{vk0}}}$$

$V_{Rd}=V_{Rd1+}V_{Rd2}$

$V_{Rd2} = 0.4*A_r*f_{yk}$

T. Triantafillou Theory:

Introduced for FRP laminates shear reinforcement, it represents the first attempt to adapt the traditional models to alternative materials. Till now it has been scarcely supported from test validations. A general efficiency factor of the reinforcement *r* is introduced, but it is not sufficiently supported from considerations related to material properties and strengthening configurations.

In addition, the proposed model introduce as limit the ultimate strain of the composite multiplied by the modulus of elasticity; which is equivalent to introduce the FRP ultimate tensile stress, assuming that any premature failure is included in the factor *r*. From this point of view it does not seem to go far from the mentioned codes where the bench mark is represented from the yielding stress of steel.

$V_{Rd}=V_{Rd1+}V_{Rd2}$

$V_{Rd1} = f_{vk}*b*d$ $\qquad f_{vk} = (f_{vk0} + ms_n)$

$V_{Rd2} = r_{frp}E_{frp}(re_{frp,u} / g_{frp})b0.9d$ $\qquad d = 0.8*l$

5.3.5 CONTRIBUTION OF FRP STRUCTURAL REPOINTING TO SHEAR CAPACITY

In the aforementioned approaches the nominal shear strength is given by the sum of the shear contributions of the masonry and the steel shear reinforcement. Previous works on RC members (De Lorenzis, 2000. [47]) demonstrated that when introducing FRP rods to integrate the steel stirrups action, the nominal shear strength can be quantified by adding a third term to account for the contribution of the FRP reinforcement:

$$V_n = V_m + V_S + V_F$$

The design shear strength is obtained by applying a strength reduction factor, f, to the nominal shear strength, as discussed later.

This design approach presents two equations that can be used to compute the contribution of FRP horizontal reinforcement to the shear capacity, V_F. A conservative criterion suggests taking the lowest value.

Similarly in the present case, a reinforcement contribution is added to the plain masonry shear strength, although a different criterion to identify V_F has to be introduced.

A first value for FRP shear strength contribution, V_{1F}, is computed when bond-controlled shear failure is the governing mechanism. The second value of FRP shear strength, V_{2F}, is estimated basing on the assumption of full development of the rod tensile capacity.

Calculation of V_{1F}

V_{1F} is the FRP shear strength contribution related to bond-controlled shear failure.
In case of mechanical anchoring, debonding can be prevented or, at least, the bond failure do not constitute the final loss of collaboration; in this situation a detailing investigation focusing on the specific solution has to be carried out. When no special anchoring is introduced, the bond failure of externally applied rods embedded into grooves can occur in different ways and locations: masonry or embedding paste can split if the tensile stress overcome their tensile strength; the rod can be pulled out from the paste; sliding in the paste-masonry interface can occur (see Section 2.4). The modality in which these failures occur is also different. In fact, splitting determines a sudden loss of collaboration with the substrate, therefore is the most brittle failure. Sliding, once occurred, conserves a resisting mechanism due to friction, and large displacements can be reached in a semi-ductile behavior. Pull out present intermediate characteristics. Related with that, different safety factors could be applied to each mode on the nominal shear contributions.

The materials involved, the interface surfaces and the profile of the rods influence these failure modes. The case of sliding of the reinforcement into the grooves appears to be the most probable: it is the less controllable due to the difficulty to obtain samples of the original masonry for laboratory tests. Pull out could be prevented choosing suitable

paste and rod profile, while splitting could be avoided with an appropriated groove depth. This latter failure mode is difficult to predict with a model, on the contrary the other two mentioned mechanisms of bond failure could be easily treated following the same analytical pattern.

Once bond properties of the masonry-paste interface and of the rod-paste interface are known or assumed from comparisons with similar assemblages, it is possible to identify which of the two bonding failure modes is expected to occur simply checking which of the two terms is bigger:

Pull out resisting force;	*Sliding resisting force;*
$p\ d_b\ t_1$;	$p\ t_2$;

where:

d_b = diameter of the rod

t_1 = max shear stress on the pull-out surface

p = perimeter of contact of the paste section with the masonry substrate (see Figure 5.8).

t_2 = max shear stress on the sliding surface

Figure 5.8: Section of two brick courses showing the perimeter of contact of the paste with masonry and bed joint.

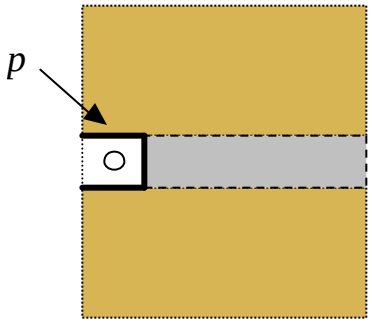

The following assumptions are considered:

1) There are not unreinforced or week horizontal layers that can determine shear sliding preventing development of diagonal shear cracks.
2) Inclination angle of the shear cracks constant and equal to 45° (see Figure 5.8).
3) Constant distribution of bond stresses along the sliding interfaces.
4) At failure, the ultimate bond strength is reached contemporary in all the rods intersected by the crack.
5) Reinforcement is evenly distributed on one or both faces of the panel and spacing between rods is constant.

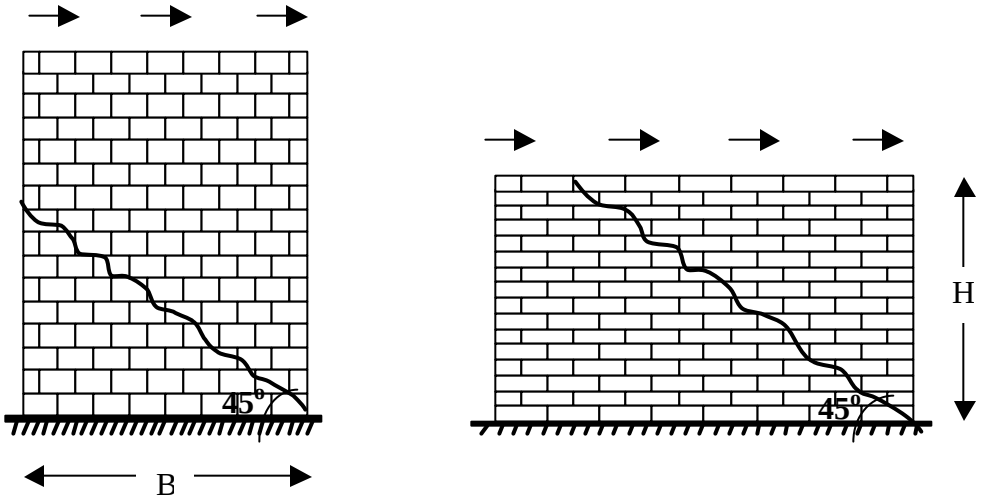

Slender Wall Squat Wall

Figure 5.8: Potential shear cracks

The shear force resisted by the FRP can be quantified as the sum of the bond forces resisted by the FRP rods intersected by a shear crack. Each rod intersected by a crack may be ideally divided in two parts at the two sides of the crack. The force in each of these rods can be calculated as the product of the average bond strength and the surface area of the shortest part, that from now on can be referred as effective length of the rod: L_{eff} .

Therefore, for each rod can be written:

$$A_f f_f = b L_{eff} t$$

Where:

b and t, depending on the most probable failure mode, are:

	in case of pull out:	in case of sliding:
	$b = p\ d_b\ t_1$;	$b = p\ t_2$;
(1)	$t = t_1$	$t = t_2 = t_0 + m\ s$

Due to their different nature, it can be assumed that t_1 is constant in all the positions of the wall reinforcement, while t_2 is much more affected from the local conditions due to position of the reinforcement. Obviously it would be onerous to calculate t_2 in each reinforced layer considering the orthogonal compressive stress s due to the self-weight and carried loads. Furthermore, under shear action the distribution of vertical loads has necessary to change to maintain the overall equilibrium. Here, a simplified and conservative method is suggested:

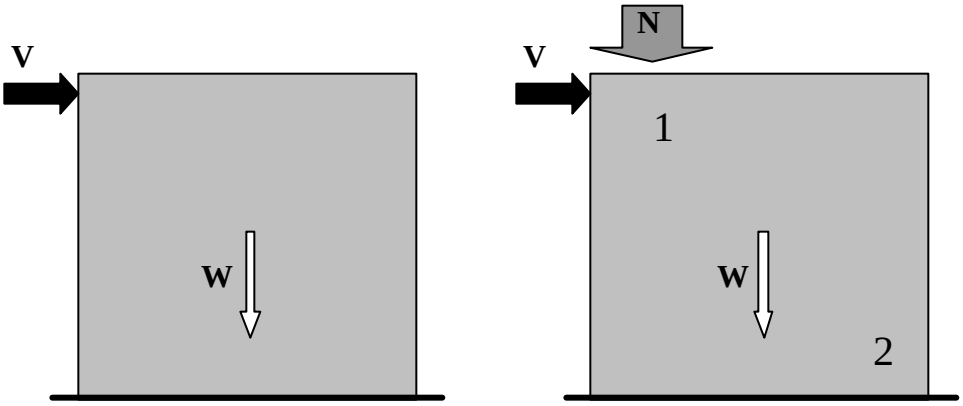

a) Non-loaded wall *b) Loaded wall*

Figure 5.9

When the wall under shear action is subjected only to its own weight (see Figure 5.9a), as the case of infill walls, the value of t_2 to be considered is the minimum, corresponding to the value t_0. Actually, this value is present only in the upper area of the wall, but has to be considered for the overall panel as the failure for sliding would be triggered from the top to the bottom once this friction strength is overcome.

When a load-bearing wall is subjected to a lateral force applied to an upper corner, for equilibrium the axial load tends to concentrate upon this corner (see Figure 5.9b). The maximum shear strength t_2 to be applied to the overall panel is the lower of the two values calculated with the Coulomb formula *(1)* in the positions 1 and 2. The compressive stress s to be considered in *(1)* is due to three quarters of total axial load in position 1 and only due to the own weight of the wall in position 2.

The FRP reinforcement contribution is calculated as:

$$V_{1F} = n\sum A_{f,i} f_{f,i} = n\, b t L_{tot}$$

Where:

n = number of the strengthened sides of the wall (1 or 2)
$A_{f,i}$ = nominal cross-sectional area of the i^{th} rod
$f_{f,i}$ = tensile stress in the i^{th} rod
τ = bond stress

L_{tot} = sum of the bonded lengths of all the rods crossed by the crack, calculated in the most unfavorable crack position (minimum total length).

The value of L_{tot} depends on the geometry of the wall, height H and length at the base B; and the spacing s of the rods (see Fig. 5.8).

Defining n_l as the number of reinforcement layers being crossed by a diagonal shear crack, which can be estimated as follows:

$$n_1 = \frac{D}{s} \qquad (2)$$

where: s = rod spacing

D = minimum dimension between *H* and *B*

Whenever the value computed using equation *(2)* is not an integer, it shall be rounded to the immediate inferior integer. The number of rods crossed by the 45° shear crack is estimated as:

$$r = n_1 - 1$$

If *r* is an odd number:

$$\boldsymbol{L_{tot} = 2s} \sum_{i=1}^{\frac{r}{2}} i$$

If *r* is an even number:

$$L_{tot} = (C+1)\, s + 2s \sum_{i=1}^{C} i$$

Where *C* is the immediate inferior integer of $\frac{r}{2}$.

Appling the above described formulas to the following example (see Figure 5.10), in which a square panel is isolated either from a slender wall or a squat wall, it possible to obtain:

$n_1 = 8$, $r = 7$, $C = 3$ and $L_{tot} = 16\, s$

as can be easily checked from the geometrical proportions.

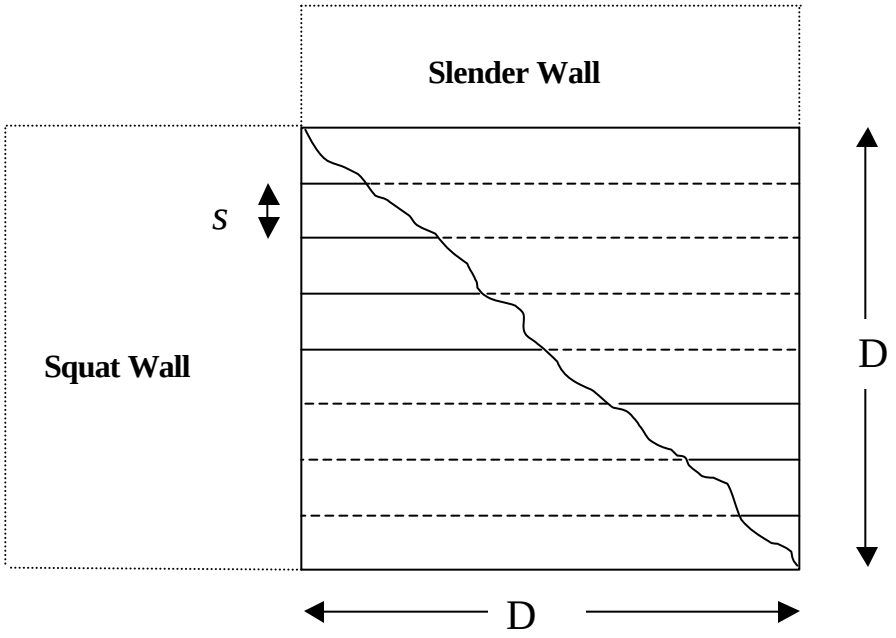

Figure 5.10

Calculation of V_{2F}

In presence of strong bonding or particular localized locking effects (see Section 4) and small rod sectional areas, tensile failure of the FRP rods having longer effective length may occur. Therefore, the shear contribution of the FRP reinforcement sometimes relies upon both debonding and rupture of the rods. V_{2F} can be calculated as sum of the contribution related to bonding limit and another part depending on the tensile strength of the rods. Thus two areas can be identified in a masonry panel (see Figure 5.11). This phenomenon can be described removing assumption 4) from the previously proposed model.

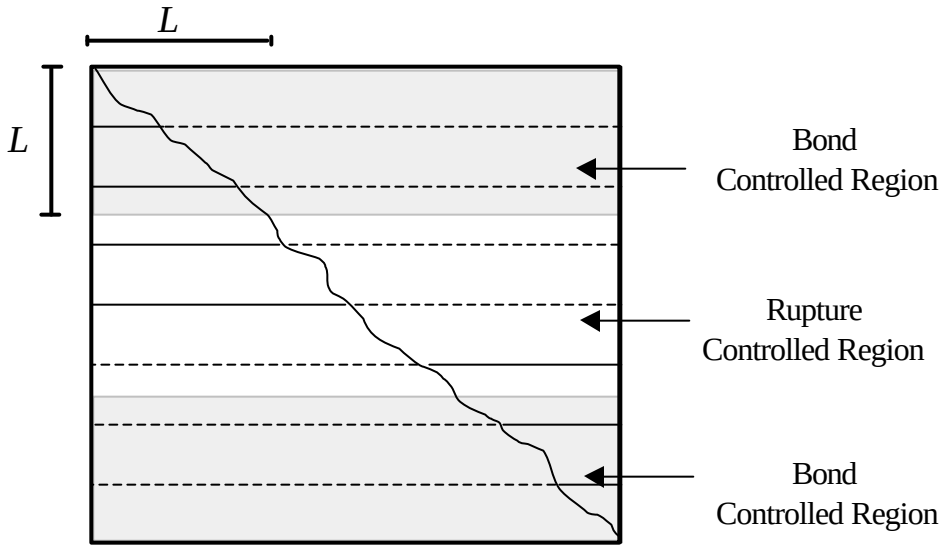

Figure 5.11: Controlling areas to calculate V_{2F}

L is defined as the length at which the rod breaks instead of being pulled-out, and can be derived from Figure 5.12:

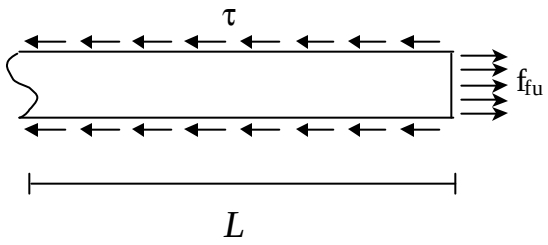

Figure 5.12.

By equilibrium:

$$A f_{f,u} = b L t$$

From which L is immediately calculated.

Nominal Shear in Bond Controlled Region (V_b)

The number of rods (r_b) in the bond controlled region can be quantified as:

$$r_b' = \frac{L}{s}$$

$$r_b = 2r_b'$$

The value of L_{tot} is calculated as:

$$L_{tot} = 2s \sum_{i=1}^{r_b} i$$

Shear in bond controlled regions now can be calculated similarly as seen for V_{1F}:

$$V_b = n\ b\ t\ L_{tot}$$

Nominal Shear in Rupture Controlled Region (Vt)

The number of rods (r_t) in the rupture controlled region can be quantified as:

$$r_t = r - r_b$$

The shear force resisted by the FRP rods in this region can be calculated as:

$$V_t = n\ r_t\ A_f\ f_{fu}$$

Where the design ultimate tensile strength $f_{f,u}$ is determined using the environmental reduction factor (see Table 5.3) for the appropriate fiber type and exposure condition:

$$f_{fu} = C_E f_{fu}^*$$

Where f^*_{fu} is the guaranteed ultimate tensile strength of the FRP rod as reported by the manufacturer.

Table 5.3. Environmental Reduction Factor for various fibers and Exposure Conditions

Exposure Condition	Fiber Type	Environmental Reduction Factor, C_E
Enclosed Conditioned Space	Carbon	1.00
	Glass	0.80
	Aramid	0.90
Unenclosed or Unconditioned Space	Carbon	0.90
	Glass	0.70
	Aramid	0.80

The shear force resisted by the FRP rods in both regions can be estimated as:

$$V_{2F} = V_b + V_t$$

5.3.6 SHEAR STRENGTH DESIGN

The ultimate shear force must comply with:

$$V_u \leq \phi V_n$$

The 1997 UBC specifies that the reduction factor ϕ is equal to 0.6. However, whenever the nominal shear strength is larger than the shear corresponding to the development of nominal flexural strength, ϕ can be equal to 0.8. For masonry structures strengthened using FRP rods, it is suggested to maintain the previously described reduction factors for the masonry and steel contributions; and to apply a conservative reduction factor f equal to 0.5 to the FRP contribution. The EC6 specifies different safety factors for the steel and masonry contributions. Obviously, this latter one is more restrictive and depends on the quality of execution of the assemblage. As the effectiveness of FRP surface mounted reinforcement is intrinsically connected with the status of the masonry support, it is suggested to maintain also for the FRP contribution the masonry safety factor. Unfortunately, when dealing with existing masonry assemblages, codes often lack indications on how to estimate suitable safety factors.

5.3.7 FINAL CONSIDERATIONS

Mechanical anchoring can prevent debonding failure, forcing the bars reaching their maximum strength. In this case, the shear contribution of the FRP reinforcement is based on the assumption that rupture of all the rods occurs simultaneously. Obviously, attention has to focus on detailing of anchoring to provide the necessary strength and fixity.

As for reinforced concrete, also the contribution of masonry interlock along the crack faces should be taken into account in the evaluation of the shear capacity. In this case, a limit value for the strain in the reinforcing rods should be introduced. In fact, this limit strain implies that narrow cracks are maintained, assuring in this way that aggregate interlock forces can still be transmitted through the crack. The suggested maximum strain for RC members is 4000 με (Khalifa et al., 1998. [56]). This strain level is confirmed in masonry assemblages by the tests performed during the current investigation, as it corresponded to presence of interlock and noticeable crack width. If data relative to the contribution from rods dowel action were available that limitation could be reconsidered.

6 CONCLUSIONS AND FUTURE RESEARCH

CONCLUSIONS

GENERAL

Unfortunately, many field applications involving the use of FRP laminates on masonry members are carried out even if not supported from the necessary experimental background. Cause of that is the implicit assumption that the high performances of FRP benefit in any case a compromised structural situation; over reinforcement is the logical consequence of this diffuse approach. Also the advantage of the external FRP applications to be removable is often used as incentive for designers to take non-evaluated risks. The present experimental investigations demonstrated the detrimental effect produced by inaccurate design and improper reinforcement distribution on the structural member.

FRP Structural Repointing has the advantage of providing remarkable structural benefits maintaining the original appearance of the masonry wall.

In addition, using FRP materials instead of steel, the Structural Repointing completely complies with durability and maintenance issues. It represents an ideal final strengthening solution. Structural repair is reversible, as it could be removed and the joints refilled with mortar once the causes of retrofitting may have changed or new materials become available. The new system introduced offers a valid alternative wheb standard retrofitting systems are often inapplicable because of the environmental exposure and aesthetic requirements.

The ease of application of the FRP Structural Repointing, added with the limited equipment requirements, results in a time saving procedure. The lightweight materials and “surgical” operations do not require the use of many scaffolding or cranes for applications at higher levels.

Anchoring FRP reinforcement to adjacent structural members (e.g. beams, columns, slabs) makes this technology suitable for bearing and non load bearing walls, infill walls, one or multi-layer walls.

From the laboratory tests, the FRP Structural Repointing has shown to dramatically improve shear and bending moment capacities under static or cyclic in-plane and out-of-plane loads. Also the residual load bearing capacity remains remarkable even after high damage levels were introduced.

Areas of applications of the FRP SR can be identified as general strengthening**,** seismic retrofitting, structural rehabilitation, structural and architectural maintenance.

PARTICULAR

The dominating failure mechanism causing the collapse of the clay brick flexural and shear specimens is related to the sliding of the epoxy mortar within the groove. The resisting mechanism is based upon friction that depends on the constituent materials and on the normal stress applied perpendicularly to their interface. Therefore, the performance of the SR method in a full-scale wall subjected to its self-weight is expected to be higher than for laboratory samples.

This mechanism determined energy dissipation during cycles of load and presented post-peak semi ductile behavior till complete collapse occur.

Block masonry walls subjected to flexural testing presented brittle failure due to splitting of the epoxy paste. This mechanism, involving the cracking of the embedding paste, tend to provoke sudden collapse of the structure.

The diagonal compressive test revealed to be effective for what concern the identyfication of fundamental mechanisms governing the behavior of the reinforced panels.

Proposed design guidelines on the masonry strengthening with FRP rods, are the first attempt of analitical approach to this subject. Obviously, as Structural Repointing was introduced in the present research, nothing is avaible as reference. The general model to evaluate the shear capacity of the laminate and rod reniforced panels is a global approach to estimate the qualitative behavior of externally FRP strengthened walls. Parameters introduced in the general model were selected to fit the experimental result of the present research and, in case of laminate reinforcement, of previous works.

FURTHER RESEARCH

The overall objective of the present study was to carry out a preliminary investigation on FRP Structural Repointing as a strengthening system. Due to its novelty, extensive experimental and analytical work is needed to characterize and predict the structural behavior of masonry members externally strengthened with this technique. The ultimate goal is to develop design formulae and construction specifications, since these are the means through which an experimental technology can become accepted field practice.

Experimental investigations on the flexural strengthening of full-size masonry panels with FRP Structural Repointing subjected to in-plane loading are currently ongoing at the University of Missouri – Rolla. The use of different standard shear tests is considered in order to isolate those factors inflluenced by the specific set up of each test.

As FRP Structural Repointing is a strengthening technique proposed with the aim to provide a product system able to solve, with aesthetic sensitivity, different structural

problems of masonry members, further studies are already oriented to increase the potentiality of the system introducing special structural elements providing a connection between the horizontal/vertical masonry courses. These connectors can be embedded with the rods. They consist of shaped FRP components, which provide vertical intra-courses collaboration to create vertical resistant bands behaving as supports for the horizontal strengthening. In addition to that, also layers connections for multi-wythe walls are under investigation. Specific solutions have been introduced using FRP special elements to solve also anchoring and splicing problems.

As far as the results presented in this dissertation are concerned, slip and strain data collected from the flexural and shear tests on masonry needs to be analyzed, in order to calculate the effect of the development length of the rods in comparison with the design predictions prospected.

Further laboratory tests and analytical investigations are needed to assess the validity of the proposed design approach and to incorporate in the design formulae the influence of all the significant variables. Also in in-situ test could reveal the actual effect of the one side FRP Structural Repointing under service load condition.

Even if at the moment some aspects of FRP Structural Repointing still need to be submitted further investigation, field applications of the technology could be performed under appropriate supervision.

For what concern the FRP laminate and hybrid laminate-rod reinforcing systems, additional experimentation on coupon and full scale walls could advance the knowledge of mechanisms related to particular set up, anchoring and boundary conditions.

APPENDIX A
In-field Experimental Project.

The Malcolm Bliss Hospital In St. Louis

A1 BACKGROUND

Test Specimens. Seven URM walls, constructed of clay units, were tested (Tumialan et al., 2000. [49]). The nominal dimensions of these walls were 2.4 x 2.4 m. (8 x 8 ft); their overall thickness, including the two wythes was 33 cm. (13 in). The upper and lower boundaries for these walls were RC beams which were cast integrally with the floor system beams. The test walls, classified as infill, belong to a masonry typology commonly used during a window time including the post-war years and the early 1960's. A section view of a typical wall is illustrated in Figure 1.

The walls under investigation consisted of two wythes of masonry units spaced at 2 cm. (0.75 in.), joined by header units placed at each fourth course, and at each fourth unit in the course in mention. The outer wythe, corresponding to the veneer wall, was built using cored units with the following actual dimensions, 9.5 cm. (3.75 in.) wide, 5.7 cm. (2.25 in.) high and 20 cm. (8 in.) long, the units had three cores of 3.75 cm. (1.5 in.) diameter. The inner wythe or backup wall was primarily constructed using tile units. The actual dimensions of the tile units were 18.75 cm. (7.5 in.) wide, 18.75 cm. (7.5 in.) high by 30 cm. (12 in.) long. Bricks were laid where brick headers were placed, their dimensions were 10.6 cm. (4.25 in.) wide, 5.6 cm. (2.25 in.) high and 21.25 cm. (8.5 in.) long (see Figure 1). The walls were finished with one-inch thick cementitious plaster, having a two-directional welded steel mesh at mid-depth. The welded steel mesh was provided to help control shrinkage of the cementitious plaster.

Two URM walls, designated as Wall 1 and Wall 2, were used as control specimens. In Wall 1 the plaster remained on its surface; whereas, in Wall 2 the plaster was removed to differentiate the impact of plaster. The remaining specimens were strengthened with different composite materials, namely GFRP, AFRP, CFRP and deformed glass rods. Thus, Wall 3 was strengthened with three 50 cm. (20 in.) wide GFRP strips attached to the plaster surface. The strengthening scheme for Wall 4 was similar to that of Wall 3, the main difference was that the GFRP strips were applied directly to the masonry, meaning without the presence of plaster. The purpose of testing this group of walls was to observe the difference in behavior, if any, in walls strengthened with FRP attached to plaster and to masonry under out-of-plane loading. One of the advantages of using composite materials is that little disruption is caused during its installation. That was the purpose of studying the behavior of walls strengthened without the removal of plaster. Thus, in the remaining walls the strengthening was carried out with the presence of plaster.

In Wall 5 and Wall 6 the strengthening geometry was similar to Wall 3. In the first case the URM wall was strengthened with AFRP; whereas, in the latter case CFRP was used as the strengthening material.

The fact that the anchorage of near-surface-mounted rods into adjacent RC members (i.e. slabs, columns and beams) is a feasible task, makes attractive their use for increasing the flexural strength of masonry walls. In that sense, Wall 7 was strengthened with eight #3 glass rods spaced at 30 cm. (12 in.) o.c. A summary of the experimental program is documented in Table A1.

Table A1: Experimental Program for Out-of-Plane Walls

Specimen	Strengthening System	Reinforcing Scheme	Attached to
Wall 1	Control	-------	Plaster
Wall 2	Control	-------	Masonry
Wall 3	GFRP Sheets	Three strips (width=20 in)	Plaster
Wall 4	GFRP Sheets	Three strips (width=20 in)	Masonry
Wall 5	CFRP Sheets	Three strips (width=20 in)	Plaster
Wall 6	AFRP Sheets	Three strips (width=20 in)	Plaster
Wall 7	Glass Rods	Eight #3 near-surface mounted rods	Plaster

Test Setup. The masonry walls were tested under two out-of-plane loads, which were distributed by 30 x 30 x 1.25 cm. (12 x 12 x ½ in.) steel plates to the external face of the wall. The loads were generated by means of a hydraulic jack using a manual pump. The force created by this jack reacted against a five foot steel girder composed of two C10x20, hereafter called Beam A, and an 11 foot steel girder composed of two C15x40, hereafter referred as Beam B. When loading, two reacting forces were created on Beam A. These forces were transmitted to the masonry wall using two high strength rods (see Figure A1), which through of the steel plates pulled the wall from its exterior face. On the reaction side, the force generated by the hydraulic jack reacted against Beam B, which transmitted the load to the upper and lower RC beams, and floor system. Beam B erected into place using an electric hoist located at the roof level. The hoist was restrained by a metal frame located on the roof of the building. In this manner Beam B could be raised or lowered, depending on what wall was being tested. A schematic representation of the test rationale is illustrated in Figure A2.

Fig. A1: Infill wall under testing

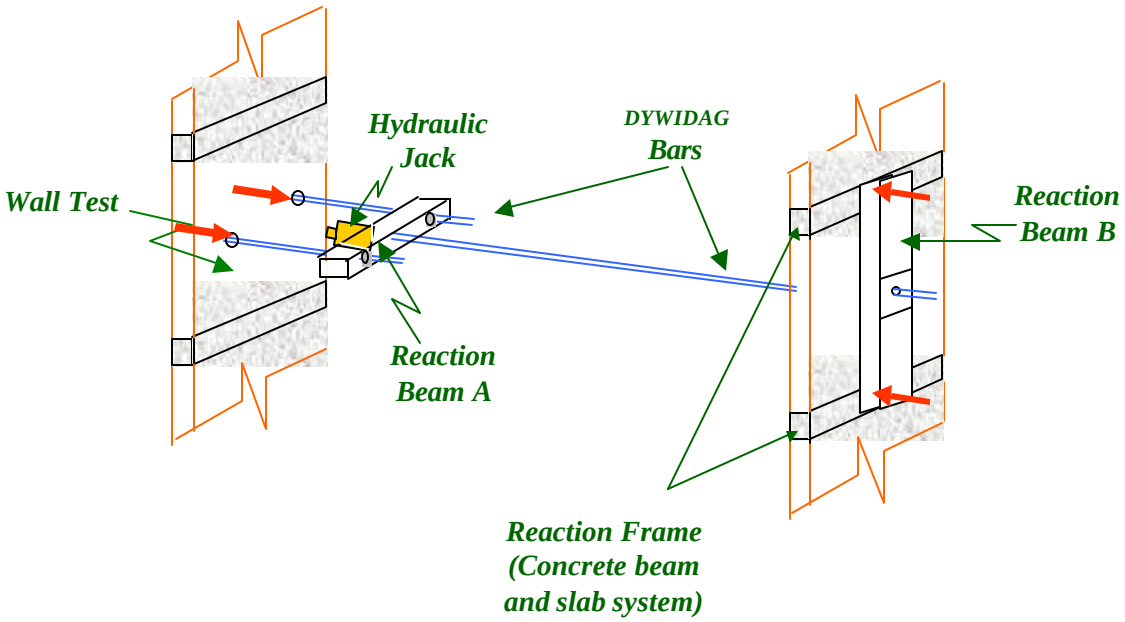

Figure A2: Out-of-Plane Test Rationale

Test Results. For most of the test walls, the first visible crack was observed running above the central brick course, along the bed joint. Following this, horizontal cracks formed at a quarter height measured from the top or bottom of the wall. Once the peak load was reached the load decreased abruptly. A mechanism of failure caused by a shear-compression effect lead to the fracture of clay tiles located either at the top or bottom region of the wall (see Figure A3).

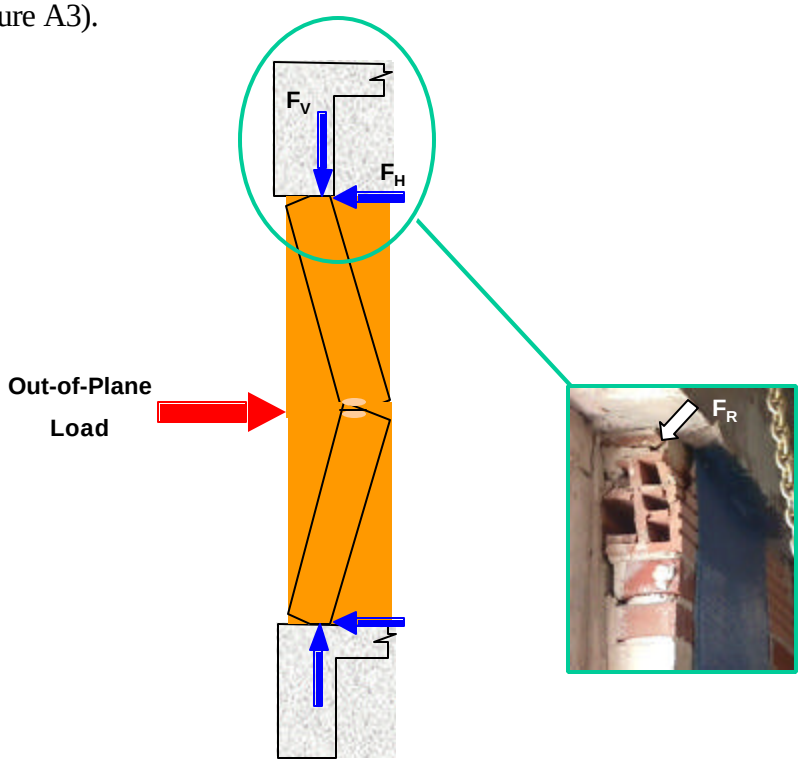

Fig. A3: Out-of-pane mechanism of failure.

Due to this progressive mode of failure, the walls were not able to develop a higher capacity compared to the control specimen (see Figure A4).

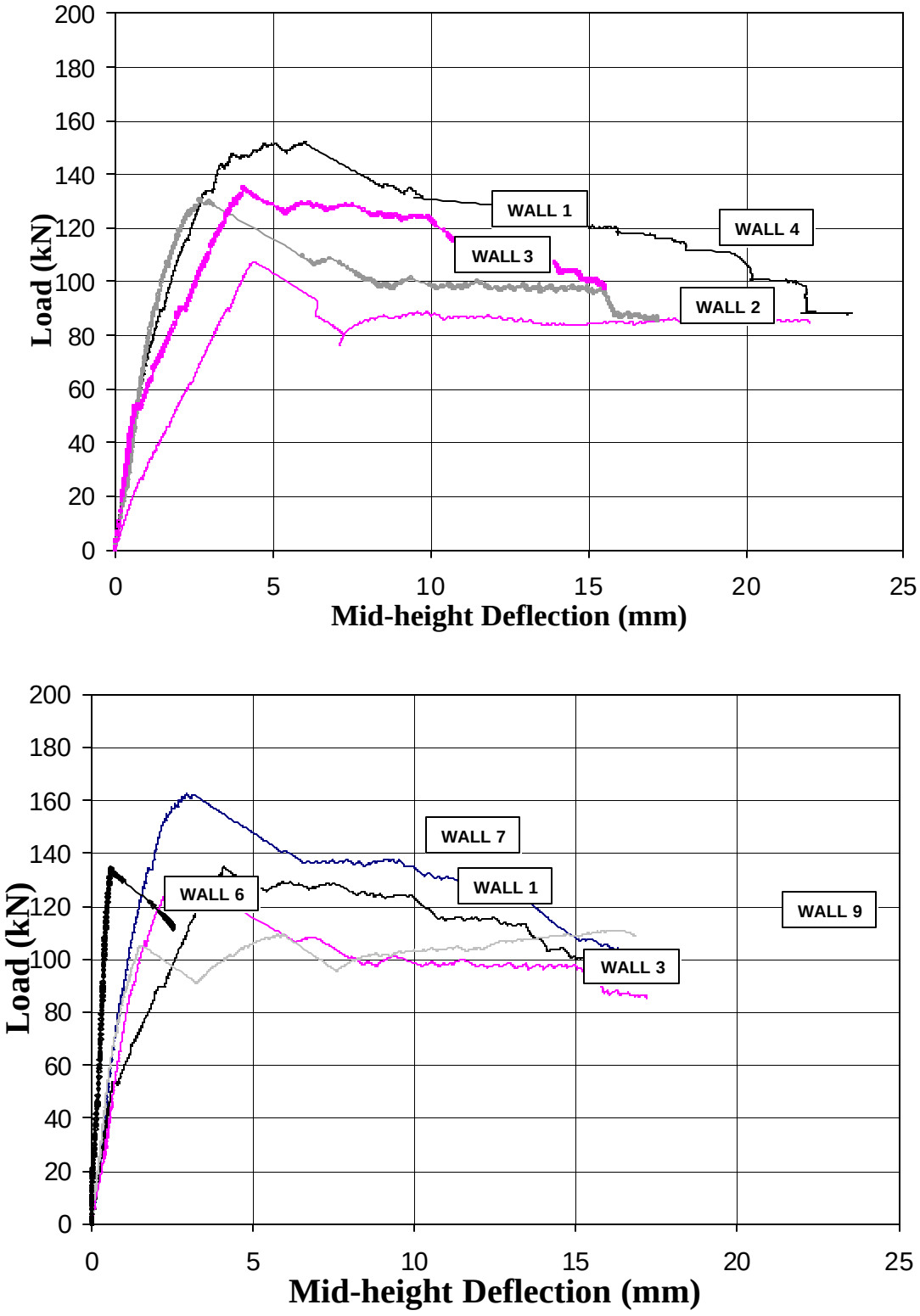

Figure A4: Behavior comparison graphs.

Mechanism of failure. The failure of the URM walls was caused by the fracture of the tile units at the uppermost or bottommost courses, caused by angular distortion due to out-of-plane rotation, and mainly by a force generated by a shear-compression combination effect. Flexural cracking occurred at the supports due to the negative moment followed by flexural cracking at mid-height due to the positive moment, as a result a three-hinged arch was formed. When the deflection increased due to out-of-plane bending, the wall was restrained against the supports, at the upper and lower boundaries. This action induced an in-plane compressive force (F_V in Figure A3), which accompanied by the shear force (F_H in Figure A3) in the support created a resultant force that caused the fracture of the tile (F_R in Figure A3). It is important to mention that normally failure caused by arching action is associated to the crushing of mortar joint; however, due to the characteristics of the tile and its placement with the holes horizontally oriented, the failure is associated to this element

A2 MATERIAL CHARACTERIZATION

One inherent difficulty when conducting a testing program in situ is to characterize the materials. In order to obtain results that can be used to explain the Malcom Bliss Hospital walls behavior, different material characterization tests needed to be performed on the site specimens.

There are standard specifications from ASTM and RILEM codes that must be observed, but sometimes is not feasible comply with those standards when dealing with field applications. That is due to the limited dimensions of the available specimens, as destructive removing operations are usually prevented. In addition, some non-standard tests can be designed with the aim of a specific application of the results, such is the case of a successive numerical analysis.

From a demolished part of the walls it was possible to remove only some bricks and two small samples. Cutting those samples, some regular specimens suitable for testing, were obtained.

Brick tests. The cored clay bricks from St. Louis hospital have been subjected to the modulus of rupture test and the halves obtained were singularly for compressive test.

Totally five veneer bricks (facings) and three solid clay bricks (cutters) constitute the statistical samples from the site walls (see Figure A5 and A6).

Although they have standard dimensions (see Figure A7), the facing bricks are no longer under production; their strong firing and the clay mix without chips of crushed bricks, coming from recycling of wasters, granted them properties that presently are difficult to reach with equivalent bricks.

Historical references from the Masonry Institute of St. Louis confirmed that the laying of the hospital walls was popular during the fifties and later. Every three layers of runners one of headers make the wythes collaborating together (see Figure A5).

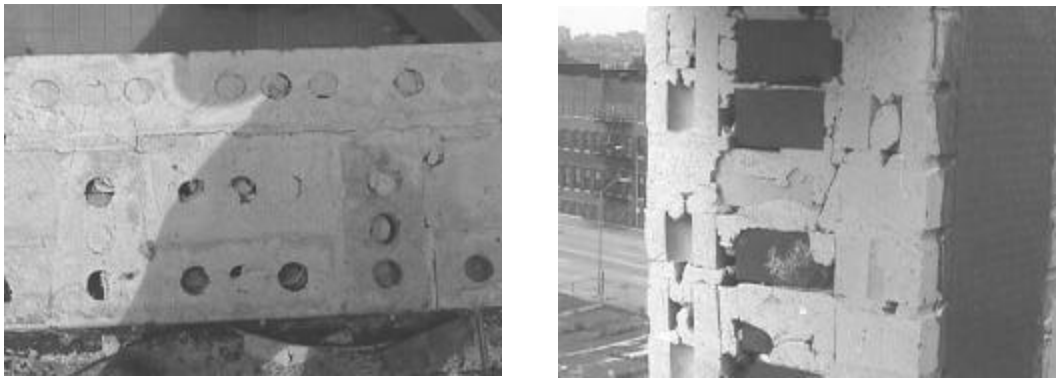

Fig.A5: Typical textures with headers and running bricks. Three wythes wall..

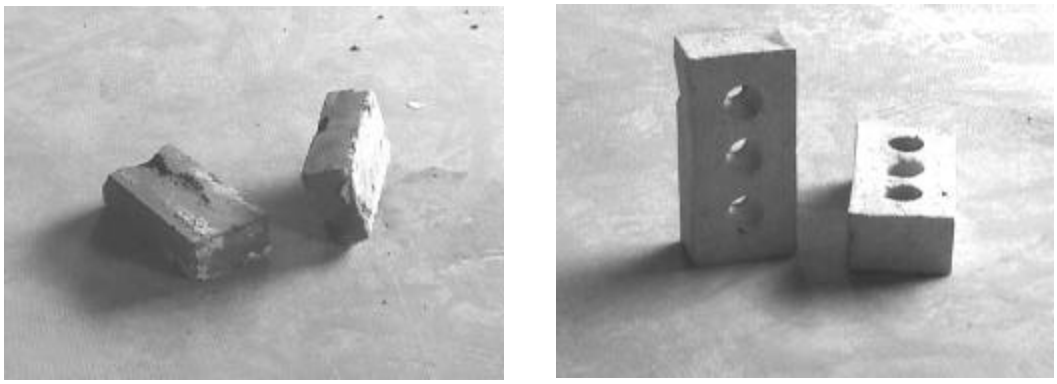

Fig. A6: filling bricks (cutters), bearing and veneer bricks (facings)

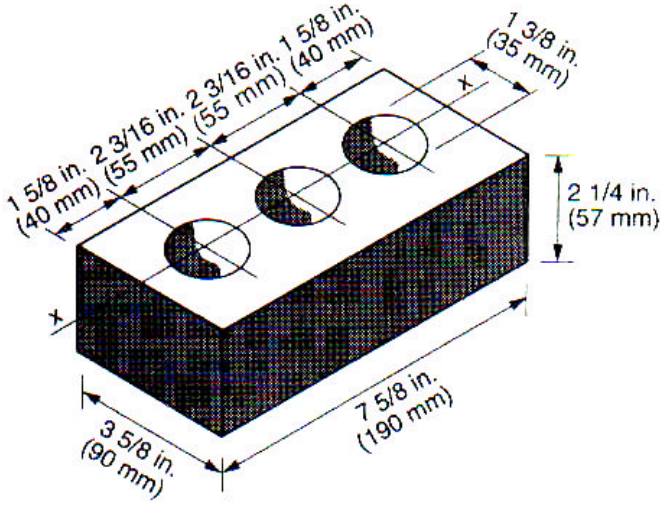

Gross Area	27.64 in.^{2}	(17,100 mm^2)
Net Area	23.20 in.^{2}	(14,215 mm^2)
Percent Solid	84 %	(83 %)
Moment of Inertia about x - axis		
Gross Section	30.27 in.^{4}	(11.54 x 10^{6}mm^4)
Net Section	29.75 in.^{4}	(11.32 x 10^{6}mm^4)
Ratio of Net to Gross	0.98	(0.98)

Fig.A7: standard dimensions.

Using the net nominal dimensions of the brick, in Table A2 the modulus of rupture and the compressive strength are calculated and the average value is given.

Table A2

VENEER

	MODULUS OF RUPTURE			COMPRESSIVE TEST		
	Load (lbs)	Fr (psi)	Fr (MPa)	Load (lbs)	Fc(psi)	Fc(MPa)
	3550	2524	17.42	35200	3034	20.94
	1475	1049	7.24	34500	2974	20.52
	3100	2204	15.21	15200	1310	9.04
	2125	1511	10.43	13900	1198	8.27
	2400	1707	11.78	23000	1983	13.68
Average	**2530**	**1799**	**12.41**	**24360**	**2100**	**14.49**

RED BRICKS

	MODULUS OF RUPTURE			COMPRESSIVE TEST		
	Load (lbs)	Fr (psi)	Fr (MPa)	Load (lbs)	Fc(psi)	Fc(MPa)
	555	188	1.30	6800	378	2.61
	360	122	0.84	4275	238	1.64
	295	100	0.69	3275	182	1.26
Average	**403**	**137**	**0.94**	**4783**	**266**	**1.83**

Mortar tests. Since it was impossible have standard tests of the mortar from the available specimens, the only way to characterize its properties was to exploit some among the most regular cylinder shaped cores of mortar trapped into the hollow bricks.

Fortunately the geometric proportion of those mortar cylinders allowed to have limited local confinement at the ends. This can be seen in the failure mode (see Figure A8).
Test on mortar cylinder specimens as big as twice the present ones are indicated as field test standard (The Brick Institute of California, 1986. [2]).

From the average compressive strength on three cylinders (see Table A4) and by comparison with the standard requirements (see Table A3 from standard ASTM C270), it was possible to identify the mortar as type N

Only the kind of hydraulic binder used to obtain the type N mortar was still unknown.
References from The Masonry Institute confirmed that still during the sixties in most of the cases, due to workability reasons, cement-lime mortar was used.

Table A3

Mortar	Type	Proportions by volume (cementitious materials)					Aggregate ratio (Measured in damp, loose conditions)
		Portland cement or blended cement	Masonry cement			Hydrated lime or lime putty	
			M	S	N		
Cement-lime	M	1	–	–	–	$\frac{1}{4}$	Not less than $2\frac{1}{4}$ and not more than 3 times the sum of the separate volumes of cementitious materials
	S	1	–	–	–	Over $\frac{1}{4}$ to $\frac{1}{2}$	
	N	1	–	–	–	Over $\frac{1}{2}$ to $1\frac{1}{4}$	
	O	1	–	–	–	Over $1\frac{1}{4}$ to $2\frac{1}{2}$	
Masonry cement	M	1	–	–	1	–	
	M	–	1	–	–	–	
	S	$\frac{1}{2}$	–	–	1	–	
	S	–	–	1	–	–	
	N	–	–	–	1	–	
	O	–	–	–	1	–	

Table 4.10 Property Specification Requirement for Mortar*
(from Ref. 4.38)

Mortar	Type	Min. average compressive strength at 28 days, psi (MPa)	Min. water retention, %	Max. air content, %	Aggregate ratio (measured in damp, loose conditions)
Cement-lime	M	2500 (17.2)	75	12	Not less than $2\frac{1}{4}$ and not more than 3 times the sum of the separate volumes of cementitious materials.
	S	1800 (12.4)	75	12	
	N	750 (5.2)	75	14**	
	O	350 (2.4)	75	14**	
Masonry cement	M	2500 (17.2)	75	...†	
	S	1800 (12.4)	75	...†	
	N	750 (5.2)	75	...†	
	O	350 (2.4)	75	...†	

* Laboratory-prepared mortar only.
** When structural reinforcement is incorporated in cement-lime mortar, the maximum air content shall be 12%.
† When structural reinforcement is incorporated in masonry cement mortar, the maximum air content shall be 18%.

Table A4

MORTAR CHARACTERIZATION

SPECIMEN	CILINDER COMPRESSION		
	Load (lbs)	Fc(psi)	Fc(MPa)
1	1400	943	6.51
2	1112	749	5.17
3	1110	748	5.16
average	**1207**	**814**	**5.61**

Fig. A8: Failure mode of the specimens tested.

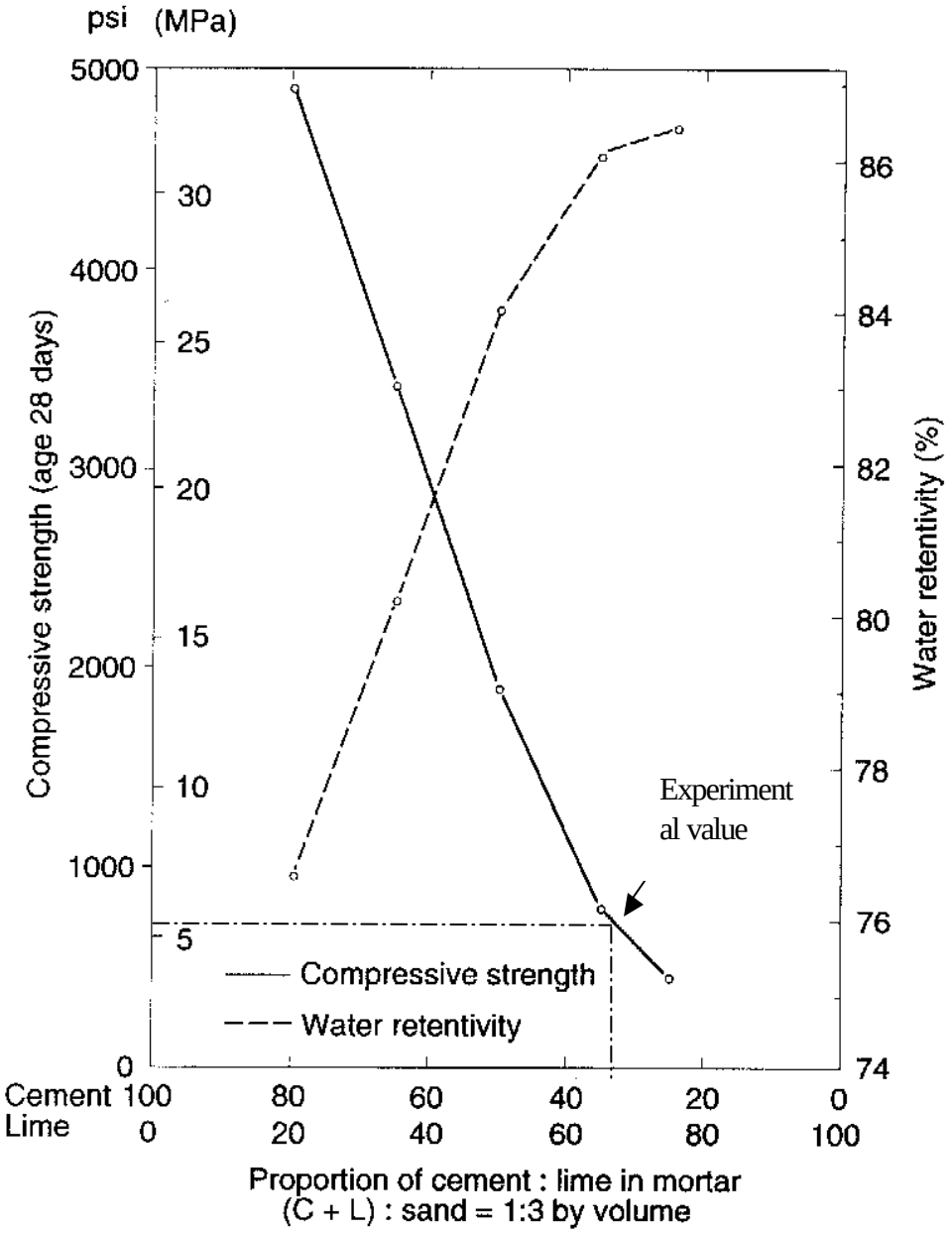

Fig.A9: *Strength-composition relationship*

The actual cement-lime ratio can be revealed only by a chemical investigation on the gypsum amount.
However, it is possible a comparison with reference graphs on the strength-composition relationship (see Figure A9). Compressive strength is greatly influenced by the amount of cement present in the mix; alternatively, water retentivity and, therefore, workability increase significantly with increasing amount of lime. Supposedly the lime-cement ratio used in tested mortar was about two.

Unit-mortar interface tests

Tensile strength. For tensile loading perpendicular to the bed joints, failure is generally caused by failure of the relatively low tensile bond strength between the bed joint and the unit. (see Figure A10).

Ultimate load:	325 lbs
Area of mortar:	2.95 in^2
Ultimate tensile strength:	f_t=110.2 psi (8.5% of f_c)

Fig. A10: Tensile test on a one-joint specimen obtained sampling the masonry assemblage.

Shear test. An important aspect in the determination of the shear response of masonry joints is the ability of the test set-up to generate a uniform state of stress in the joint.
In order to obtain as much specimens as possible from the same irregular sample from the hospital walls, the use of couplets seemed to be the most rational (see Figure A11).
Nevertheless, to avoid major secondary effects a particular configuration was used. (see Figure A12)

Fig. A11: Stress distribution in the couplets. Specimen tested.

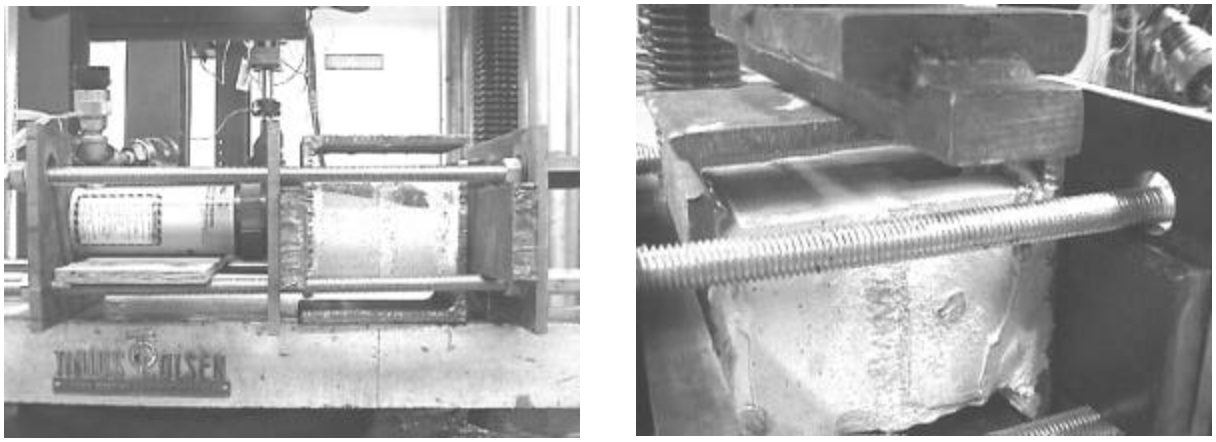

Fig. A12: Test apparatus

The steel plates, glued by epoxy paste, allowed shear transmission and joint lateral deformation.
Having six specimens it has been possible to tests them under shear action and contemporary applying different values of compressive stress at the joint; using this method, the coulomb friction law of the joint was obtained.

$$t = m\,s + t_0 \qquad \text{(typical value } 0.5<\mu<0.7\text{)}$$

Applying dial gages for a sensitive manual reading the stress strain relationship were found for each specimen. The behavior was linear for all the lateral compression levels.
At the two highest lateral loads an interlock mechanism was visible after the opening of the crack and a noticeable request of pressure of the pomp to avoid dilatation in the joint.
The profile of the crack in the joint was located in the brick-mortar interface.

Masonry properties

Prisms tests. Compression tests of masonry prisms are used as the basis for assigning Youg modulus and design stress.

The standard ASTM E447-74 describes test equipment, procedures and reporting of prism tests.
Two methods are allowed each one with specific geometry limitations.

Method A: […] height to thickness ratio not less than two.
Method B: […] the height of the prism shell be at least twice the thickness and a minimum of 15 inches.

Unfortunately, it was possible only obtain three two-layers and one three layers specimens (see Figure A13). However the crack at failure did not revealed inclined patterns typical of high influence of confinement at the ends. Therefore the only foreseeable effect of having non-standard specimens is a higher stiffness due to the limited number of vertical joints.

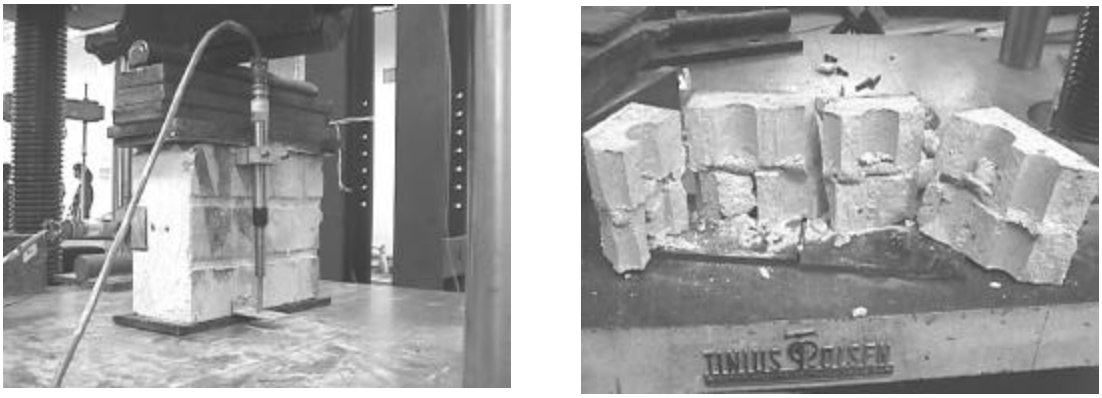

Fig. A13: Test set up of the prisms for compressive tests. Failure pattern.

The masonry prism characteristics obtained are the following:

Compressive strength	f_m=	1300 psi	
Modolus of elasticity	E_m=	1100 ksi	$E_m=846f_m$ (see Figure A15)
Compressive strain	ε_m=	0.0039	(typical value 0.0035)
Poisson ratio	ν =	0.16	(typical value 0.15)

All the specimens had a similar compressive stress; the average value is 1303 psi.
The stiffness instead varied noticeably among the different specimens.
As the specimens derived from the same part of the site wall, secondary effects due to their geometry and the test set-up were, with the scarce sensitivity of the data acquisition system, most likely the cause of that inconsistency. The stiffness value of the first specimen was reputed the one most significant, because of accompanied with a close to theoretical forecasts stress-strain relationship.

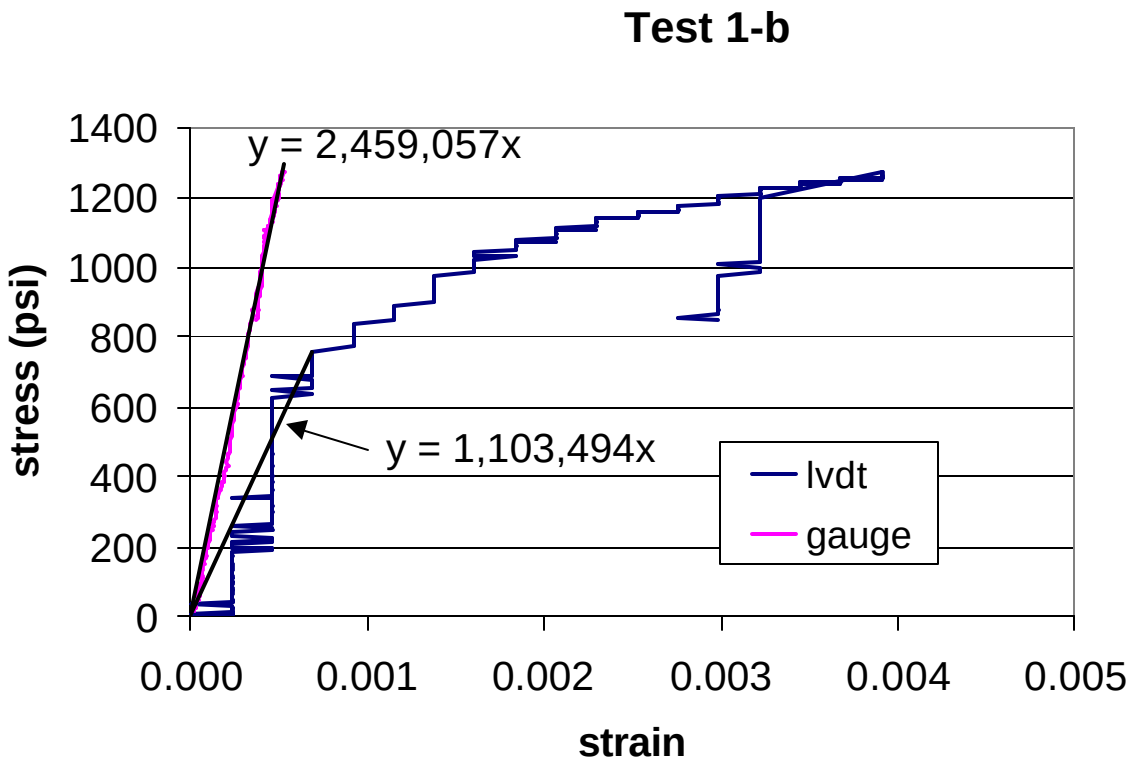

Fig. A14: Stress-Strain relationship of a tested specimen

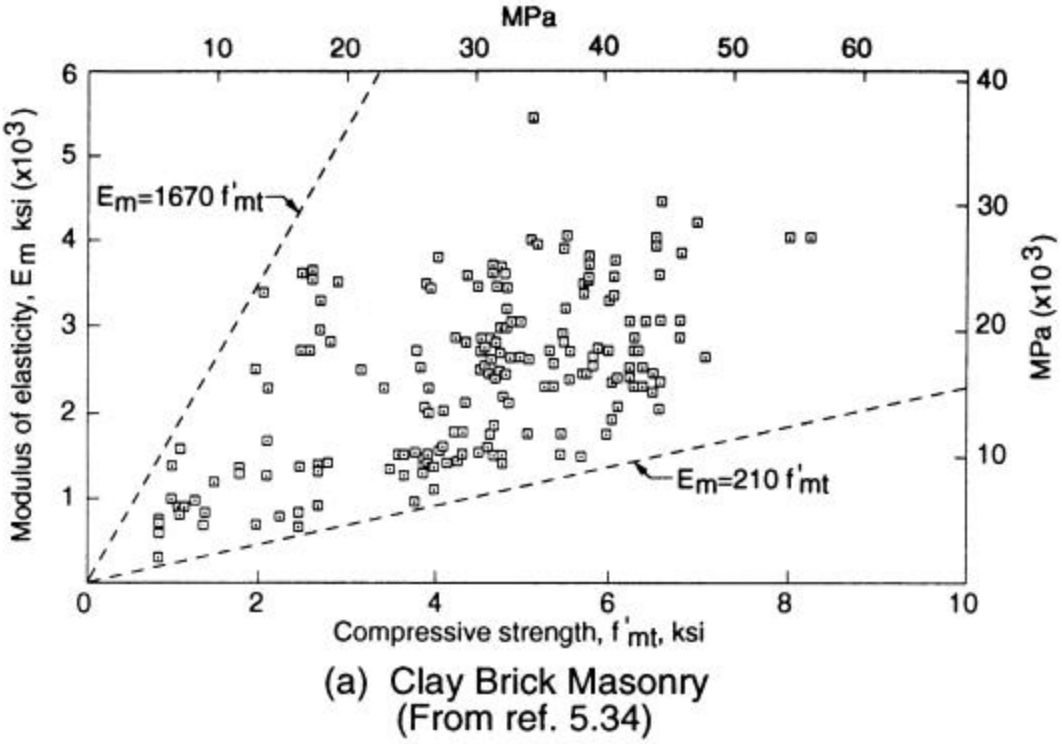

Fig. A15: Range of the Modulus of Elasticity- Compressive strain ratio.

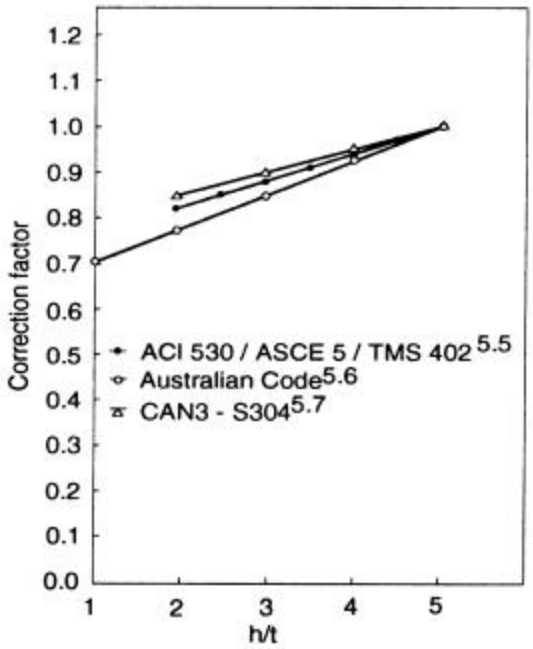

Fig. A16: Clay brick masonry reduction ratio

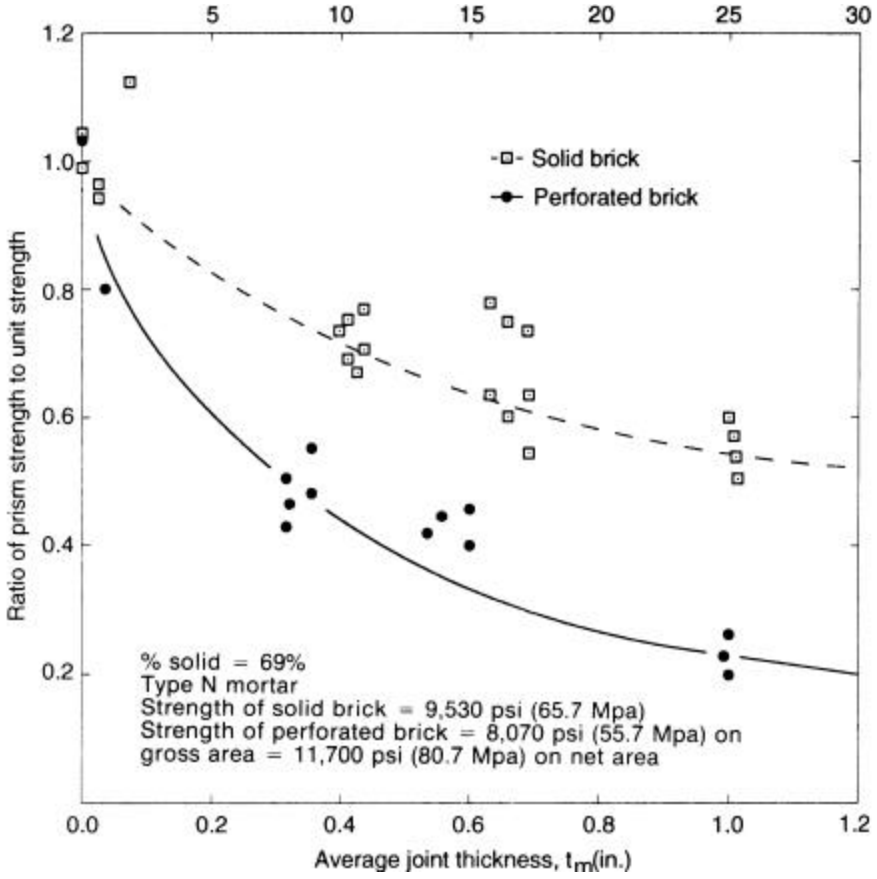

Fig. A17: Average joint thickness related to the ratio of prism strength.

A compressive strength reduction factor is usually applied to take into account the slenderness of real walls compared with the test prism. ASTM code has a linear reduction with the height to thickness factor between two and five. Extending this line to the h/t factor of the specimen tested it was possible obtain a precise reduction factor.
This procedure can be supported by the fact that other codes, as the Australian one, allowing inferior ratios, have a wider range of reduction factors. (see Figure A16)

As a further validation of the performed material characterization, a comparison with experimental data provided by other authors (Sahlin, 1971. [1]) and relative to bricks used in the same period of time is proposed (see Figure A17). The compressive strength obtained from the prism tests can be related to the one of the bricks and compared with reference graphs showing the relation of the masonry-brick ratio with the thickness of the joints. The average joint thickness of the specimens tested was half inch and the experimental ratio of prism strength to unit strength is 0.620. In the former graph their intersection point fits with the solid brick curve. (The kind of cored brick tested have a net cross sectional area parallel to the bearing plane 84% of the gross area; so they are regarded as solid bricks. In fact the reference where the graph comes from defines perforated or hollow bricks the ones with the net-gross area ratio between 40% and 75%).

A3 ANALYTICAL MODEL

From the material characterization data, using formulas relative the arching effect and assuming the absence of tensile strength, it is possible to describe the unreinforced wall behavior.

Arching mechanism. An unreinforced wall restrained at the top and bottom and subjected to out-of-plane load tends to crack in correspondence tensile stress concentrations. Those cracked areas are located mid-height, on the side opposite to the load, and close to the ends on the side of the acting load. Masonry in these regions do not contribute to bear the lateral load, hence there must be a compressed band crossing the depth of the wall from one side to the other and back, constituting an arch structure between the supports. This phenomenon, called arching mechanism, provides further flexural capacity; in fact, as an arch, the uncracked sections of the wall are working in compression. A simple model to describe this phenomenon is three hinges arch, as excluding the dead material, the wall consists in two segments connected by a mid-height hinge and rotating around the supports as rigid bodies (see Figure A18). The limit of this rotational mechanism is the opposition, offered by the restrains, to the vertical component of the displacement.

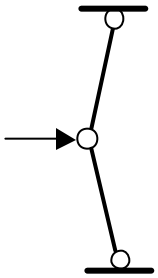

Fig. A18: Three hinges arch model

Snap through. An arching mechanism can only take place when the segment rotation is small enough so that an internal compression strut can develop. When the loading increases to the extent that the segment rotates beyond its limit, the wall will "snap through" if the compressive strain were less than which would result in crushing.
A derivation by Angel et al. (Drysdale, 1994 [3]) based on geometrical concepts and material strain offers criteria to establish the limit slenderness of the panel after which snap-through is the governing failure mode:

$$\left(\frac{h}{t}\right)_{max} = 0.981\sqrt{\frac{2}{e_{max}}}$$

Excluded this mechanism in the case under investigation, its now possible to consider different approaches to phenomena of crushing at the edges.

Crushing. When a wall submitted to horizontal load and arching effect is uniform, meaning that there are not different materials constituting its wythes, and those different layers collaborate as only one reacting section under bending action; then its the moment capacity can be calculated by equations based on the equilibrium conditions that exist when the wall snaps-through in two pieces:

$M_{max} = \sigma_u/4\ (d - d\sigma_u/E\varepsilon_m)^2$; where: $\varepsilon_m = \dfrac{\sqrt{d^2 + \frac{h^2}{4}} + \frac{h}{2}}{\sqrt{d^2 + \frac{h^2}{4}}}$ (Cohen and Laing, 1956)

Or:

$$M_{max} = \frac{s_u d^2}{4}\left(1 - \frac{e_u h^2}{2d^2}\right)^2$$ (Sven Salin,1971. [1])

The configuration of the barrier wall with external veneer usually does not match the former assumptions, therefore other models are needed.

Considering the specific case of Wall 2, the unreinforced wall without plaster, a simple approach based on equilibrium is here proposed:

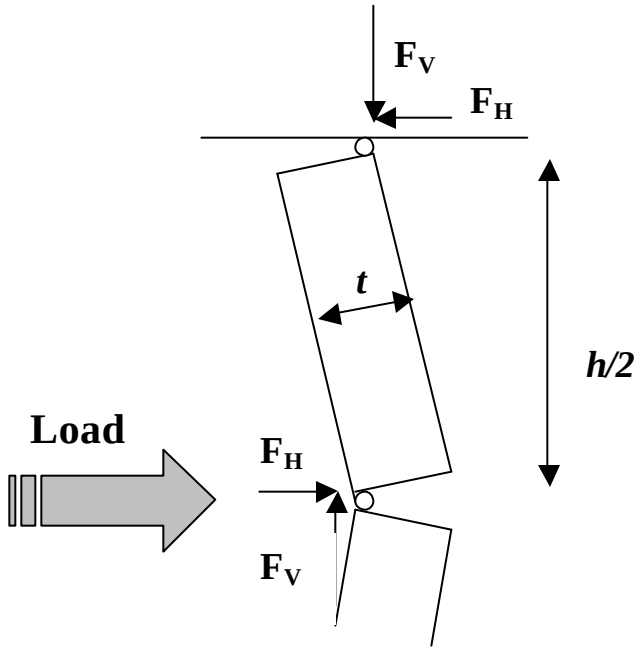

Equilibrium:

$F_V \times t = F_H \times (h/2)$

$F_V = (F_H \times h) / (2 \times t)$

Where: F_H= Load/2

For control Wall 2 we had: **h = 8'**
t = 12"
Load = 24 kips

Obtaining: **F_V = 48 kips**
F_H = 12 kips

Dividing the support reaction by the length of the wall we can compare it with the component of the ultimate diagonal compressive load from the tile test (see Figure A18):

F_H/96" = 125 lbs/in ; T/Ö2 = 190 lbs/in

Therefore the crushing of the tile was mainly due to the vertical reaction of the support.
Theoretically this vertical component was concentrated only on a bearing width of (from Angel, et al.1994):

$$b = (h/4)\left[1 + \sqrt{1-(e_{max}/2)(h/t)^2}\right] = 5.90"$$

Where: $e_{max} = e_{cu}(0.73-0.016h/t)$ (assuming that ε_{cu}=0.0035)

Assuming a linear stress distribution on the bearing width, the maximum compressive stress on the tile's edge is:

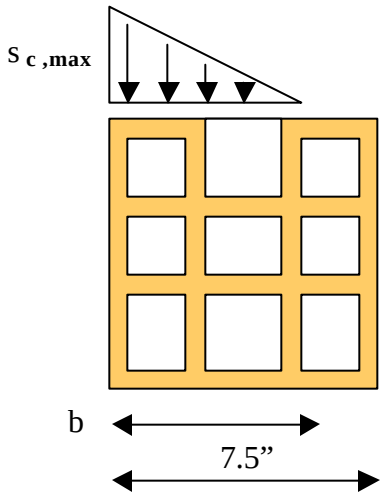

$s_{c,max} = 2[F_V / (8' \times 5.90")] = 170$ psi

Fig. A18: Tile shear test

This value of ultimate bearing stress, obtained with reasonable assumptions for a qualitative description of the phenomenon, is confirmed from the compressive test on the tiles; clearly, having the presence also of a horizontal component, due to shear, it is reasonable have:

$$s_c < s_\wedge$$

Therefore equilibrium relations, applied to Wall 2, seem to explain the actual crushing failure.

For the other walls, the FRP reinforcement caused a gain of stiffness that prevented a clearly located mid-height hinge formation; but still the vertical compression, due to the wall bending, combined with contribute of the horizontal reaction are the reason of the tiles crushing.

At higher load levels the proportions of the horizontal and vertical components of the support reaction change. That happens because of different rotations at end tiles due to different flexural stiffness.

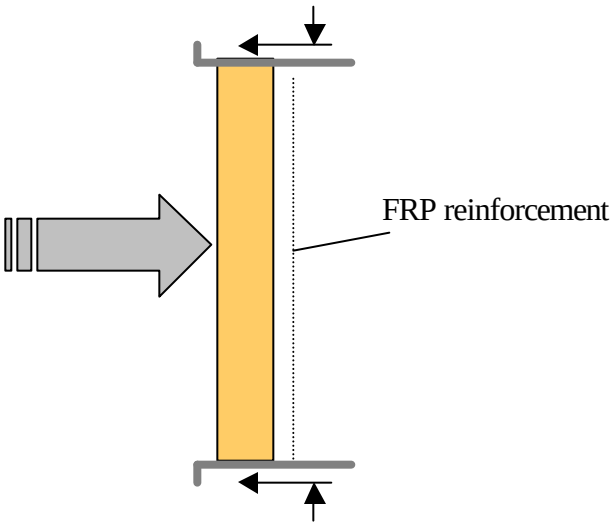

In order to find an arching effect-load relation, first, by means of an iterative process, the constant of elasticity of the springs of a statically indeterminate configuration was searched.

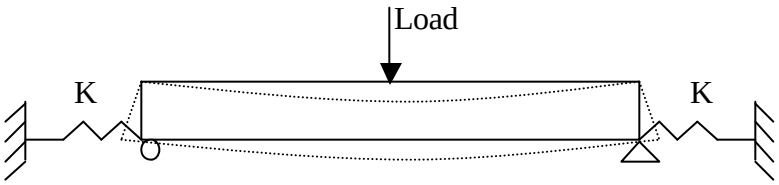

Because of the inconsistency of the strain and displacement data from the site tests, after some iteration this way seemed to be inconclusive.

Another way attempted consisted in calculating the deformations of the tiles due to the end rotations. In fact from the rotation angle φ and the deformation δ in the tile corresponding to the ultimate strain (assumed ε_{cu}=0.0035) it was possible to obtain the length x of the uncracked section.

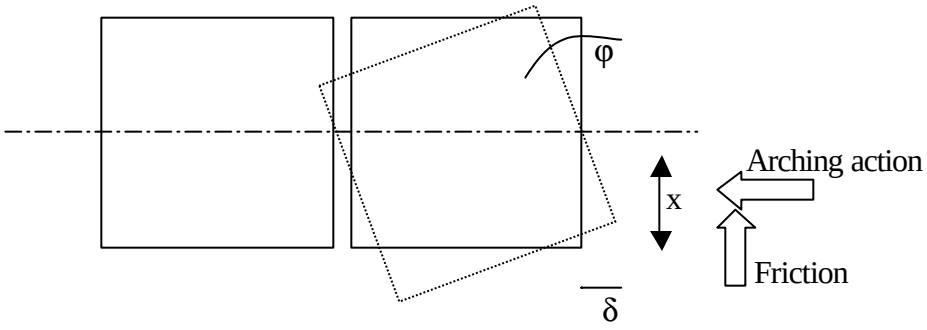

Assuming an appropriate distribution of the stresses in the contact area and imposing the ultimate compressive stress in the edge, it could be possible to evaluate the axial component of the reaction and its eccentricity.
Unfortunately, the data from inclinometers were inconsistent and it was not possible to find out the actual rotation.

Another approach evaluated consisted in calculating the arching action using the Coulomb friction relation of the mortar obtained from the laboratory tests:

$$\mathbf{F_V = 1/m\ (F_H - T_0)}$$ where T_0 is the friction without load

In this case the attempt was improper as the component T_0 itself was sufficient to bear the load.

Considering that the improvement obtained by reinforcement was not dramatic, it is feasible to assume, at failure of each wall, the same value of vertical component derived from the equilibrium relations previously used.
That means that at failure the distribution of the compressive stresses, their resultant and its application point are the same for every wall.
So, the fixed parameters introduced are:

Vertical reaction component **N=48 kips**
Eccentricity **e=(t/2)-(b/3)=4”**

These assumptions allow defining the static model of the wall. As there were rotations at the ends, fixed supports clearly do not represent the actual connections; at opposite, as the end rotations are always smaller than the theoretical ones related to the simply supported scheme, an intermediate condition was needed.

As both the vertical reaction and its eccentricity are function of the mid-height load, the actual system has at the ends two torsion-spring supports. Their behavior is assumed to be linear elastic.

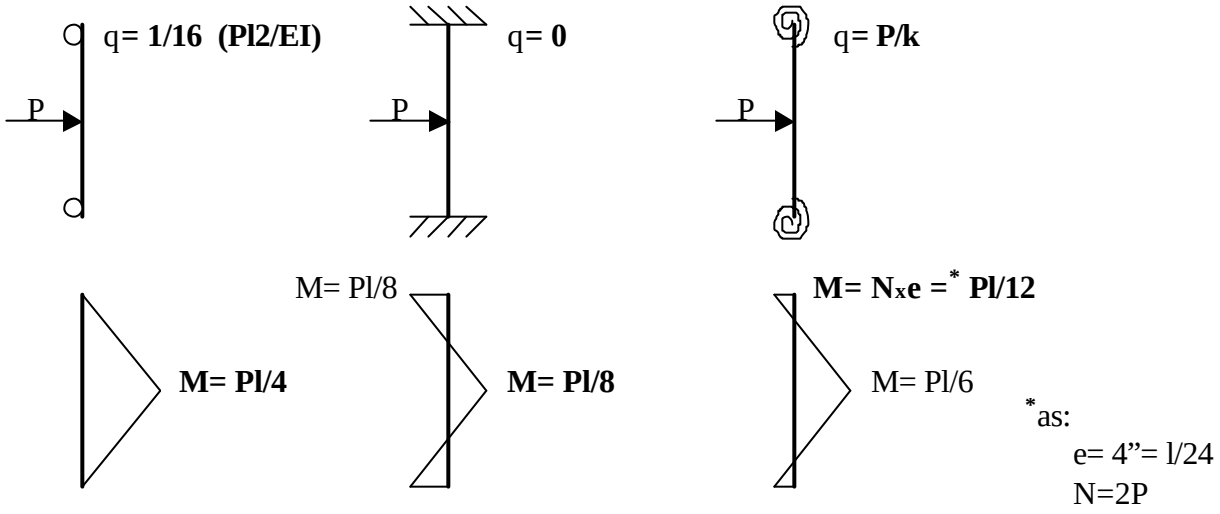

Theoretical bending capacity under axial load of FRP retrofitted walls

Not many approaches have been proposed on this subject and only a few tests validate some assumptions, rating reduction coefficients on failure mode and material properties.

In order to obtain an upper limit to compare the actual behavior of he walls, equations obtained from equilibrium of the section (Triantafillou, 1998. [15]) are introduced, while material properties were found both from material test characterization and references.
In the model, reinforcement is considered linear elastic up to failure and the ultimate performance properties are the ones declared by the manufacturer without reduction factors recommended for design.

A rectangular stress block is the constitutive law adopted for masonry, where stress and strain ultimate values are taken accordingly with the veneer test performances.

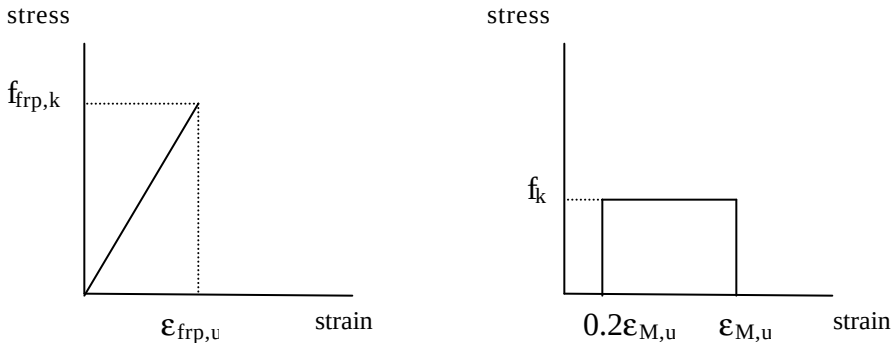

Unless particular failure mechanisms previously occur, as peeling or delamination modes, crushing of masonry or FRP fracture determine the bounds of the bending capacity. In order to fully develop the masonry performance and to obtain the less brittle failure (especially when design is focused on ductility), the fracture of FRP is avoided increasing the reinforcement ratio.

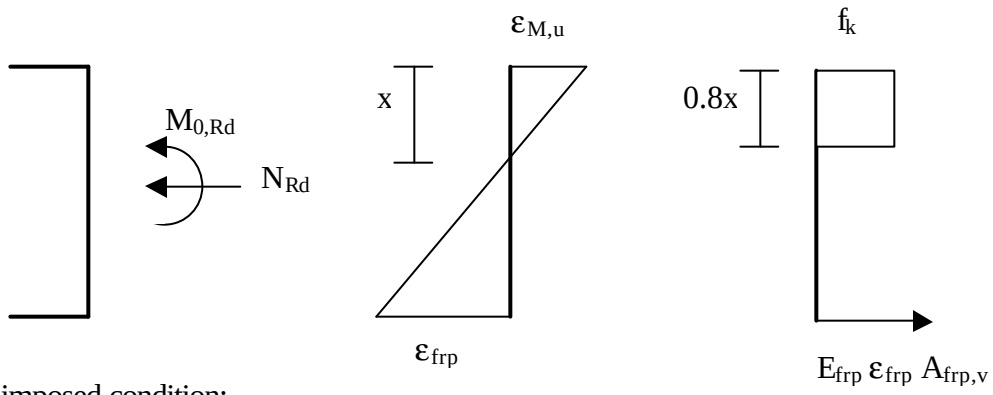

In the imposed condition:

1) $\rho_v > \rho_{lim}$ where: $\rho_v = A_{frp,v}/l\,t$

ρ_{lim} is derived in the following expression:

2) $\omega_{lim} = \varepsilon_{M,u}\,E_{frp}/f_k \quad \rho_{lim} = \varepsilon_{M,u}/\varepsilon_{frp,u} = [0.8/(1+\varepsilon_{frp,u}/\varepsilon_{M,u}) - N_{Rd}/l\,t\,f_k]$

condition 1 correspond to the following:

3) $\omega_v > \omega_{lim}$

When condition 3 is accomplished, the failure is due to masonry crushing.

The normalized bending capacity of the section is obtained:

4) $M/l\ t^2\ f_k = \omega_v/2\ \ (1-x/t)/x/t\ +\ 0.4\ x/t\ \ (1-0.8\ x/t)$

Where:

5) $x/t = 1/1.6\ [N/l\ t\ f_k\ -\ \omega_v\ +\ \sqrt{(\omega_v - N/l\ t\ f_k)^2 + 3.2\ \omega_v}\ ]$

Those expressions allow obtaining the maximum resistant moment in a cross section in relation to the normal stress and the parameter ω_v.

Example:

Wall 4, reinforced with three sheets of GFRP applied directly on the masonry was the one presenting the laminate strengthening best performance (see Figure A3).
From its load-displacement curve a failure load is assumed equal to 30 kps.

Assuming, as discussed above, a vertical reaction N due to the arching effect as calculated from the equilibrium for the unreinforced wall, the former equations give:

$\rho_v = A_{frp,v}/l\ t = 723*10^{-6}$ as: fiber thickness= 0.0139 in^2
sheet width= 20 in
$A_{frp,v}$ =0.0139*20"*3=0.834 in^2
t = 12 in
b = 96 in

$\omega_v = \varepsilon_{M,u}\ E_{frp}/\ f_k\ \ \rho_v = 0.02960$ as: $\varepsilon_{M,u}$ =0.0039
E_{frp} =10.5 Msi
f_k =1000 psi

$\omega_{lim} = \varepsilon_{M,u}/\varepsilon_{frp,u} = [0.8/\ (1+\varepsilon_{frp,u}\ /\ \varepsilon_{M,u})\ \ -\ \ N_{Rd}\ /\ l\ t\ f_k] = 0.01724$

as: $\varepsilon_{frp,u}$ =0.02
l = 96 in
N_{Rd} = 48 kips

Therefore: $\omega_v > \omega_{lim}$

x/t =0.2 in

$M/l\ t^2\ f_k$ = 0.1264 lbs*in

From the maximum mid-height moment it is now possible to obtain the theoretical lateral force that determines a failure due to the crushing of the masonry in the compressed side:

$P_{max,th}$=6*M/l=109.2 kips.

Using the same formulas to evaluate the theoretical moment capacity at the ends, using the correspondent f_k value, a good approximation of the actual premature failure load is obtained:

$P_{prem,th}=12*M/l= 28$ *kips*

Obviously in the last case the formulas were applied in the unreinforced case, that means without the condition $\omega_v > \omega_{lim}$, as the end sections are compressed on the FRP side. The value obtained is close enough to the actual ultimate load to validate the assumptions on the vertical load and its eccentricity.
In the following graphs, with normalized parameters, show the relations expressed in 4) and 5), the theoretical and the premature actual failure, the limit and actual reinforcement normalized ratio.

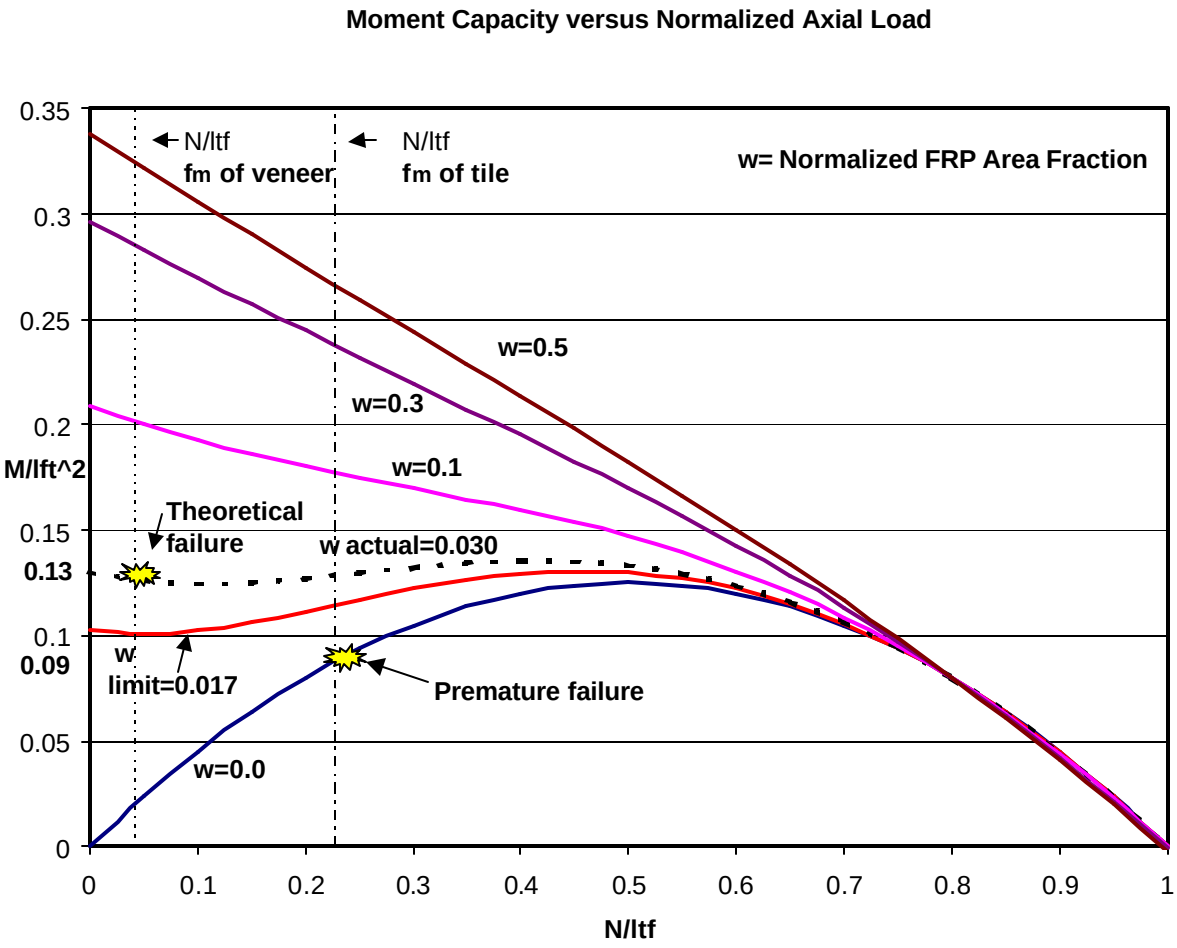

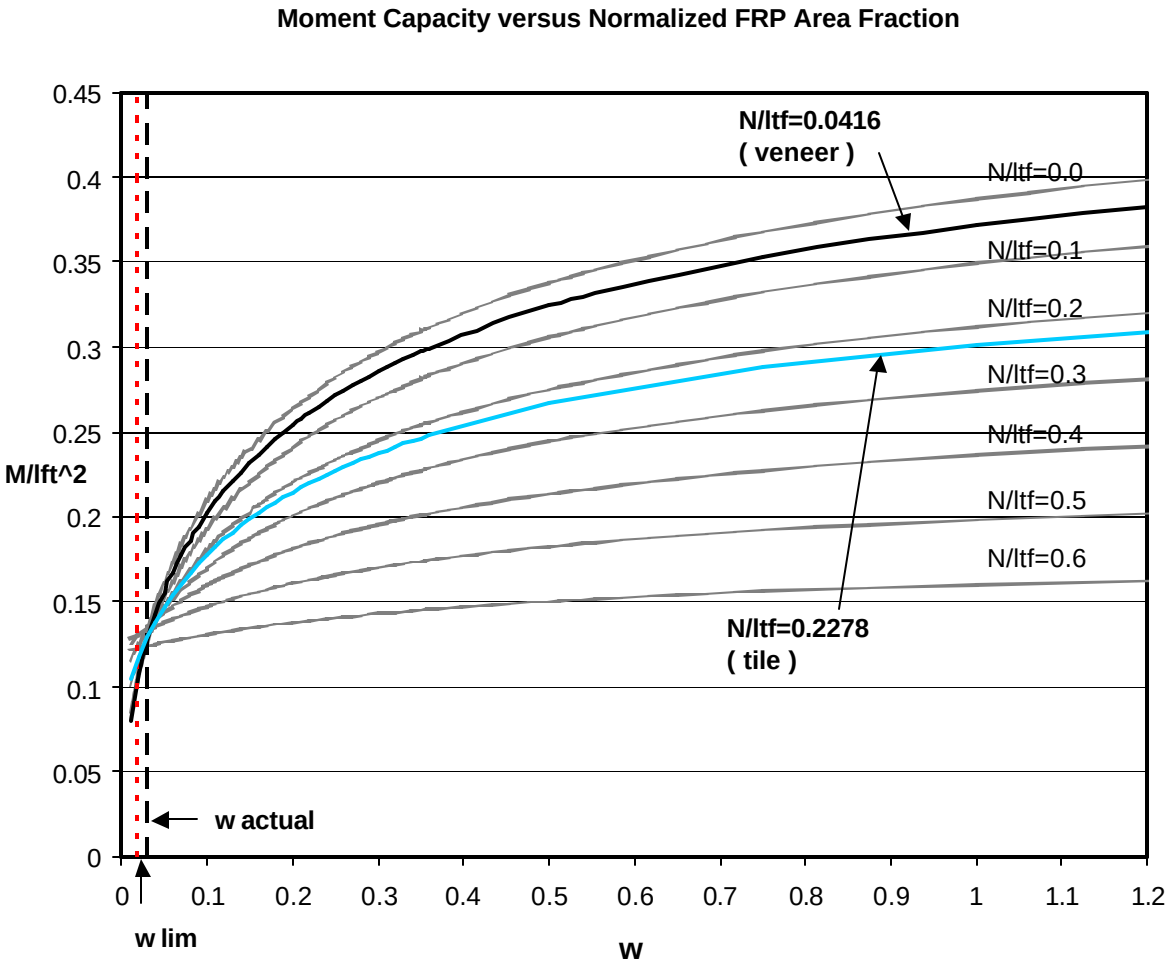

In the first graph, the fact that the actual omega curve is almost flat in a wide range of the normal action minimizes evaluation errors of the theoretical bending capacity. In the second graph it is clearly expressed the theoretical improvement that still is possible to obtain increasing the reinforcement ratio.

The arching effect plays a contradictory role reducing the mid-height moment and contemporary inducing a bending action where a one side-reinforced wall is weak.
This redistribution of moments is related to the strength and stiffness of the wall, which depend on the material properties and the reinforcement amount.

Those considerations stimulate to find alternative reinforcement solutions for a better exploitation of the wall potentiality and of the FRP retrofitting technique.

Retrofitting alternative approaches

As it is not feasible to apply any kind of vertical reinforcement on the outside veneer to absorb the tensile stresses due to the ends moment, the crushing of the tiles can be prevented only changing the boundary condition at the supports eliminating the

vertical force; but in order to guarantee the horizontal reactions this solutions is onerous to be realized.

The compressive strength anisotropy of the tiles revealed by the material characterization (see Figure A19) suggests the possibility to involve the horizontal direction in order to better exploit the tiles potentiality.

Figure A19: Evaluation of the tiles compressive anisotropy.

Creating RC columns at the vertical edges of the wall it would be possible to create the necessary supports to change the panel structural scheme from vertical to horizontal, or even bi-directional (square slab restrained on all the edges). In this way, tiles are involved in compression in the direction parallel to the holes, which is the ideal condition. Provided that some reinforcement could be installed horizontally on the outer part, together with the vertical FRP laminate action on the inside face this two ways strengthening could be seen as a suitable approach to out-of-plane cyclic actions.

This hypothesis has to face the problem of strengthening the external part of the wall. In fact on the veneer it would not be feasible to apply any kind of visible reinforcement without compromising the look of the façade. Furthermore, a traditional reinforcement based on steel, would be exposed to detrimental weathering. Obviously, application issues should be considered as a limit of a traditional strengthening approach.

It was exactly in response to the mentioned problems that a program of investigation on the use of FRP rods reinforcement on masonry was developed.

APPENDIX B
MATERIAL CHARACTERIZATION

B1 MORTAR

Mortar used is available in bags in a dry premixed composition of masonry cement and sand, and is classified as Type N according to the standard ASTM C270. Type N mortar has been chosen to reproduce masonry assemblages similar to the most common typologies of the Midwest, among which the project presented in Appendix A is included. Standard tests (ASTM, 1999. [22]; RILEM, 1997. [25]) were performed to characterize compressive and tensile properties of the mortar used in the experimental program (see Figure B1).

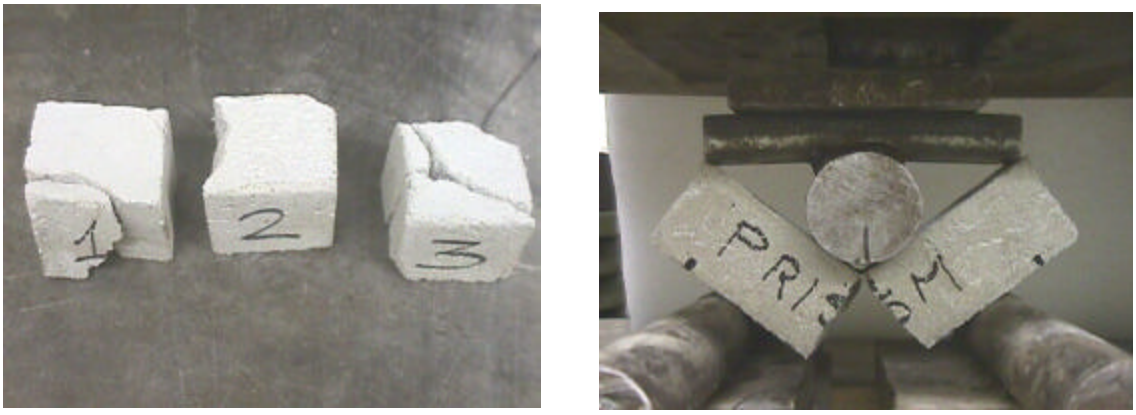

Fig. B1: Compressive tests on mortar cubes. Modulus of rupture test on a mortar prism.

B2 CONCRETE BLOCK MASONRY

Concrete blocks used were the eight-inch width (20.3 cm) for load bearing walls, in sash and half sash shapes. The standard blocks have nominal dimensions of 8x8x16 in. The actual block dimensions are 3/8 in. less than the nominal values, to allow for a standard mortar joint thickness (see Figure B2).

Three specimens were subjected to standard prism tests (ASTM Standards. [20]). Stress-strain relations were obtained by vertical and horizontal displacement data acquisition. The everage compressive strength obtained was f'm=904 psi (gross area). As the prisms involved presented a height to width ratio minor than five (see Figure B3), guidelines from different reference suggest the application of corrective factors. The ACI 530/ASCE and 5/TMS 4O2 propose a corrective factor of +7% in correspondence of a height to width ratio equal to three. Thus, the corrected compressive strength is f'm=967 psi (gross area). Since the average mortared area of the blocks used is 50%, the net compressive strength is equal to f'm=1934 psi (net area).

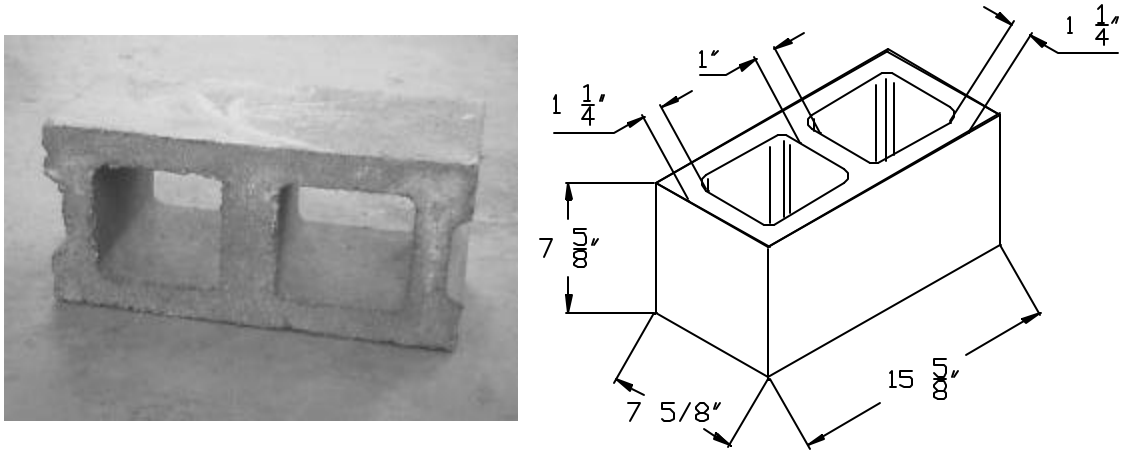

Fig. B2: Standard hollow concrete block.

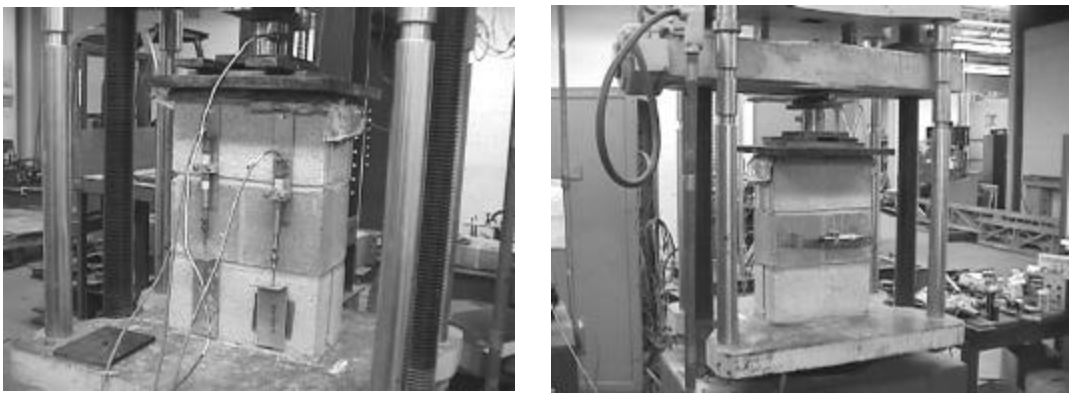

Fig. B3: Concrete block masonry specimens under compressive test.

From reference on similar experimental results (Drysdale et al., 1994. [3]), from the masonry net compressive strength and the type of mortar is possible to approximate the compressive strength of the concrete block in f'_b=3200 psi.

The UBC standard requires for hollow load bearing concrete units a minimal compression strength (gross area) of: 1000 (Grade N-I) or 700 psi (Grade N-II). The different grade depends on the certified compliance of the blocks with specified water absorption limits. Therefore, block used in the present research can be considered as grade N-II.

Present information indicates that the ultimate tensile strength of grade N concrete masonry units ranges somewhere between 50 and 200 psi. On this subject there are not

specific requirements from codes except for the California Concrete Masonry Technical Committee (CCMTC), which requires 135psi minimum.

Modulus of elasticity is not generally determined for the individual masonry units and is not specified in most standards. Current codes refers to Em=750f'm.

A report by Atkinson and Kingsley (1985) points to a more realistic value around 550f'm, while a Poisson ration of 0.28 was recorded in the same specimens. At present shear modulus of concrete masonry is set at 0.4 Em.

B3 CLAY BRICK MASONRY

In order to product results from the laboratory tests that could, in a latter date, be used as reference values to plan further in-field experimentations on the Malcolm Bliss Hospital (see Appendix A), it was decided to build tests specimen that cold reproduce as much as possible the masonry assemblage fundamental characteristics of the site walls.

As different manufacturing procedures occurred in the last decades, it was necessary select and test many different bricks (see Figure B4) before it was possible to identify the type with the most similar characteristics. The fact that nowadays fragments of crushed brick are recycled in the mix to produce new brick, diminishes the modulus of rupture of the current production, while the compressive strength is less influenced. Fortunately, it was still possible to find similar characteristics in a kind of brick that is also quite diffuse in the Midwest area. The selected kind of brick was subjected to standard tests providing a complete series data (see Section 4.2).

Compressive strength and the complete stress-strain relationship of the masonry assemblages were obtained referring to both American and European standards (ASTM, 1999. [20]; RILEM, 1997. [25]). Four stack bond prisms and two Rilem panels offered representative material characteristics (see FigureB5).

Twelve triplets were tested with especially designed equipment to find the friction relation of the mortar joints (see Figure B6), lately used in the analytical model to predict the shear capacity of the wallettes. As can be seen, the shear strength of the panels was slightly lower than the corresponding values find testing the triplets (see Figure B7).

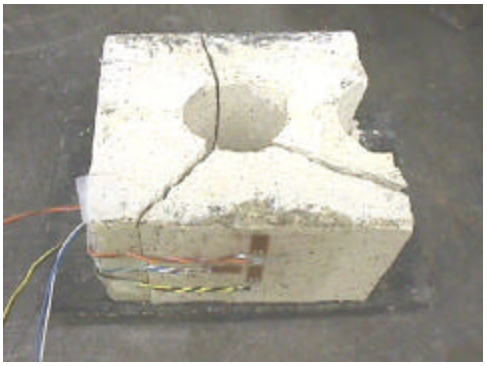

Fig. B4: Selected bricks of current production. Instrumented compressive test on the halves obtained after the modulus of rupture test.

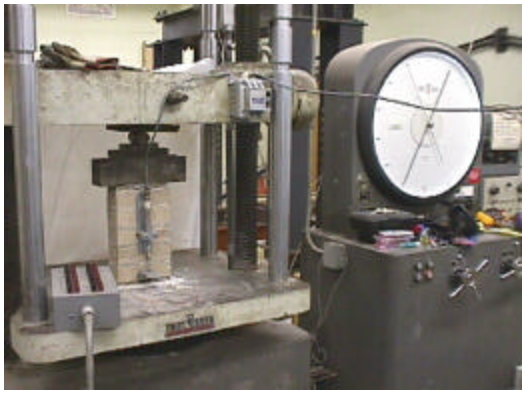

Figure B5: Specimen for compressive test. Test set up and equipment.

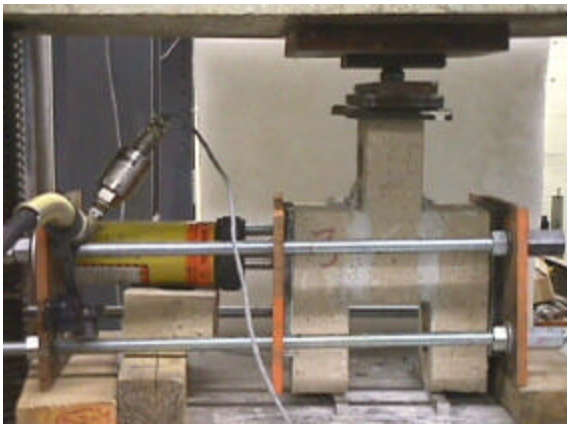

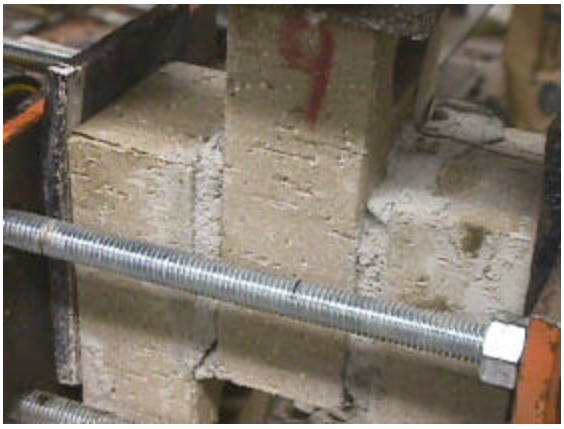

Fig. B6: Equipment designed to apply compressive and shear stress on the tested joints.

Lateral load reached in some specimens the compressive strength limit.

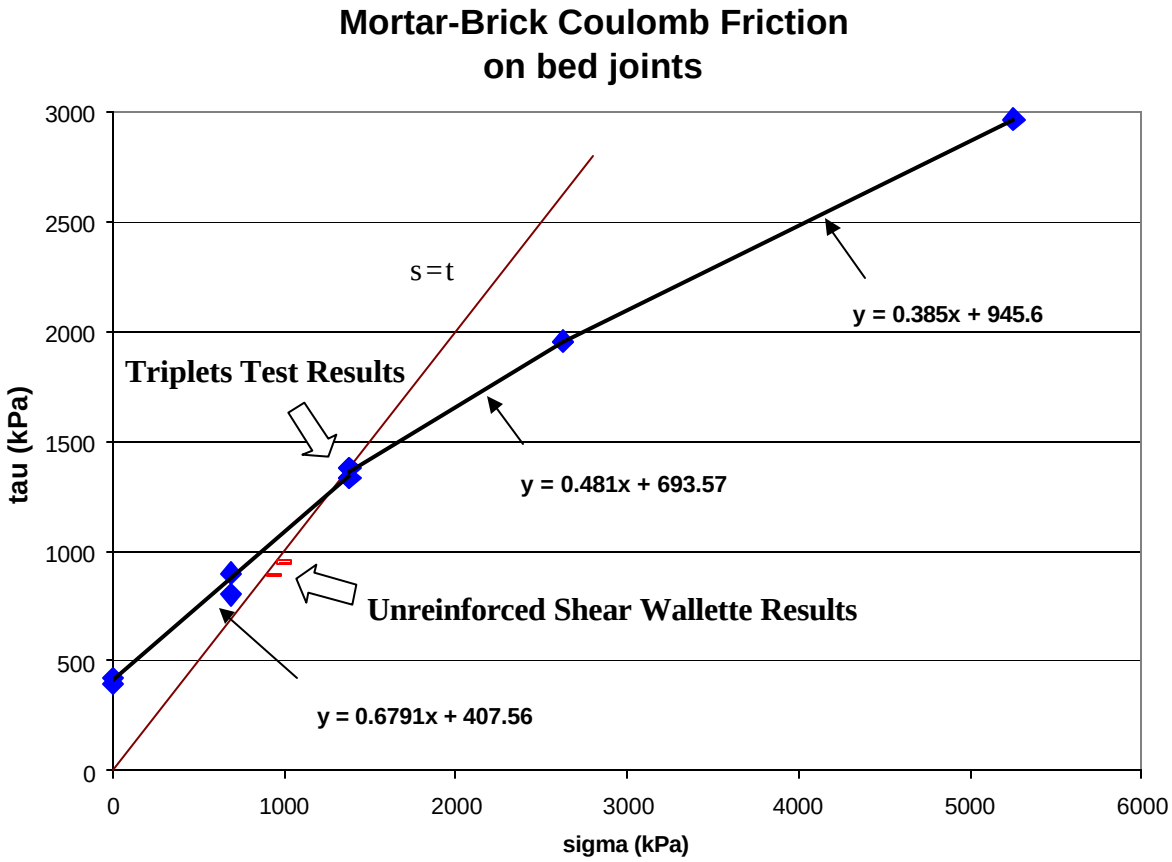

Fig B7: Comparison between the friction relation triplets from the triplets and the shear tests on the unreinforced specimens.

B4 EPOXY PASTE

The epoxy resin used in the experimental program is produced by Master Builders Technologies and is commercially known as Concresive Paste LPL. It is a two component adhesive with long pot life. All the fundamental performance data are furnished by the manufacturer.

Cylindrical samples of both the epoxy paste and the epoxy mortar (designed mix of epoxy paste, pure quartz sand and coloring pigments) were taken during the installation, to be tested in the same period in which the wallettes were tested (see Figure B8).

Accurate mixing speed allowed obtaining a mix with reduced void amount and, most important, the small empty cells, being embedded in the material, are isolated from each other. Thus the epoxy mortar, theoretically, has not porosity, ensuring perfect protection of the reinforcement from environmental conditions.

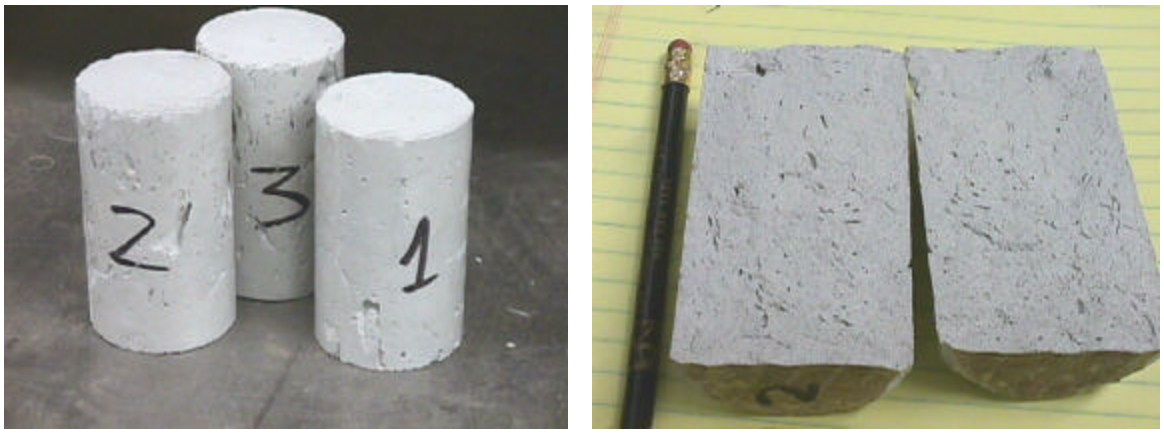

Fig. B8: Epoxy mortar cylindrical samples subjected to compressive and splitting tests.

B5 GFRP RODS

GFRP rods used in the experimental program are produced by Hughes Brothers. They present exterior wound fibers and sand coatings. Data exposed in section B5 are provided by the manufacturer. The principal characteristics are listed in Table B1.

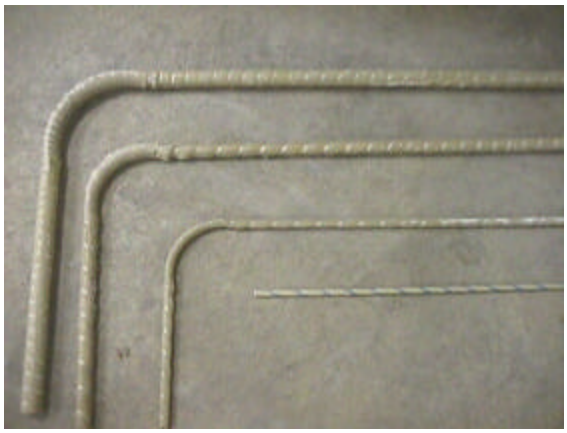

Table B1

Hughes Brothers GFRP Rebar

Bar Size	mm	6
Cross Sectional Area	mm^2	34.84
Nominal Diameter	mm	6.35
Tensile Strength	Mpa	900
Tensile Modulus	Gpa	40.8

Fig B9: Bent GFRP rods.

Bends are fabricated by shaping over a set of molds or mandrels prior to thermoset of the resin matrix (see Figure B9). Research has shown that bends typically maintain 38% of the straight bar ultimate tensile strength.

Bends are limited to shapes continuing the same circular directions; otherwise lap splices are required.

Suggested lap splicing lengths are equal to forty times the rod diameter.

Accelerated aging tests indicate that after simulated 50 years of service life the rods experienced a 25% degradation in tensile strength and 4% change in modulus of elasticity.

Creep tests indicated that if sustained stresses are limited to less than 60% of short-term strength, creep rupture does not occur in GFRP rods. Environmental factors such as moisture can affect creep rupture performance.

Based on proposed ACI design guidelines, it is recommended that computed tensile stress does not exceed 25% of minimum ultimate tensile strength.

B6 GFRP LAMINATES

GFRP laminates used in the experimental program are produced by MBT and are commercialized as M-Brace system (see Figure B10).
The principal characteristics provided by the manufacturer are listed in Table B2.

Table B2

MBrace EG 900 E-glass LAMINATE

Fiber Areal Weight Density	oz/yd^2	27
	g/m^2	915
Tensile Strength k-LB/inch of sheet width		3.5
Ultimate Strength	Mpa	1730
	ksi	251
	kg/cm^2	17647
Tensile Strength for Design	MPa	1517
	ksi	220
	kg/cm^2	17000
Tensile Modulus	MPa	72400
	ksi	$10.5x10^3$
	kg/cm^2	$0.71x10^{12}$
Design Thickness	in./ply	0.0139
	mm/ply	0.353
Tensile Elongation, Ultimate, percent		2

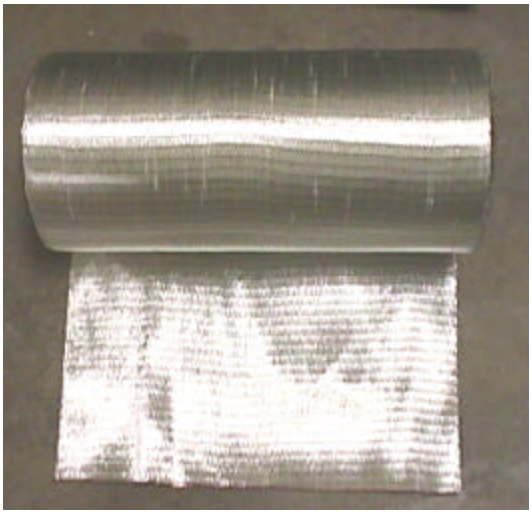

Fig. B10: GFRP fibers used in the wet lay-up applications.

APPENDIX C

FINITE ELEMENT MODEL

In order to better identify the stress redistribution consequent to the application of the SR and adjust design assumptions describing the physical phenomena, a micro model was implemented by a commercially available finite element code. A 3D mesh was adopted, simulating the micro structure of the wall. Bricks and mortar joints were discretized with 20-node brick elements. Constitutive laws of materials, including the softening part (Lourenco, 1996. [10]), and failure domains were introduced as obtained from an evaluation of units and masonry assemblages. The model used is based upon the smeared crack approach and the Drucker-Prager model. The yield surface is hyperbolic with associated softening type flow. The hyperbolic domain was established fitting the experimental data available on friction (see Figure C1). The bold black line was reproduced in the numerical simulation. The non-linear associated plastic flow was calibrated on the experimental results of unreinforced panels, in order to simulate the sliding phenomena, at least in the initial stage. The use of smeared crack approach is preferable when the position of cracks is unknown. Unfortunately this tool cannot reproduce macro-cracks propagation, because of the localization of relative displacement inside the body. This situation generates numerical instability and the convergence of the solution becomes impossible.

The model refers to the double-wythe wallettes, hence has a plain of symmetry on the z=3 direction, and areas around the two loaded corners are subjected to forces along the x=1 (horizontal as the bed joints) and y=2 (vertical) directions. Stress (S) and Strain (E) contours are associated to each direction: es. E11 is the strain along axes x.

Materials involved have been defined with the following constitutive laws:

-Bricks: elastic-plastic with softening failure domain (Drucker-Prager). Data are obtained from the experimental results of compressive and tensile strength.

-Mortar: elastic-plastic with softening failure domain (Drucker-Prager). Data are obtained from the experimental results of compressive and tensile strength. Interface properties are obtained from date from triplet tests.

-FRP reinforcement: elastic up to failure, either in compression and in tension (this limitation was related to the software used). Modulus of elasticity and tensile strength are obtained from the manufacturer data.

The model of the unreinforced panel, Wall 9, is reported in Figure C2. Simulation of the test condition is reported in Figure C3, where stress and strain distributions along the x and y axes. Two conditions are represented: at the maximum load and at advanced sliding. The typical stepped failure pattern along the mortar joint is perfectly simulated by the model and readable from the strain contours. The discrepancy from the

experimental test is on the maximum sustained load: the model result to be more than 10% conservative.

Wall 10 simulation is represented in Figure C4. A view of the strain distribution in horizontal (E11) and vertical direction (E22) is shown, together with the stress distribution (S11 and S22) at the last step of load. The limit of the modeling strategy implemented is here evident in the discrepancy on the maximum capacity and in the maximum splitting: 78% and 25% of the experimental results, respectively.

The strain contours on the x and y directions perfectly match the strain distribution experimentally measured by gauges (see Section 4.4).

Figures C5, C6 and C7 shows the Wall 11 simulation contours during different steps. The calculation was stopped after 40 steps because of the convergence problems related to the limits of the smeared crack strategy.

Some results obtained, such as applied load-rod strain relations, are consistent with the experimental records from strain gauges applied on the FRP rods: after an almost linear phase, were the relative horizontal displacement is negative, we observe the formation of micro-cracks in almost all mortar joints and then, in the central part of the panels these cracks becomes very large (see Section 4.4). The numerical model confirms that FRP reinforcement acts to absorb tensile action and, keeping close cracks, permits ductility load enhancement.

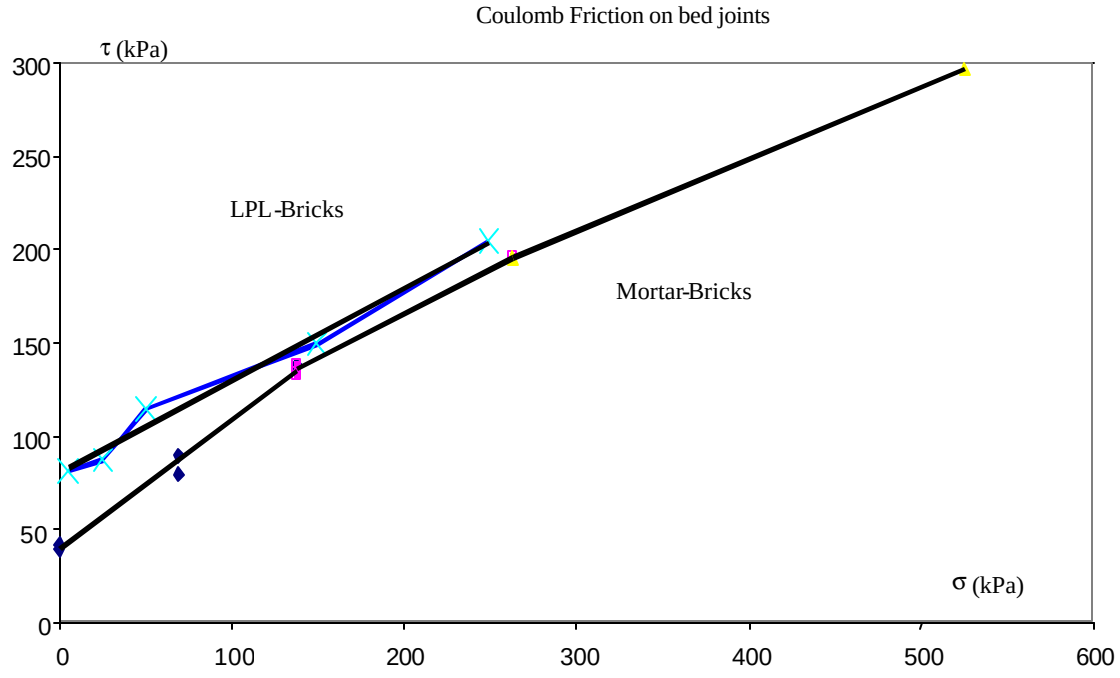

Fig. C1: Experimental Coulomb friction domains, bold line has been implemented in the numerical analysis

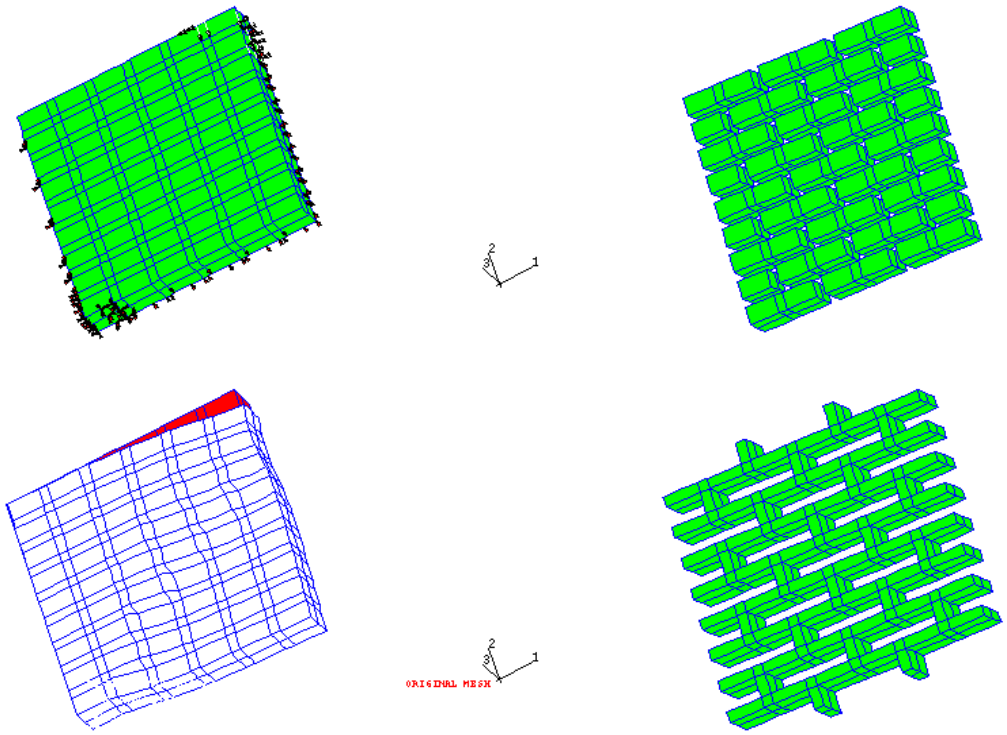

Fig. C2: Wall 9: Boudary conditons, bricks mesh, mortar joints mesh, deformed configuration compared with the original configuration.

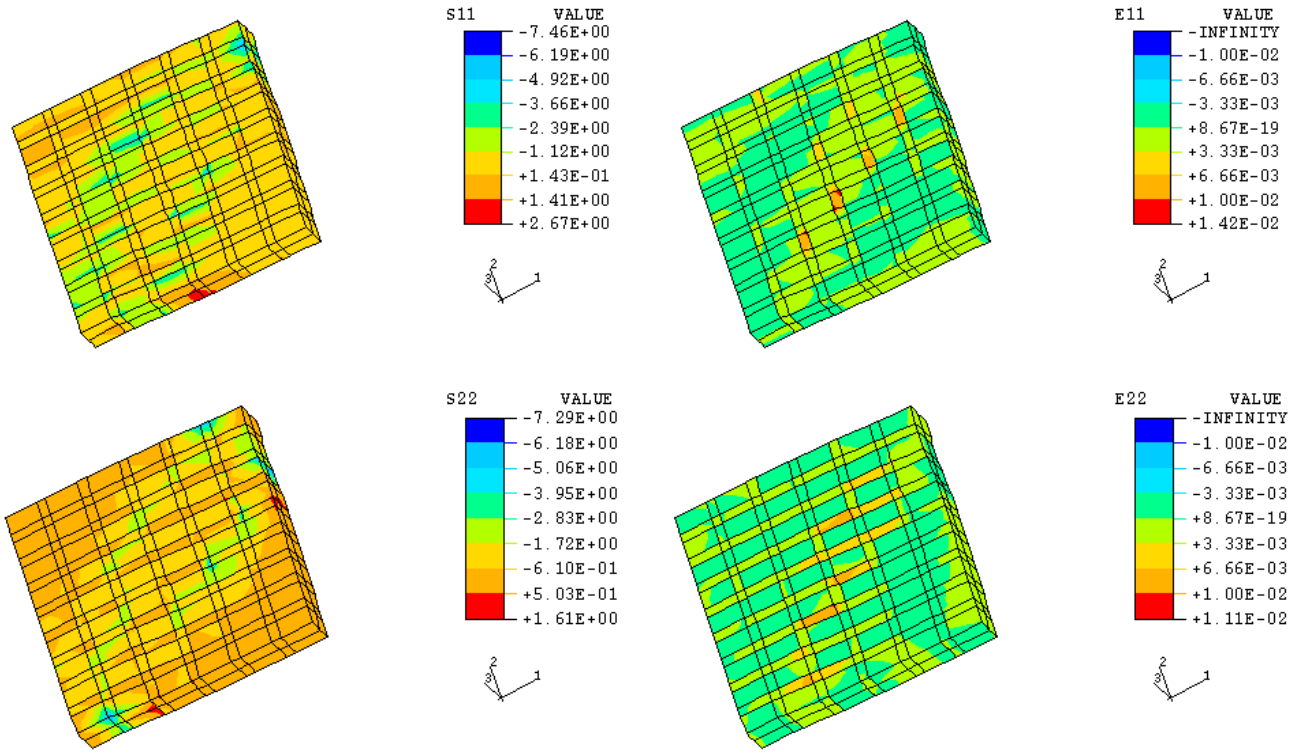

Figure C3 a: Wall 9. Loading Step 10, load=64kN decreasing, crack already developed.

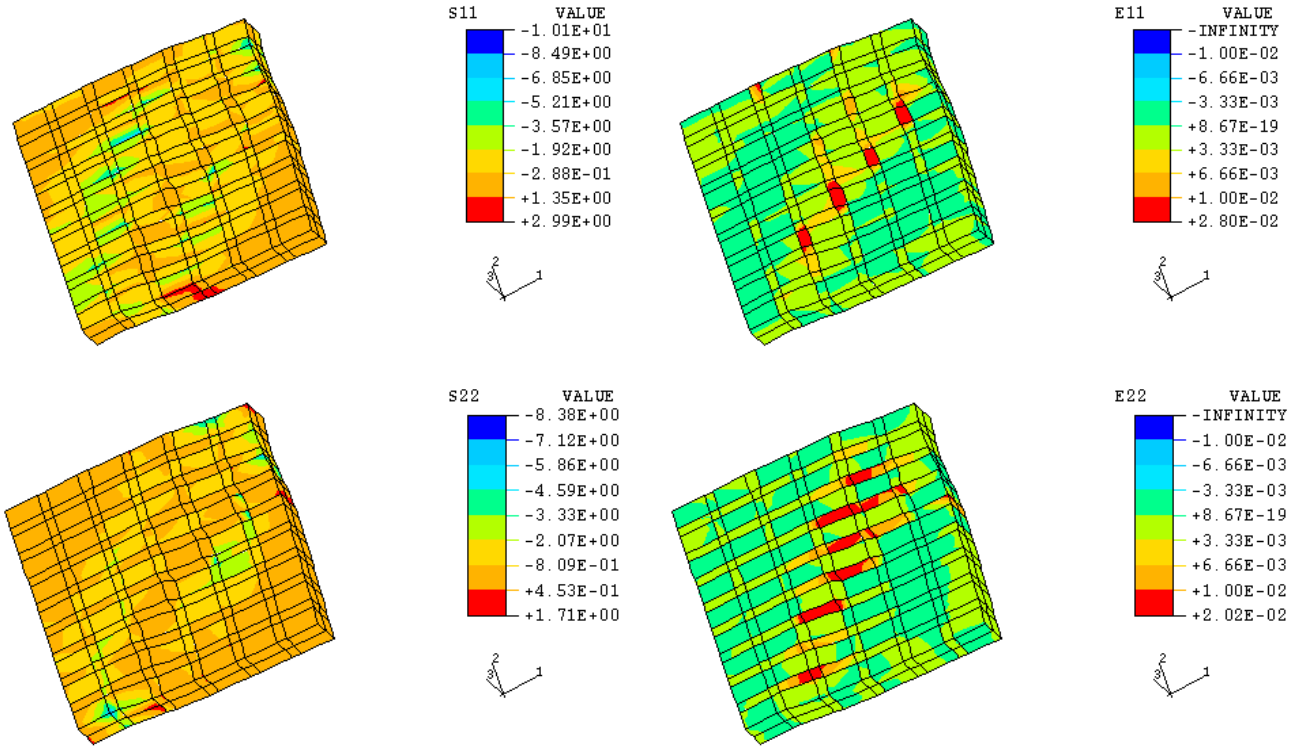

Figure C3 b: Wall 9. load=55kN, decreasing as large displacement are in progress.

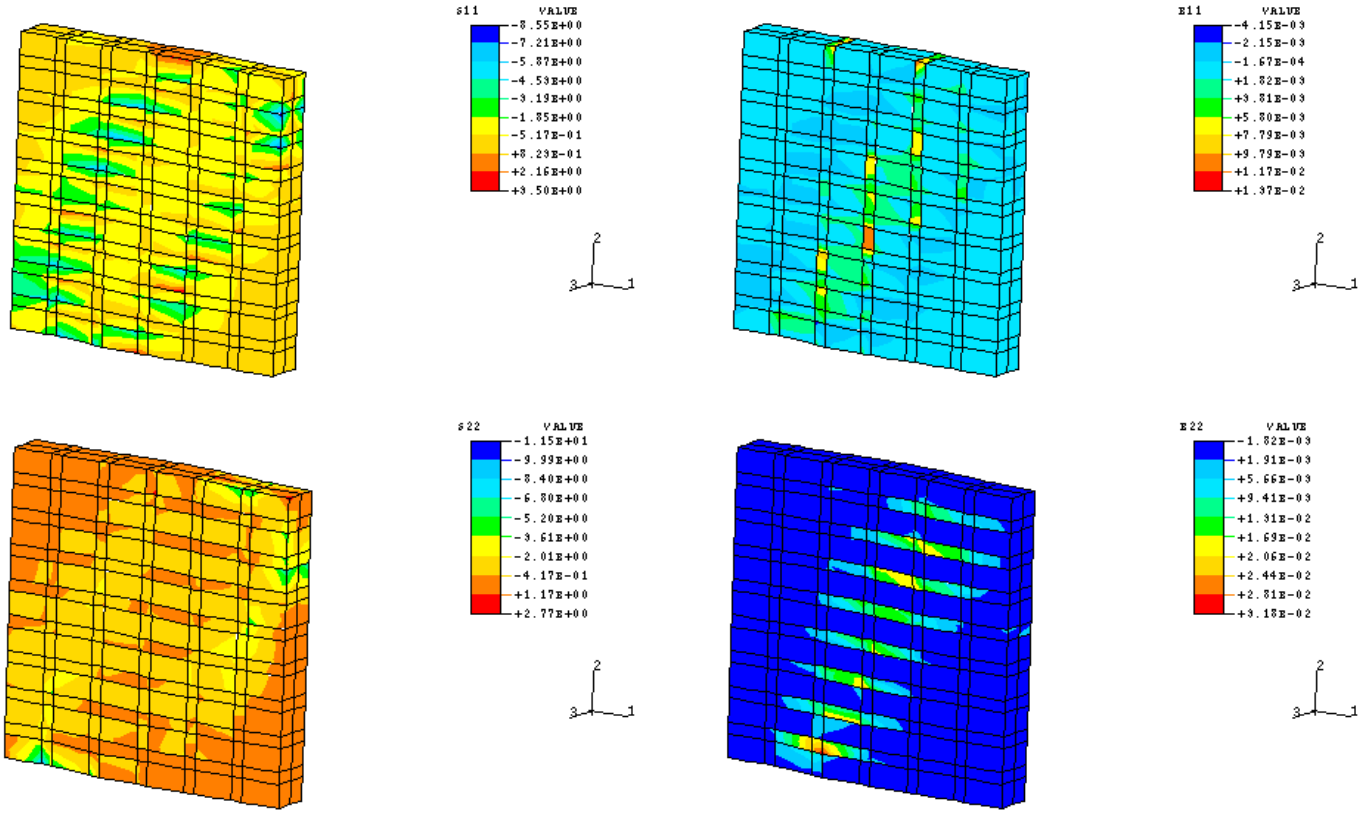

Fig. C4: Wall 10. Stress (S) and strain (E) distribution at the last step of loading.

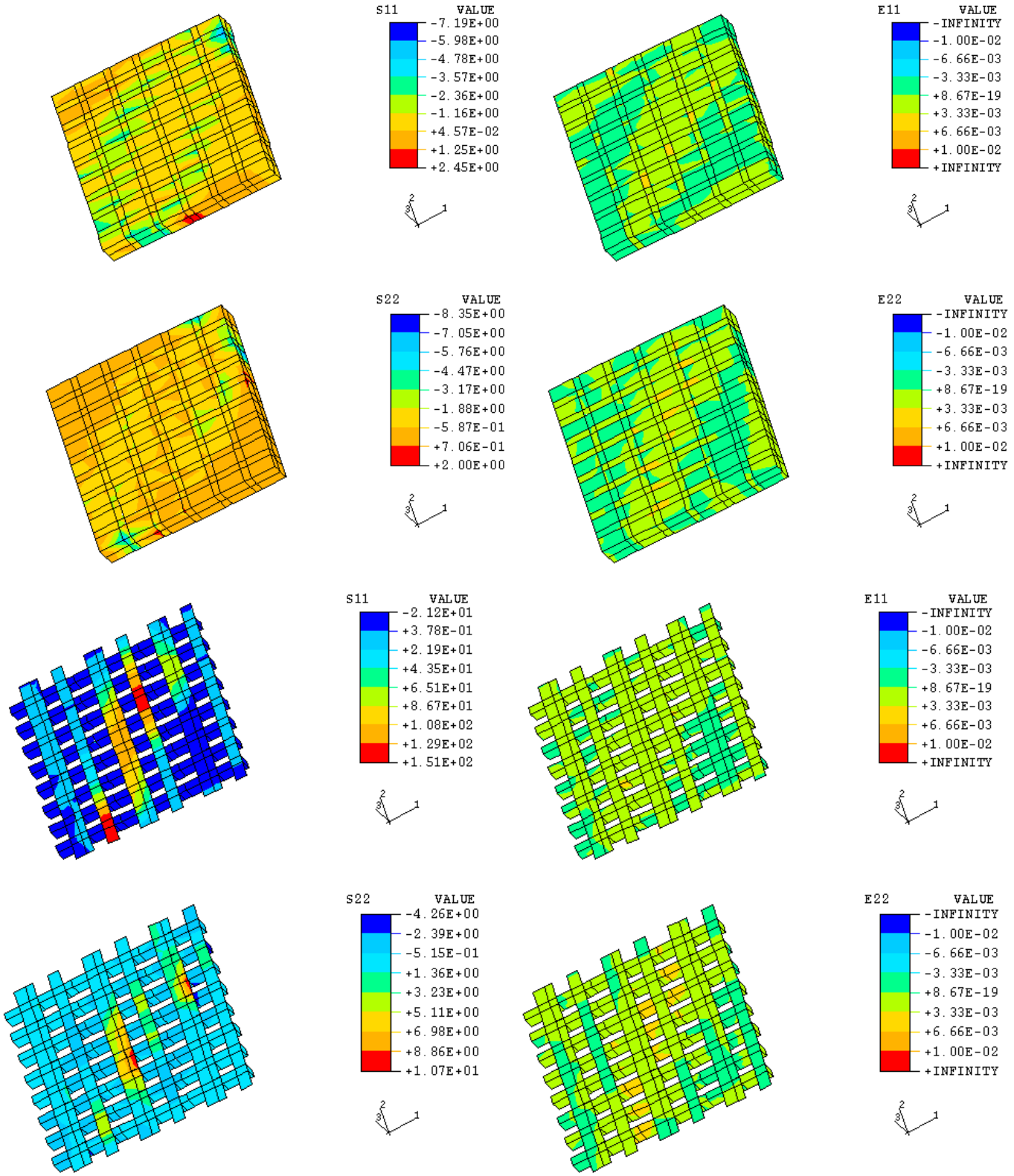

Fig. C5: Wall 11. Step 10, load 87 kN amplification =10. Top: stress and strain distribution on the masonry panel. Bottom: stress and strain distribution on the FRP strips and into the joints with the embedded rods. Load is increasing and splitting is starting.

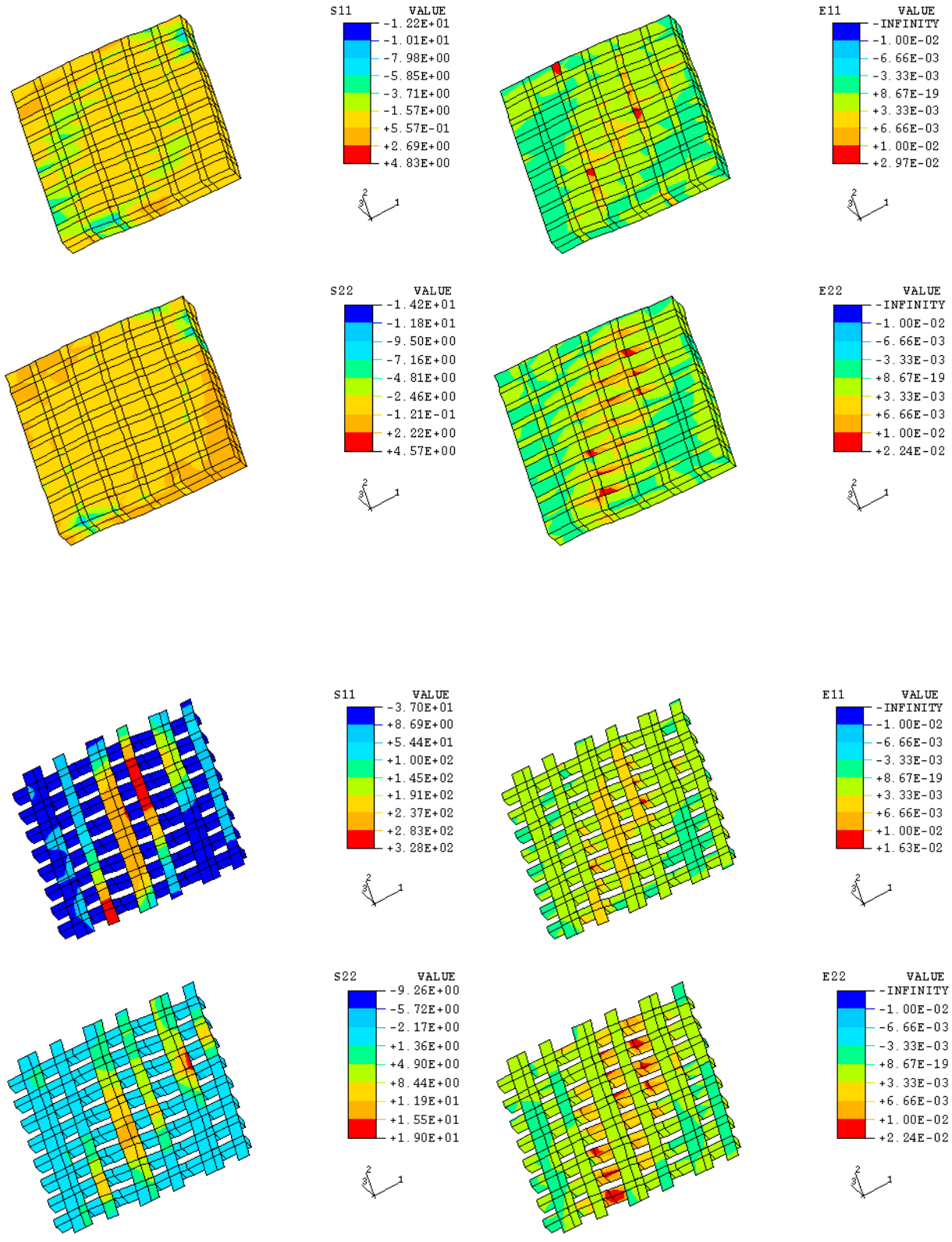

Fig. C6: Wall 11. Step 20, load 109 kN amplification =10. Top: stress and strain distribution on the masonry panel. Bottom: stress and strain distribution on the FRP strips and into the joints with the embedded rods.

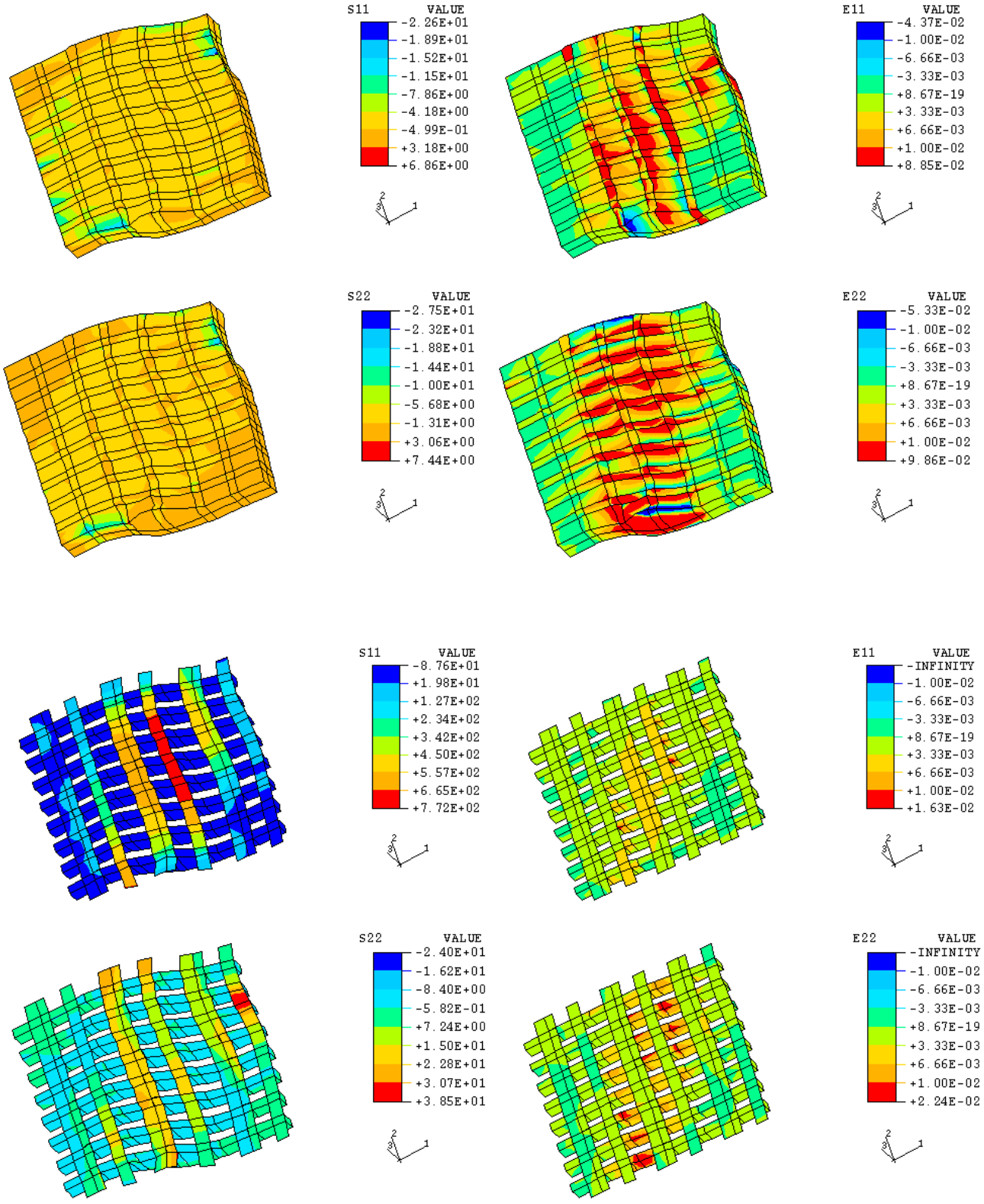

Fig. C7: Wall 11. Step 40, load 148 kN amplification =10. Top: stress and strain distribution on the masonry panel. Bottom: stress and strain distribution on the FRP strips and into the joints with the embedded rods. The maximum load reached correspond to wide displacements that cannot be further followed by the model.

Deformations of the panel and strain of the rods, continuously recorded during the diagonal compressive tests, were simulated within the model. This allowed representing different strengthening configurations and different wall scales, in order to be able to rapidly investigate many "What if" cases as preliminary analysis for further experimental tests or field applications. In addition, once different parameters such as FRP material, rod diameter and paste bonding properties are characterized, it is possible to evaluate the most suitable set of products to be applied on the considered masonry assemblage. Boundary conditions such as restrain position and load distribution can also be changed to take into account a series of variables a strengthened wall can be submitted to. Introducing creep phenomena or dynamic inertia conditions, long term static loading or cyclic events can be examined by the model in a wide range of configurations and receive validation from just a few selected experimental tests.

In order to develop the present model for further applications on different masonry assemblages, detailed characterizations of the mortar-brick interface are necessary.

Bibliography

[1] Structural Masonry. By Sven Sahlin, Copyright 1971 by Prentice-Hall Inc., Englewood Cliffs, New Jersey 1971.

[2] Reinforced Grouted BRICK Masonry Construction. By The Brick Institute of California, revised by James E. Amrhein, S.E. and Michael W. Merrigan of the Masonry Institute of America, Los Angeles, California, July 1986.

[3] Masonry Structures Behavior and Design. By Robert G. Drysdale, Ahmad A. Hamid, and Lawrie R. Baker, Copyright 1994 by Prentice-Hall Inc. Englewood Cliffs, New Jersey 1994.

[4] Masonry Structures. By Frederick P. Spalding, Copyright 1921, published by John Wiley & Sons Inc., New York and Chapman & Hall, limited, London 1921.

[5] Reinforced Masonry Engineering Handbook Brick and Other Structural Clay Units. By J.E. Amrhein, published by the Masonry Institute of America, Los Angeles, California in cooperation with Western States Clay Products Associated, San Francisco, California 1972.

[6] Proceedings of the Fourth North American Masonry Conference. Hosted by the Dept. of Civil Engineering, School of Engineering, and Applied Sciences at the University of California, Los Angeles, California August 16 - 19, 1987.

[7] Symposium on Masonry Testing. published by the American Society for Testing and Materials, Baltimore, Md. February 1963.

[8] The Masonry Society, Limit States Design of Masonry - Draft Report. March 1991.

[9] 1998 Annual Book of ASTM Standards. Section 4 - Construction, Volume 04.01 Cement, Lime, Gypsum. Copyright 1998 American Society For Testing And Materials, West Conshohocken, PA.

[10] Computational Strategies for Masonry Structures. By P. B. Lourenco copyright 1996, published by Deft University Press, Stevinweg 1, 2628 CN Delft, the Netherlands.

[11] Uniform Building Code, 1988 Edition. copyright 1988 by the International Conference of Building Officials, Whittier, California, published May 1, 1988.

[12] Concrete Masonry Handbook for Architects, Engineers, Builders. By Frank A. Randall, Jr., and William C. Panarese, Portland Cement Association.

[13] Construcciones De Albanileria. By Angel San Bartolome, Pontificia Universidad Catolica Del Peru Fondo Editoral 1994

[14] A Manual of Facts On Concrete Masonry. by the National Concrete Masonry Association

[15] Strengthening of Masonry Structures Using Epoxy-Bonded FRP Laminates. by Thanasis C. Triantafillou, Member ASCE, from the Journal of Composites for Construction, May 1998.

[16] Flexural and Shear Response of Reinforced Masonry Walls. by P.B. Shing, M. Schuller, V.S. Hoskere, and E. Carter, from the ACI Structural Journal. November-December 1990

[17] Mechanics of Masonry in Compression. by W. Scott McNary and Daniel P. Abrams, M. ASCE from the Journal of Structural Engineering, Vol. 111, No. 4, April, 1985.

[18] Design of masonry structures Euro Code 6, 1998. Part 1-1. UNI ENV 1996-1-1. UNI, Milan.

[19] Standard Test Methods for Sampling and Testing Brick and Structural Clay Tile. ASTM Standards, C 67 - 97, copyright 1999

[20] Standard Test Methods of Conducting Strength Tests of Panels for Building Construction. ASTM Standards, E 72 - 98, copyright 1999

[21] Standard Test Methods of Sampling and Testing Concrete Masonry Units. ASTM Standards, C 140 - 97, copyright 1999

[22] Standard Specification for Mortar for Unit Masonry. ASTM Standards, C 270 - 97a, copyright 1999

[23] Standard Test Method for Diagonal Tension (Shear) in Masonry Assemblages. ASTM Standards, E 519 – 81 (reapproved 1988), copyright 1999.

[24] Standard Test Methods for Flexural Bond Strength of Masonry.
ASTM Standards, C 1390-80 (reapproved 1993), copyright 1997.

[25] Materials and Structures, Supplement March 1997, pp 12-16, A review of the work of the RILEM Committee 127-MS: Testing masonry Materials and Structures. prepared by R.C. de Vekey

[26] Materials and Structures. Vol. 29, October 1996, pp 459-475, MS-B.4 Determination of shear strength index for masonry unit/mortar junction.

[27] Earthquake Spectra. Volume 12, No. 4, November 1996, pp. 825-844, Out-of-Plane Strength of Unreinforced Masonry Infill Panels. by Daniel P. Abrams, M.EERI, Richard Angel, and Joseph Uzarski, M.EERI

[28] Glass Fiber Reinforced Polymer Rebar. Hughes Brothers, INC., Seward, Nebraska

[29] Influence of the Characteristics of the Units on the Strength of Block Masonry. Article by R.G. Drysdale and Ahmad A. Hamid.

[30] Ultimate Strength Behavior of Hollow Concrete Masonry Prisms Under Axial Load and Bending. Article by Ivan J. Becica and Harry G. Harris

[31] Prism Tests for the Compressive Strength of Concrete Masonry. Article by G.A. Hegemier, G. Krishnamoorthy, R.O. Nunn, T.V. Moorthy, research sponsored by the National Science Foundation.

[32] Compression Characteristics of Concrete Block Masonry Prisms. Article by Hong E. Wong and Robert G. Drysdale. Masonry: Research, Application, and Problems. ASTM STP 871, J. C. Grogan and J. T. Conway, Eds., American Society for Testing and Materials, Philadelphia, 1985, pp. 167-177

[33] Modulus of Elasticity of Concrete Block Masonry. Article by Ahmad Hamid, Ghassan Ziab, and Omar El Nawawy

[34] Flexural Behavior of Reinforced Concrete Masonry Members. Article by Macher K. Tadros, Department of Civil Engineering, University of Nebraska, Omaha, NE

[35] Flexural Strength of Reinforced Block Masonry Walls. Article by Sami M. Fereig and Ahmad A. Hamid

[37] Reinforced Masonry Design 3rd Edition. By Robert R. Schneider and Walter L. Dickey, Copyright 1994, 1987, 1980 by Prentice-Hall, Inc.

[38] The Masonry Society, Limit States Design of Masonry, Draft Report. March1991 TMS Report

[39] ASTM Standard Specifications for Brick and Applicable Testing Methods for Units and Masonry Assemblages and BIA Standard Specification for Portland Cement - Lime Mortar for Brick Masonry, BIA Designation MI- 72. By the Brick Institute of America 1750 Old Meadow Rd, McLean, Virginia. Copyright of the American Society for Testing and Materials, October 1975.

[40] Building Code Requirements for Masonry Structures (ACI 530-98/ ASCE 5-98/ TMS 402-98), Commentary on Building Code Requirements for Masonry Structures (ACI 530-98/ASCE 5-98/TMS 402-98), Specification for Masonry Structures (ACI 530.1-98/ASCE 6-98/TMS 602-98), Commentary on Specification for Masonry Structures (ACI 530.1-98/ASCE 6-98/TMS 602-98), working draft, August 1998. By the Masonry Society, Boulder, Colorado.

[41] Masonry Limit States Design Standard, Draft. By The Masonry, American Concrete Institute, and the American Society of Civil Engineers, April 1992

[42] "A comparision of the laboratory test methods used to determine the shear resistance of Masonry walls". Bernardini A., Modena C., Turnsek V., Vescovi U., Studio tratto dal programma di collaborazione tra l'Università di Padova e l'istituto ZRMK di Ljubljana.

[43] Analisi sperimentale e modellazione di una tecnica di consolidamento per strutture murarie, Zago R., Tesi di laurea, Università di Padova, a.a. 1996-'97.

[44] Analisi sperimentale del comportamento di volte murarie rinforzate con FRP, Valdemarca M., . Tesi di laurea, Università di Padova, a.a. 1997-'98.

[45] Sperimentazione e modellazione del comportamento a taglio di pannelli murari rinforzati tramite FRP, Marchetti M., Tesi di laurea, Universita`di Padova, a.a. 1998-99.

[46] Mechanical Effects of Bed Joint Steel Reinforcement in Historic Brick Masonry Structures, Binda L., Modena C., Valluzzi M.R., Zago R., Structural Faults+Repair 99, 8th International Conference, London, UK, 1999.

[47] Strengthening of RC Structures with Near-Surface Mounted FRP Rods, De Lorenzis L., MSc. Thesis, Department of Civil Engineering, University of Missouri - Rolla, Rolla (MO), USA, 2000

[48] Anchorage System for Externally Bonded FRP Laminates Using Near Surface Mounted FRP Rods, Gose S., Nanni A., CIES Report, University of Missouri - Rolla, Rolla (MO), USA, 1999

[49] Field Evaluation of Unreinforced Masonry Walls Strengthened with FRP Composites subjected to Out-of-Plane Loading, Tumialan G., Tinazzi D., Myers J., Nanni A., American Society of Civil Engineers (ASCE) Structures Congress 2000 - Philadelphia (PA), USA, 2000

[50] Strengthening of Masonry Assemblages with Fiber Reinforced Polymer Rods and Laminates, Tinazzi D., Modena C., Nanni A., Advanced with Composite 2000, Milan, ITALY.

[51] The effect of horizontal reinforcement on strength and ductility lf masonry walls, Tomazevic M., Report to the research community of Slovenia. Ljubljana - Slovenia 1984, 85.

[52] Simulazione numerica della risposta di pannelli murari consolidati mediante materiali compositi. di A. Rocco, S. Sorace, G. Terenzi, Universita` di Udine, Universita` di Firenze, Italy

[53] Provisional Design Recommendations for Concrete Reinforced with FRP bars.
Working Document, reported by the ACI committee 440 FRP reinforcement, January 2000. (Still under evaluation).

[54] Building Code Requirements for Reinforced Concrete and Commentary, ACI-318-95, (1995). American Concrete Institute, Detroit Michigan.

[55] Flexural Behavior and Design of Reinforced Concrete Using FRP Rods, Nanni A., Journal of Structural Engineering, V.119, No.11,pp.3344-3359, 1993.

[56] Contribution of Externally Bonded FRP to Shear Capacity of RC Flexural Members, Khalifa, A.; Gold, W.J.; Nanni, A.; and Abdel Aziz, M. I. (1998). Journal of Composites for Construction, Vol. 2, No. 4, pp. 195-202.

[57] Anchorage System for Externally Bonded FRP Laminates Using Near Surface Mounted FRP Rods, Gose S.C.; Nanni A. CIES Report 99-7, University of Missouri - Rolla, Rolla (MO), USA, 2000

[58] An Introduction to composite materials, Derek Hull, Oxford University Press, 1998.

[59] Principles of Polymer Engineering, N.G. McCrum, C.P. Buckey, C.B. Bucknall Oxford University Press,1997.

[60] Masonry Construction Strenghtened With Fiber Composites In Seismically Endangered Zones, Shwegler, Published by: 10th European Conference on Earthquake Engineering. Vienna, Austria, 1994.

[61] Composite Strengthening System – Design Guide, MBrace ™ (1998), Master Builders Technologies, Cleveland, Ohio, pp. 3.2-3.6.

[62] Waterfront Repair and Upgrade, Advanced Technology Demonstration Site No. 2: Pier 12, NAVSTA San Diego, Site Specific Report SSR-2419-SHR, Warren, G.E. (1998), Naval Facilities Engineering Service Center, Port Hueneme, CA.

[63] Characterization of CFRP Bars Used as Near-Surface Mounted Reinforcement, Yan, X.; Miller, B.; Nanni, A.; and Bakis, C.E. (1999). Proceedings 8th International Structural Faults and Repair Conference, M.C. Forde, Ed., Engineering Technics Press, Edinburgh, Scotland, 1999, 10 pp., CD-ROM version.

[65] Myriad Convention Center Floor System Reinforcement, Hogue, T.; Cornforth, R.C.; and Nanni, A. (1999). Proceedings of the Fourth International Symposium on Fiber Reinforced Polymer Reinforcement for Reinforced Concrete Structures, C.W. Dolan, S. Rizkalla and A. Nanni, editors, American Concrete Institute SP-188, pp. 1145-1161.

[66] Upgrading the Transportation Infrastructure: Solid RC Decks Strengthened with FRP, Alkhrdaji, T.; Nanni, A.; Chen, G.; and Barker, M. (1999), Concrete International, American Concrete Institute, Vol. 21, No. 10, October, pp. 37-41.